The Dissertation Committee for Gary Lynn McGregor Certifies that this is the approved version of the following Dissertation:

New Tissue Damage Model for Pressure and Thermal Injuries and its Practical Application

Committee:

Kenneth R. Diller, Supervisor

Michael S. Sacks

Joseph J. Beaman

James W. Tunnell

Christopher G. Rylander

New Tissue Damage Model for Pressure and Thermal Injuries and its Practical Applications

by

Gary Lynn McGregor

Dissertation

Presented to the Faculty of the Graduate School of
The University of Texas at Austin
in Partial Fulfillment
of the Requirements
for the Degree of

DOCTOR OF PHILOSOPHY

The University of Texas at Austin

August 2021

Dedication

To my wonderful loving family and friends.

Acknowledgments

I want to give a special thank you to my advisor Dr. Ken Diller. He set a high standard for being a scientist and engineer and always pushed me to achieve the best possible outcome regardless of the challenges. The personal development, lessons, and growth I have experience under his mentorship will last a lifetime. He is always positive and willing to give as much time as anyone needs, regardless of how busy he might be. I never saw a day that Dr. Diller did not smile.

I would like to thank my committee for their guidance and support throughout this journey. A special thanks to Dr. Michael Sacks for his insightful help in simulations and his great engineering sense of humor.

I would like to give a special thank you to my friend and colleague, Dr. Bruno Rego. I had little chance to collaborate with others due to research project differences. Bruno not only provided great in-depth discussions regarding our simulation work but was the mental catalyst for the injury model presented in this dissertation.

Finally, I would like to thank all my wife, family, and friends who have been so supportive of my dreams and goals during graduate school. I can not thank you enough for all the love you have given me.

Abstract

New Tissue Damage Model for Pressure and Thermal Injuries and its Practical Applications

Gary Lynn McGregor, PhD

The University of Texas at Austin, 2021

Supervisor: Kenneth R. Diller

A new novel approach for modeling coupled thermal and pressure injuries will be demonstrated here for medical and consumer products. The analysis shows the benefits an injury model has in a complex Multiphysics environment. This dissertation consists of three manuscripts submitted to publication. The basic coupled injury model between applied temperature and pressure is submitted to J Heat Transfer for a special issue on bioheat transfer research. The kinetics of the injury model are derived by optimized fitting to a complex experimental data set from the Iaizzo lab at the University of Minnesota. A second paper models the combined effects of pressure and temperature to simulate development of injury in soft tissue overlying the ischial tuberosity for a person sitting on a heated vehicle seat. Pressure reduces perfusion of blood leading to ischemic injury. Elevated temperature accelerates the injury process. This is submitted to the Society of Automotive Engineers Journal on Transportation Safety. The third paper presents a new analysis of tooth injury that can occur during the use of whitening products based on

hydrogen peroxide (H_2O_2) gel applied in conjunction with laser activation. The analysis models diffusion of H_2O_2 through enamel and dentin into the pulp where it can cause inflammation and swelling. Heating by absorption of laser light also causes inflammation to be accelerated. Swelling of the pulp within the rigid tooth cavity results in pain and necrosis. This work is submitted to the Journal of Dental Research.

Table of Contents

List of Tables

List of Figures

Chapter 1: Introduction

There is a growing need for rapid development of innovation in medicine to ensure consumer products and medical devices are safe. Mathematical modeling of injury has roots dating back to the late ’40s has been employed to help mitigate potentially harmful events [1–6]. With the advances in software and hardware processing power, the improvements in computers are playing a pivotal role in advancing medicine in a multitude of areas [7]. Without a model to understand injury and its causation, pure reliance on animal and human experiments is expensive to run and requires an internal review board (IRB) before any are carried out. Some types of experiments may not even be able to be carried out due to ethical reasons.

Having a way to test if a product or device is safe earlier in the design phase can be potentially game-changing from a cost and safety perspective. The FDA has approved medical simulation as a pillar of the approval system [8]. Computer simulation does not replace actual product testing for validation and verification. What it does provide is a way for defining design direction while narrowing the number of necessary experiments. This is all accomplished by letting the development team know if the physical parameters of the device in question could potentially be harmful before the testing stage. Two areas where simulations can have a substantial impact on development are medical devices and consumer products.

Having the ability during the development process to predict if a product could be potentially harmful to a patient or consumer is essential[9].

There is a strong need within the medical device and consumer product industries for better prediction tools [7,9,10]. Several areas within product development benefit from Injury simulation. One is to lower the number of experiments needed for validations and verification. Experiments cost time and money. Eliminating unnecessary experiments, especially those related to animal and human tests, is valuable. The improved up-front development helps the product have the highest possible impact. More time can be invested in refinement with the ability to predict harmful situations and reduce unknowns in the development cycle and to prevent potentially harmful products from reaching the marketplace. Some products are developed with scientific experiments that do not require human trials. If the understanding of the experiments is misinterpreted, the product could become potentially dangerous. For example, many hundreds of lawsuits have been filed as a result of injury attributed to cryotherapy units that were developed and brought into the marketplace with essentially no experimental testing of modeling simulations. Medical simulation helps understand how the products will affect a more extensive user demographic. Humans vary in age, weight, size, and genetics. There is also the factor of preexisting medical conditions such as spinal cord injury (paraplegic) and conditions that affect blood flow throughout the body, such as diabetes, Buerger's disease, Raynauld's disease, and peripheral artery disease (PAD). Understanding the confounding aspects of these conditions may help improve clinical outcomes by providing the correct dosage or protocol of a device in question-based on human variability. An effective therapeutic treatment for one person could be potentially harmful to another. Injury modeling in the development process has significant benefits. This leads to the question, what is injury modeling, and how does it fit into the product development?

Injury modeling and simulation is an broad field reaching into all areas of medicine [7]. Models can be empirical, based on first principles, or a hybrid of the two as a structurally informed empirical model. The focus here will be on structurally informed, coupled thermal and mechanical models. These two types of injury will be defined in the following sections, but it is important to note that there is a range of conditions in which the two are coupled together. The definition of injury for the paper is to establish the percentage (%) viable cells in a unit of tissue volume. The model is run by dependent and independent variables, such as temperature, time, stress, strain, blood flow, and inflammation.

Thermal injury (TI) or burns results from the application of heat to the extent that the rising temperature in the tissue denatures proteins [2–6]. Thermal injury modeling was given heavy emphasis after World War II (WWII) [3]. The body of work that laid the foundations was from Pennes for calculating bioheat transport and Mortiz and Henriques series of paper on understanding burns and the development of an empiricall model. This early model, which persists to this day, is based on the Arrhenius equation for chemical activation. Since the original model was proposed, a large body of work has been built on its foundation to improve the model's prediction capabilities, as seen by Diller, Pearce, Bishop, He, and Feng [11–17].

Moritz and Henriques showed that thermal injuries happen above 44°C [2]. At this temperature maintained on the surface of skin, it would take 7 hours to produce a second-degree burn [2]. The Arrhenius model is very successful at the simulation of thermal injuries above 55°C [16]. Modeling challenges and research focuses are on the temperature ranges between 44-55°C due to large jumps in time for injury formation [16]. The 44-46°C is especially sensitive [2]. Not only is the 44-46°C problematic in accurate prediction for conventional modeling methods, but it

is in a temperature range that closely couples it to mechanical parameters for increasing the rate of injury [18–21]. Adding a mechanical load to the heated tissue, blood flow that is critical in regulating temperature, is impeded, in an ischemic environment. This falls within the cross-over point of a pressure injury.

Pressure injuries, also known as pressure ulcers, are defined by the National Pressure Injury Advisory Panel (NIPAP) as " localized damage to the skin and underlining tissue, as a result of pressure or pressure in combination with shear " [22]. According to the NIPAP, the number of "pressure injuries are estimated to approach 11.6 billion annually in the U.S." [22]. It is also estimated that 34% of the PI reported in the hospital are caused by a medical device [10]. Classically, pressure injury research focuses on the mechanical loading of the tissue [23–27]. The three underlining causes of PI are direct deformation, inflammation, and ischemia [28]. A large study conducted by Iaizzo in the mid-'90s showed that PI can be modulated by temperature [18–21]. It was documented that temperature could act as prophylactic or promoter of PI formation, depending on its range compared to physiological base line [19]. In the Iaizzo studies, Kokate et al. demonstrated the groundwork for an injury model. Zeevi et al. applied this model a 3D FEM analysis of potential pressure injury formation using different seat cushions [18,29]. The original model is a great start but has limitations by being a polynomial fit to the experimental data and therefore can not express the percentage of tissue viability [18]. The original model overlapped burn temperatures leading to faster injury prediction times with an applied load. With the critical temperature overlap, a new injury model is necessary to accurately predict tissue damage from medical devices, and consumer products in the domain where thermal and mechanical induced injury causation overlap.

With a focus on improving the design of medical devices and safe consumer products, a motivation to develop an injury model that engineers could use was born. An injury model will be demonstrated based on a unique new equation and simulation methods. The value of this simulation approach is not just crucial for the TI or PI, but the sensitive overlap region to two injury types have that are typically ignored in traditional modeling methods.

Research Focus

The underlying focus of the present research is developing a mathematical model for thermal and pressure injuries and the existing coupling. This is followed with novel simulation applications of the model to two consumer products. The first section is the development of the injury model. The second section applies the model to vehicle seat heating and its effects on a human subject with and without a spinal cord injury. The third section summarizes the application of injury modeling to a complex system in dental tooth whitening treatments. The thesis comprises a large body of work that is synthesized into several publications. Further detailed information from this study is included in the appendix.

[1] Pennes, H., 1948, "Analysis of Tissue and Arterial Blood Temperatures in the Resting Human Forearm," J. Appl. Physiol., pp. 5–34.

[2] Moritz, a. R., and Henriques, F. C., 1947, "STUDIES OF THERMAL INJURY II. The Relative Importance of Time and Surface Temperature in the Causation of Cutaneous Burns.," Am J Pathol, **23**, pp. 695–720.

[3] Henriques, F. C., and Moritz, A. R., 1947, “STUDIES OF THERMAL INJURY I. The Conduction of Heat to and through Skin and the Temperatures Attained Therein. A Theoretical and an Experimental Investigation.,” Am. J. Pathol., **23**(4), pp. 530–549.

[4] Moritz, A. R., 1947, “STUDIES OF THERMAL INJURY III. The Pathology and Pathogenesis of Cutaneous Burns An Experimental Study,” Am. J. Pathol., **13**(6), pp. 915–941.

[5] Moritz, A. R., Henriques, F. C., Durtra, F. R., and Weisiger, J. R., 1947, “STUDIES OF THERMAL INJURY IV. An Exploration of the Casualty-Producing Attributes of Conflagrations; Local and Systemic Effects of General Cutaneous Exposure to Excessive Circumambient (Air) and Circumradiant Heat of Varying Duration and Intensity,” Arch. Pathol., **43**(5), pp. 466–488.

[6] Henriques, F. C., 1947, “STUDIES OF THERMAL INJURY V. The Predictability and the Signinficance of Thermally Induced Rate Processes Leading to Irreverible Epidermal Injury,” **43**(5), pp. 489–502.

[7] Winslow, R. L., Trayanova, N., Geman, D., and Miller, M. I., 2012, “Computational Medicine: Translating Models to Clinical Care,” Sci. Transl. Med., **4**(158).

[8] Morrison, T. M., Dreher, M. L., Nagaraja, S., Angelone, L. M., and Kainz, W., 2017, “The Role of Computational Modeling and Simulation in the Total Product Life Cycle of Peripheral Vascular Devices,” J. Med. Devices, Trans. ASME, **11**(2).

[9] Haimy, A., Kopplin, K., and Gefen, A., 2018, “Device-Related Pressure Ulcers from a Biomechanical Perspective,” Lect. Notes Bioeng., **26**(1), pp. 37–41.

[10] Gefen, A., Alves, P., Ciprandi, G., Coyer, F., Milne, C. T., Ousey, K., Ohura, N., Waters, N., and Worsley, P., 2020, “Device-Related Pressure Ulcers: SECURE Prevention,” J. Wound Care, **29**(Sup2b), pp. S1–S52.

[11] Hensley, D. W., Mark, A. E., Abella, J. R., Netscher, G. M., Wissler, E. H., and Diller, K. R., 2013, "50 Years of Computer Simulation of the Human Thermoregulatory System," J. Biomech. Eng., **135**(2), p. 021006.

[12] Roselli, R., and Diller, K. R., 2011, *Biotransport: Principles and Applications*, Springer Science & Business Media.

[13] Diller, K. R., 2015, *Therapeutic Recruitment of Thermoregulation in Humans by Selective Thermal Stimulation along the Spine*.

[14] He, X., and Bischof, J. C., 2003, "Quantification of Temperature and Injury Response in Thermal Therapy and Cryosurgery," Crit. Rev. Biomed. Eng., **31**(5–6), pp. 355–422.

[15] Pearce, J. A., 2013, "Comparative Analysis of Mathematical Models of Cell Death and Thermal Damage Processes," Int. J. Hyperth., **29**(4), pp. 262–280.

[16] Pearce, J. A., 2015, "Improving Accuracy in Arrhenius Models of Cell Death: Adding a Temperature-Dependent Time Delay," J. Biomech. Eng., **137**(12), pp. 1–7.

[17] Feng, Y., Oden, J. T., and Rylander, M. N., 2008, "A Two-State Cell Damage Model under Hyperthermic Conditions: Theory and in Vitro Experiments," J. Biomech. Eng., **130**(4), pp. 1–10.

[18] Kokate, J. Y., Leland, K. J., Sparrow, E. M., and Iaizzo, P. A., 1997, "Critical Thresholds for Pressure Ulcer Formation in a Porcine Model," Wounds, **9**(4), pp. 111–121.

[19] Iaizzo, P. A., Kveen, G. L., Kokate, J. Y., Leland, K. J., Hansen, G. L., and Sparrow, 1995, "Prevention of Pressure Ulcers by Focal Cooling: Histological Assessment in a Porcine Model.," Wounds A Compend. Clin. Res. Pract., **7**(5), pp. 161–169.

[20] Hansen, G. L., Sparrow, E. M., Kokate, J. Y., Leland, K. J., and Iaizzo, P. A., 1997, "Wound Status Evaluation Using Color Image Processing," IEEE Trans. Med. Imaging, **16**(1), pp. 78–86.

[21] Kokate, J. Y., Leland, K. J., Held, a M., Hansen, G. L., Kveen, G. L., Johnson, B. a, Wilke, M. S., Sparrow, E. M., and Iaizzo, P. a, 1995, "Temperature-Modulated Pressure Ulcers: A Porcine Model.," Arch. Phys. Med. Rehabil., **76**(7), pp. 666–673.

[22] European Pressure Ulcer Advisory Panel, National Pressure Injury Advisory Panel, and Pan Pacific Pressure Injury Alliance, 2019, *Prevention and Treatment of Pressure Ulcers/Injuries: Clinical Practice Guideline*, The International Guideline.

[23] Bouten, C. V., Oomens, C. W., Baaijens, F. P., and Bader, D. L., 2003, "The Etiology of Pressure Ulcers: Skin Deep or Muscle Bound?," Arch. Phys. Med. Rehabil., **84**(4), pp. 616–619.

[24] Linder-Ganz, E., and Gefen, A., 2004, "Mechanical Compression-Induced Pressure Sores in Rat Hindlimb: Muscle Stiffness, Histology, and Computational Models," J. Appl. Physiol., **96**(6), pp. 2034–2049.

[25] Linder-Ganz, E., Shabshin, N., Itzchak, Y., and Gefen, A., 2007, "Assessment of Mechanical Conditions in Sub-Dermal Tissues during Sitting: A Combined Experimental-MRI and Finite Element Approach," J. Biomech., **40**(7), pp. 1443–1454.

[26] de Groot, H., and Rauen, U., 2007, "Ischemia-Reperfusion Injury: Processes in Pathogenetic Networks: A Review," Transplant. Proc., **39**(2), pp. 481–484.

[27] Linder-Ganz, E., Shabshin, N., Itzchak, Y., Yizhar, Z., Siev-Ner, I., and Gefen, A., 2008, "Strains and Stresses in Sub-Dermal Tissues of the Buttocks Are Greater in Paraplegics than in Healthy during Sitting," J. Biomech., **41**(3), pp. 567–580.

[28] Amit Gefen, 2018, “The Future of Pressure Ulcer Prevention Is Here: Detecting and Targeting Inflammation Early,” EWMA J., **19**(2), pp. 7–13.

[29] Zeevi, T., Levy, A., Brauner, N., and Gefen, A., 2018, “Effects of Ambient Conditions on the Risk of Pressure Injuries in Bedridden Patients—Multi-Physics Modelling of Microclimate,” Int. Wound J., **15**(3), pp. 402–416.

Chapter 2: Mathematical Model for Combined Effects of Heat Transfer and Pressure in Causing Soft Tissue Injury

The work contained in this chapter has been submitted to the Journal of Heat Transfer for publication[1].

Gary McGregor contributed to the conception and development of the mathematical model, development of code, experiments, analysis, and drafting of manuscript.

[1]This is a slightly modified version of the article submitted for publication to align with the dissertation format.

ABSTRACT

Pressure and thermal injuries affect millions of lives every year. Both types of injury have been a focal priority for the medical community to understand and treat since World War II. Typically, each injury mechanism is studied in isolation due to differences in the primary factors causing the trauma. The serial confluence of applied tissue deformation, inflammation, and ischemia imposed over time combine to cause mechanically derived injury, whereas high or low temperatures are causative factors for thermal injuries. Modeling and simulation analyses have been used to develop an understanding of both types of injury pathways to predict threshold conditions for the onset of damage and to develop methods of prevention. Although thermal and mechanical injury processes are often viewed independently, prior experiments have demonstrated that these two phenomena may have active cross-coupling. Temperature can act as a prophylactic or accelerant to pressure injuries, depending on its magnitude, to radically alter the shape, position, time, and final disposition. In the present study, we developed a finite element model to predict injury as a function of time, temperature, mechanical deformation, and local blood perfusion. The model embodies an equation with constitutive terms that are relevant to physiological processes that govern the development of injury. The current model is a composite derived from regression of experimental data and conformation to the physiological structure. It expresses highly nonlinear coupling across the domains of thermal, mechanical, and fluid transport and is solved for composite hard and soft tissue geometry combinations. We evaluated the model for a broad range of trauma conditions defined by subject morphology, mechanical loading, temperature, and time. Moreover, we implemented the model within a finite element framework to estimate the risk of injury for specific stress conditions via large-scale simulations.

INTRODUCTION

There were over 3 million burns and pressure ulcers (PUs, also known as pressure injuries) reported in 2017 in the United States, of which 2.5 million were reported as PUs [1,2]. The PU is a complex injury formed as a consequence of ischemia, direct deformation, and inflammation [3]. Soft tissue is deformed under physical loading, such as created by a sitting or lying position, that, when maintained for long periods of time, will lead to a PU. When tissue is deformed, it causes a lack of local blood flow to supply the metabolic needs of the cells in the affected region, allowing for the accumulation of metabolic waste while starving the cells of nutrients and oxygen. If the condition perpetuates, cellular necrosis will start to set in, and cell death will occur [3–5]. Burns, on the other hand, result from the denaturing of proteins during exposure to temperatures above 43°C [6]. Both types of injury have traditionally been studied separately, although in their classic study of burns in the late 1940s, Moritz and Henriques performed a very limited evaluation of the effect of applied pressure on their standard thermal exposure protocols [6,7]. In the mid-1990s, Iaizzo et al. conducted a well-designed large-scale study on a porcine model to investigate the relationship between temperature, mechanical loading, and time [8–11]. The study stands as the largest and most comprehensive of its kind and (to the authors' knowledge) has not been replicated since. The results document how temperature can modulate PUs and the complex coupled relationship between temperature and pressure in injury causation [8–11]. The study also showed that lowered temperature is prophylactic in combination with mechanical loading, while an elevated temperature may act as an accelerant to

mechanical loading to cause PU formation [8]. An ancillary observation of the studies was that elevated local pressure stress increased the rate at which burns occurred [8].

There has remained persistent mischaracterization of pressure injuries occurring in conjunction with exposure to relatively low temperatures as being full-thickness burns [8]. Gefen has published a series of papers addressing PUs as a function of microclimate, including temperature and humidity [5,12–14]. This work, including modeling of the injury process, is linked to an international community of researchers studying the diverse factors that contribute to pressure-derived injuries [15,16]. Gefen has developed extensive criteria for determining the onset of PUs, including via modeling and simulation. One simulation used a computational damage model developed by Kokate et al. based on the original Iaizzo porcine data [12]. The damage model used an algebraic equation to fit the data for time, temperature, and mechanical loading to yield threshold conditions for injury occurrence [9]. The model was a significant step forward in injury prediction based on these three confounding factors. However, this model is limited by the fact that effective optimization techniques were not used when estimating the best-fit coefficients, and by its polynomial form, which does not provide the best representation of the physical data.

In contrast to PUs, thermal injury processes have been extensively measured and modeled since the 1940s, based primarily on the Arrhenius rate equation [6,7,17–24]. A drawback to many burn models is that while they are effective for the prediction of trauma in short exposure times at high temperatures, they are less accurate with lower temperatures at longer time scales [17,18]. Researchers in the thermal injury field have proposed various methods to compensate for this issue, though with limited success [18,21,25,26]. The

model proposed herein addresses the need to estimate thermal injury within the lower temperature ranges that are often encountered in conjunction with mechanical loading injuries.

The goal of this study was to develop an injury causation model for soft tissue that embodies the coupled effects of temperature, applied pressure, and localized blood perfusion over time. Constitutive property data for the model was derived by optimized fitting of mathematical functions to data from the Iaizzo porcine study. The injury model constitutive coefficients were derived with the intention of being physiologically relevant (as opposed to merely a consequence of a curve fit to the source data). This objective has been a major challenge to achieve. The model is presented in a rather simplified initial foray to serve as a platform for future development of coupled injury analyses that embody more rigorous physical and physiological assumptions.

METHODS

Research data used for the model.

To the authors' knowledge, the largest and most comprehensive experimental study on pressure ulcer formation with temperature modulation was the set of trials conducted by the Iaizzo lab on a porcine model [8–11]. Swine were anesthetized, and three arrays of four 57-mm diameter heated and weighted disks were applied along the dorsal flanks anterior to posterior with varying disk temperature, duration, and force, as shown in Table 1. A total of 70 animals were studied, yielding 840 sites for analysis of injury resulting from specific combinations of simultaneous thermal and mechanical stress. The animals

were observed for up to 7 days following the stress and then euthanized so that tissue damage could be evaluated histologically. Consistent with traditional studies of PU formation and burn injury occurrence, tissue damage was assessed at four different depths: in dermis, epidermis, fat, and muscle. Tissue damage was assigned an injury rating by a blinded observer on a coarse scale consisting of 0 for no damage, 1 for some damage, or 2 for severe damage. Acute exposure times lasted for 2, 5, or 10 hours. The four constant surface pressures applied were 10, 50, 100, or 150 mmHg and the six surface temperatures were between 25°C and 50°C at 5°C increments. Thus, although the matrix of experimental conditions was large, the temporal, thermal, and mechanical resolutions were limited, making it a challenge to fit a mathematical expression to the experimental data to determine values for the constitutive properties that govern the model injury process.

Experimental Condition	Values of Experimental Condition
Applied Temperature (^{0}C)	25, 30, 35, 40, 45, 50
Applied Loads (mmHg)	10, 50, 100, 150
Exposure Time (hrs)	2, 5, 10

Table 2.1. Values of mechanical, thermal and temporal variables applied during determination of temperature enhanced pressure sores as measured at four different tissue depths. In total, 288 different injury assessments were made. [9]

Summary data from the Iaizzo experiments are presented in Fig. 1 [9]. Several features of this data set are readily apparent: there is a very sparse resolution for the time

of exposure and for the degree of resulting injury. In some cases, data is missing. Our analysis approach was to fit a mathematical expression to predict the progressive development of tissue damage using the three predictor variables (pressure P, temperature T, time t) together with optimally estimated constitutive coefficients. In addition to the bar graph (Fig. 1), Iaizzo et al. also includes a tabulated nonnumerical summary of each experimental point that gives a complete qualitative description of the data. Using select archival experimental data from the Iaizzo study, we created, as completely as possible, a continuous data set of injury outcomes as a function of T, P, and t. An interpolated numerical map was fit to this data set to provide a smoother and more comprehensive representation of the experimental outcome that we then used for our injury model development. In essence, this process amounted to reverse engineering of the experimental data. Data from the original graphs and table were cross-referenced to each other to assemble the more continuous experimental data sets shown in Fig. 2 that were used to build the injury model. These data have an increased level of internal consistency and were used for optimizing the constitutive coefficients of our model to provide an injury prediction tool.

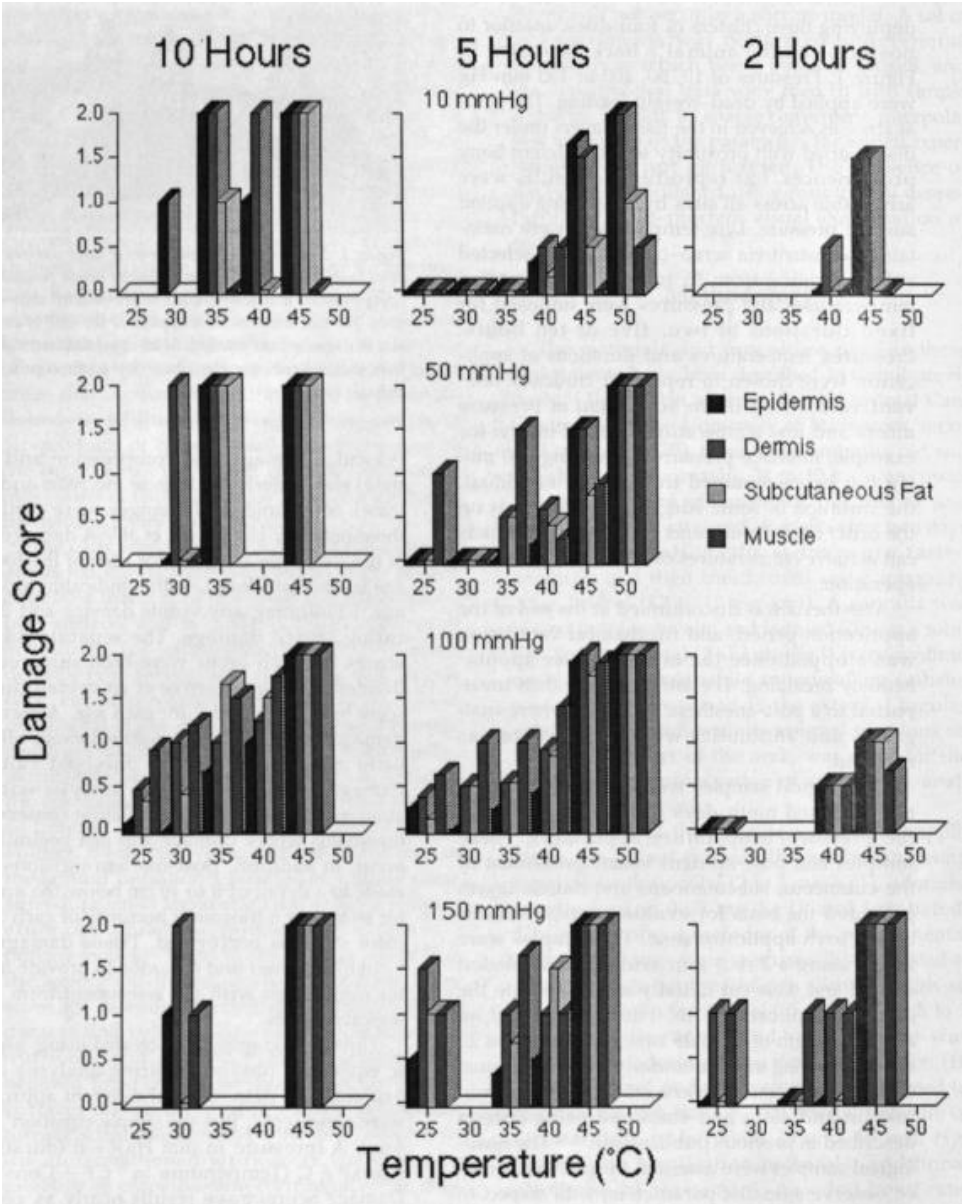

Fig. 2.1. Data for damage measured at four different tissue depths for specific combinations of surface temperature, pressure loading, and exposure time, reproduced from Kokate et al [9]. Note that damage data is missing for many combinations of temperature and pressure. Some missing data is supplied in a complementary table using qualitative descriptors of injury outcomes. Increasing pressure, temperature, and time all exacerbate injury. The damage score values were correlated between the table and Fig. 1 to develop Fig. 2.

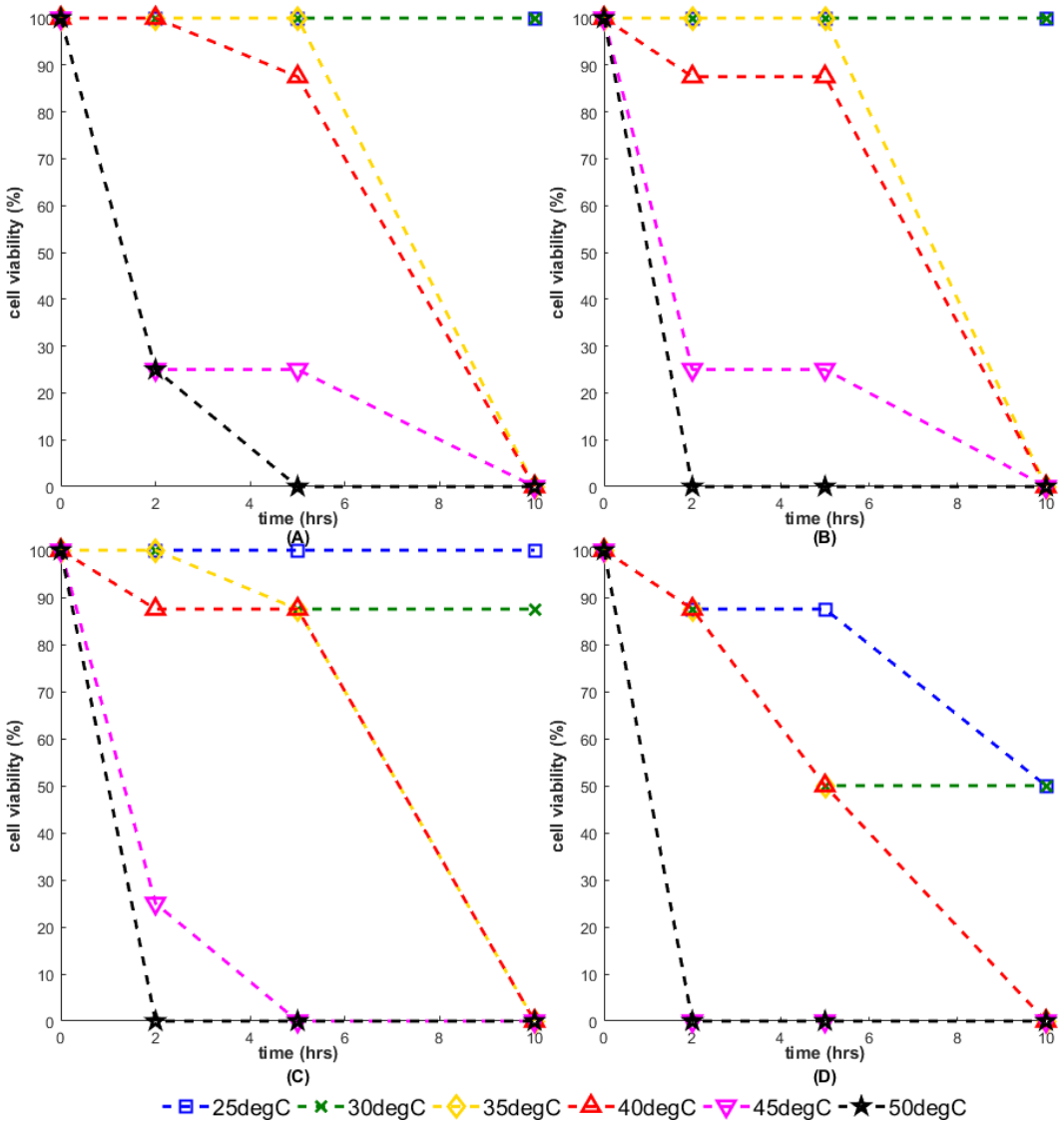

Fig. 2.2. Inversion of the tissue damage data in dermis only from Fig. 1, now expressed in terms of viability. The four plots (A), (B), (C), and (D) separate the data for pressure loading of 10, 50, 100, and 150 mmHg, respectively to enable the response trends to be observed more clearly. Note that the resolution of the data in terms of viability and time is very limited, resulting in overlap that compromises interpretation. The original purpose of the data was to show that heat can modulate pressure injury onset. The coarseness of the experimental setpoints was sufficient to show causation. The biological nature of the onset of injury is more gradual and would have little to no overlap until complete cell death.

Development of the coupled mathematical model for injury causation.

The Iaizzo experimental data presented an opportunity to develop a predictive model for the coupled interaction between applied temperature and pressure in soft tissue injury causation. A successful model needs to embody both the mechanisms of interaction between elastic and thermal stresses in soft tissues as well as the physiological response, including blood flow modification, inflammation, and necrosis. Inputs to the model are constitutive property values and macroscopic initial and boundary conditions applied to the tissue. The actual injury occurs at the cellular and molecular levels, but explaining the macroscale manifestation of insult in terms of the microscale response to applied stresses requires a detailed understanding that is beyond the scope of this process model. For example, Xue et al. presented a model for cutaneous tissue PU formation using a first-principle approach based on a multicomponent cascade of biochemical reactive processes [27]. However, a macroscopic data set such as that used in the present study is difficult to match with a bottom-up modeling methodology. Rather, we have pursued an approach to building a model that is based directly on the macroscopic physically measured parameters of the Iaizzo study. An advantage of this approach is that the resulting model will have a minimum set of variables, thereby reducing uncertainty in interpreting the outcome. The present model affords an injury equation as a simple function of time, temperature, pressure, and tissue constitutive properties.

A key component of developing a working injury model is the determination of effective constitutive tissue properties to match the behavior embodied in the experimental

data. To this end, it is realized that when heat and mechanical forces are applied to the surface of a composite tissue, there will result a spatial and temporal distribution of temperature and elastic stress within the tissue as a function of its thermal and mechanical properties and anatomy. The values for many key kinetic coefficients and tissue properties must be determined via an optimal fit of the model to the available data. Since the data set is sparse along the temperature, pressure and time dimensions, achieving an optimal fit of the model to this data involved a huge computational effort. The original experimental data was comprised of only temperature and pressure boundary conditions and injury outcomes at incremental tissue depths and times. Although it is acknowledged that important gradients in temperature and stress will develop over time within the tissue after it is loaded, for the sake of obtaining values for the model coefficients, the tissue was assumed to be isothermal and isobaric during the injury manifestation process. This same assumption was used by the Iaizzo group in their own injury prediction model [9]. During the fitting procedure, the temperature and pressure were assumed to be uniform throughout all four components of the tissue system to facilitate a match between the model and data. In contrast, when the full model is applied during injury process simulations, a prime outcome is the actual transient spatial distribution of temperature and pressure within the tissue that regulates the kinetic processes of injury. An example of the model prediction of injury when spatial variations in temperature and pressure are included can be seen later in Fig. 13.

It is assumed in the model that the dominant factor in the accrual of mechanical injury is depressed perfusion that persists over time. Ischemia is one of the major

contributors to PU, but not the only one. Mechanical distortion of cells and tissue moisture are also acknowledged as important factors [4,12,14]. Depressed perfusion was adopted as the single precipitating injury factor as there is a paucity of other data to motivate the model, with the realization that a more comprehensive set of precipitating factors that can be added to the model in future iterations. Additional terms such as elastic deformation can be included for injury induction if they are a function of local stress.

Although the Iaizzo experimental data set reported the tissue behavior for applied pressures of 10, 50, 100, and 150 mmHg, 120 mmHg was defined for purposes of the injury model as the threshold above which perfusion was driven to zero, based on mechanical stress overcoming the average systolic blood pressure. The baseline state of zero applied pressure was equated to 100% perfusion. Perfusion was assumed to decrease linearly with increasing elastic stress until total ischemia occurred at 120 mmHg. To determine coefficient values for fitting the model to the Iaizzo data, a linear relationship was thus assumed between the perfusion ω and the pressure P applied to the surface (and assumed to be transmitted uniformly throughout the tissue system), as in Eq. (1):

$$\omega = \begin{cases} 1 - \frac{P}{120\ \text{mmHg}} \text{ for } 0 < P < 120\ \text{mmHg} \\ 0 \text{ for } P \geq 120\ \text{mmHg} \end{cases} \quad (1)$$

Note that the perfusion scale is normalized between 0 and 1. Note also that a nonlinear response of blood flow to mechanical loading, which results in an internal distribution of stresses, may readily replace the above linear simplification when such a relation is available.

In the same manner, for fitting the model to the experimental data, the temperature imposed on the surface was assumed to be propagated uniformly through all tissues. The tissue damage data from Fig. 1, defined on a scale from 0 to 2, was converted by a linear inversion to cell viability Ω on a scale of 100% to 0% using

$$Cell.Viability = \frac{2 - Damage.Score}{2} \times 100\% \quad (2)$$

The resulting transformed viability data are presented in Fig. 2 for the four levels of pressure loading that were applied.

The original data was reassembled, interpolated, and graphed using Excel and MATLAB® to define a continuous function describing injury that could be incorporated into the algorithm for fitting coefficients. Several types of mathematical functions have been applied previously to describe pressure-induced injures [9,12,28,29]. However, after reviewing the existing equations, it was apparent that none could be adapted to fit the goal of modeling both PUs and burns over a wide range of stressor variables. Thus, a new set of constitutive relations was composed for the coupled thermal and mechanical injury processes.

We developed a novel approach to model cell viability based on concepts traditionally used in clinical studies for survival analysis (i.e., to represent patient survival over time in the presence or absence of a disease condition and/or therapeutic intervention). Fundamentally, we sought to describe the evolution of cell viability over time using temperature and perfusion as quantitative predictors. (Note: in this model, we have assumed perfusion to be a direct and proportional consequence of applied mechanical

stress, although other relevant surrogate responses that may initiate injury, such as cell deformation, could be substituted or added.) For this purpose, we adopted a survival model as originally proposed by Cox [30], which considers predictors that independently act on the baseline survival function (which in the present study is cell viability over time). Central to Cox's framework is a "proportional hazards condition," which states that the predictor variables are multiplicatively related to the hazard function (i.e., the instantaneous rate of decrease in viability that may vary with time). We assume that cell viability decreases monotonically with time, following a baseline hazard function, and that the effects of temperature and pressure modify the hazard rate in a multiplicative fashion.

Determining injury model coefficients.

Survival analysis is often performed to model the survival of individual subjects who can be tracked separately over the course of a clinical study. The time at which death occurs for each subject (or not, if a subject survives over the entire period of observation) is noted, and a probabilistic survival function (such as Cox's proportional hazards model) is then fit to the data using maximum likelihood estimation, to obtain a set of optimal coefficients that describe the effect on survival of each predictor variable considered. This modeling procedure attempts to answer the question, "given each subject's conditions/attributes, what coefficients best predict whether each individual will still be alive at every measurement time t_i?" In the present study, since it was not possible to track the survival of individual cells, we used the same survival function derived from Cox's approach (see details below), but instead fit the model to the survival data directly using

least-squares regression rather than fitting the survival state of individuals (which would be true/false as a function of time and predictor variables).

Based on the theoretical framework of Cox's proportional hazards model, the hazard function has the form

$$h(t \mid \vec{x}) = h_0(t) \exp\left(\beta_1 x_1 + \cdots + \beta_p x_p\right), \tag{3}$$

where h is the hazard function, h_0 is the "baseline" hazard function, t is time, x is a vector of state variables (e.g. temperature, perfusion), and β is a vector of p coefficients. We modeled the baseline viability using a Weibull distribution, such that viability decreases over time following

$$F(t) = 1 - \exp\left(-\lambda^k t^k\right). \tag{4}$$

Then the baseline hazard is defined as

$$h_0(t) = \frac{F'(t)}{1 - F(t)} = k\lambda^k t^{k-1}, \tag{5}$$

where λ is a scaling coefficient and k is a "shape"/exponent coefficient. The overall survival function is then defined as

$$S(t \mid x) = \exp\left(-\int_0^t h(\tau \mid x)\, d\tau\right) = \exp\left(-\lambda^k t^k \exp\left(\beta_1 x_1 + \cdots + \beta_p x_p\right)\right). \tag{6}$$

Since scale coefficients must be positive, it is convenient to re-write Eq. (6) using a transformed coefficient $\lambda^* = \ln \lambda$, which maps λ ∈ (0, ∞) to λ* ∈ (–∞, ∞). Re-writing the survival function as

$$S(t \mid x) = \exp\left(-\int_0^t h(\tau \mid x)\, d\tau\right) = \exp\left(-\exp\left(\lambda^*\right)^k t^k \exp\left(\beta_1 x_1 + \cdots + \beta_p x_p\right)\right), \tag{7}$$

an unconstrained least-squares optimization is then performed for the complete coefficient vector $\vec{\theta} = \left[\lambda^*, k, \beta_1, \ldots, \beta_p \right]$. In the present study, we considered the temperature T and perfusion ω as predictor variables with coefficients β_T and β_ω, respectively (such that p = 2, corresponding to 4 total model coefficients). By analogy to survival, we modeled the viability Ω using

$$\Omega(t, T, \omega) = e^{-\int_0^t [(e^{\lambda^*})^k k \cdot e^{\beta_T \cdot T(\tau) + \beta_\omega \cdot \omega(\tau)} \cdot \tau^{k-1}] d\tau}, \quad (8)$$

which under constant temperature and perfusion simplifies to

$$\Omega(t, T, \omega) = e^{-(e^{\lambda^*})^k \cdot t^k \cdot e^{\beta_T \cdot T + \beta_\omega \cdot \omega}}, \quad (9)$$

The coefficient values were identified in a two-step optimization process. First, the coefficients of the baseline viability function were estimated while ignoring the effects due to temperature and perfusion (i.e., holding $\beta_T = \beta_\omega = 0$). Then, the resulting estimates for λ* and k were used as initial guesses when fitting the full survival model. This protocol was chosen to ensure numerical stability during the optimization process since the values of the different model coefficients can sometimes differ by orders of magnitude.

To quantify the uncertainty in the optimal coefficient set resulting from least-squares fitting, we examined the likelihood function of our coefficient set in the neighborhood of the identified optimum. Exploiting the fact that least-squares optimization is equivalent to maximum likelihood estimation under the assumption of zero-mean normally distributed residuals r, we first obtained an estimated covariance matrix for the coefficient set using the Jacobian computed during least-squares minimization. Specifically, for a Jacobian matrix **J**, the covariance matrix of the estimated coefficients is

itself estimated using $\widehat{\boldsymbol{\Sigma}} = [\mathbf{J}^{\mathrm{T}}\mathbf{J}]^{-1}s^2$, where $s^2 = \frac{1}{n-4}\sum_{i=1}^{n} r_i^2$ is the unbiased estimate of the residual variance (with the 4 in the denominator corresponding to the total number of coefficients in the model) and n is the number of data points. The vector of standard errors $\hat{\sigma}_i$ for the coefficients can then be obtained by taking the square root of the diagonal elements of $\widehat{\boldsymbol{\Sigma}}$. The 4-dimensional likelihood function was computed within a neighborhood of $\pm 4\hat{\sigma}_i$ around each optimal coefficient value, under the assumption that residuals were normally distributed with a mean of zero and variance of s^2. Bivariate marginal likelihoods were then computed for every possible pair of coefficients by integrating through the remaining coefficient directions, as were univariate marginal likelihood functions for each individual coefficient. For visualization of results, every marginal likelihood was normalized with respect to its maximum value. Coefficients were optimized using a custom MATLAB® script, relying primarily on the vectorized `lsqcurvefit()` function for nonlinear least-squares regression, which executed in ~0.1 s per tissue type. Likelihood functions were computed numerically on a 31^4 grid centered at the optimal coefficient set (~45 s per tissue type), and trapezoidal integration was performed for the aforementioned marginalizations (~0.02 s per pair of coefficients). Values for the optimized coefficients are shown in Table 2.

Mathematical Model Fit and Coefficient Optimization	Values
Epidermis R^2	0.87
Epidermis Optimum λ^*, k, β_T, β_ω	-6.86, 1.86, 0.26, -0.011
Epidermis Standard Error λ^*, k, β_T, β_ω	0.48, 0.3, 0.035, 0.0033
Dermis R^2	0.86
Dermis Optimum λ^*, k, β_T, β_ω	-8.67, 1.35, 0.24, -0.0059
Dermis Standard Error λ^*, k, β_T, β_ω	0.79, 0.22, 0.029, 0.0028
Fat R^2	0.85
Fat Optimum λ^*, k, β_T, β_ω	-8.25, 1.12, 0.2, -0.029
Fat Standard Error λ^*, k, β_T, β_ω	0.92, 0.19, 0.024, 0.0042
Muscle R^2	0.91
Muscle Optimum λ^*, k, β_T, β_ω	-6.02, 1.44, 0.2, -0.044
Muscle Standard Error λ^*, k, β_T, β_ω	0.41, 0.18, 0.02, 0.0046

Table 2.2. Optimized values of coefficients in the injury model obtained by fitting to the data set from Kohate, et al. [9].

RESULTS - MODEL PREDICTION OF INJURY.

Figs. 3-6 show the predicted accrual of injury over time for specific combinations of applied pressure and temperature as of function of depth into the tissue in comparison with the experimental data to which the model was fit. Each plot is for an incremental tissue depth starting with the epidermis (Fig. 3), to dermis (Fig. 4), fat (Fig. 5), and muscle (Fig. 6). Note that the model data presents a continuous curve in comparison with the discrete experimental data points. Fig. 7 shows a 3D surface view of the predicted development of

injury over time for different applied temperatures (25°C, 35°C, and 45°C) for an applied pressure of 100 mmHg. The global trends of the prediction follow the experimental data well, with R^2 values for goodness of fit of the model to the data falling within the range of 0.85 – 0.91 (Table 2). Given the level of uncertainty in the experimental source data values, this level of fit has exceeded expectations. The injury model, by graphical observation and by numerical evaluation, demonstrates the ability to follow a complex multivariable phenomenon. Striving for a more accurate modeling match is not warranted at the current time due to the sparseness and uncertainty in the experimental data. The model captures an overall impression of a rich physiological process involving injury formation under a complex load.

The spatial distribution of injury formation is related to the pressure load and temperature, plus the susceptibility the different tissue types to stress. Under high-pressure loads, PU's are likely to form in the deeper tissue of the muscle, whereas for low loads, the superficial layers of tissue are more susceptible to injury. Temperature can act as either retardant or accelerant for the onset of injury within a range centered about the the normal physiological state (about 34-37°C). At lower temperatures, thermal effects are progressively prophylactic to pressure induced injury. Above the threshold for thermal denaturation (about 43°C) [6,7,21–24], low grade burns occur in addition to pressure damage. One of the prime messages from the Iaizzo study is that temperature actively modulates pressure injury [cite]. This behavior is not surprising since the development of pressure injury is dominated by rate dependent processes that are temperature sensitive.

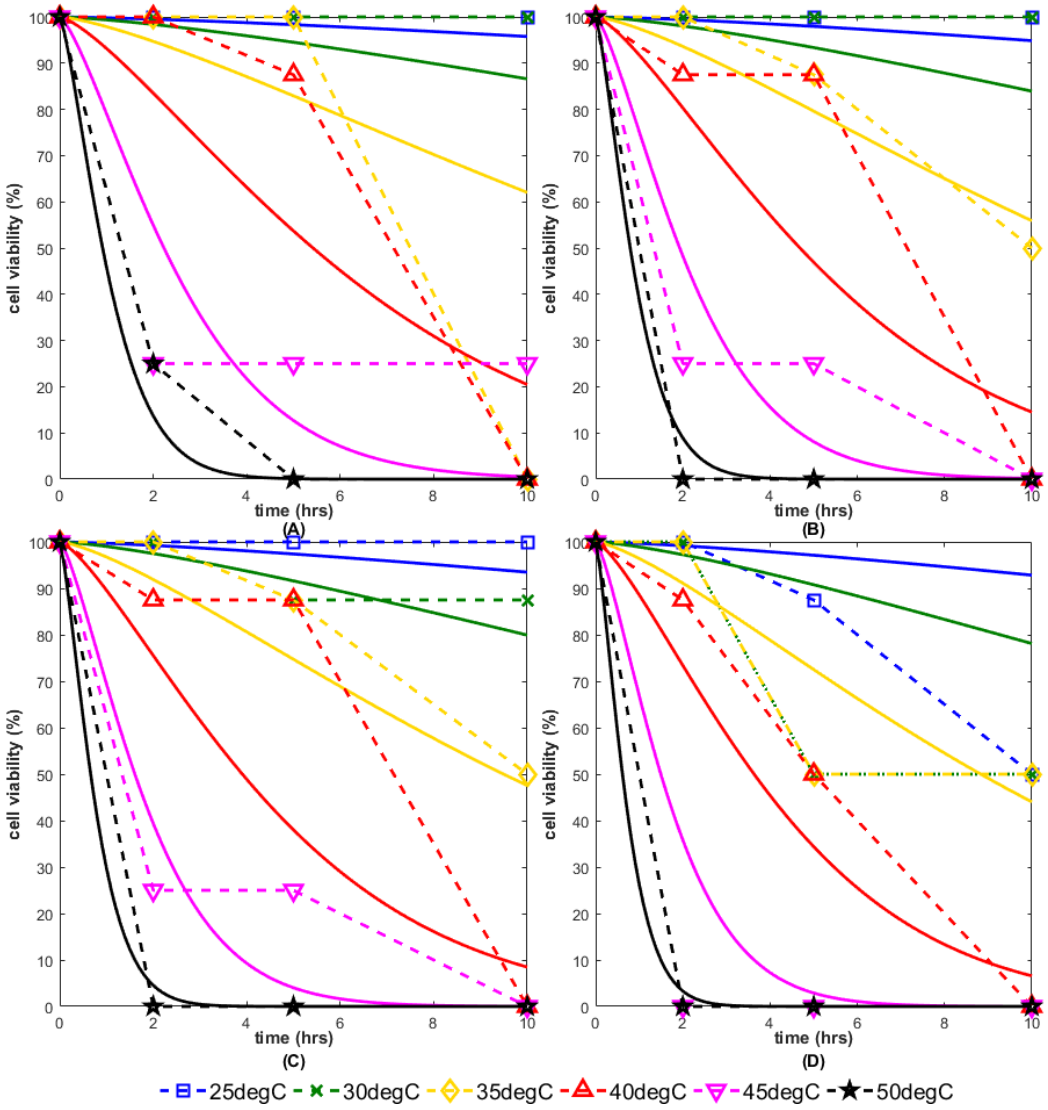

Fig. 2.3. Epidermis injury model fit to the experimental data from publication [9]. Solid lines denote the model predictions, while the dotted lines are a linear interpolation of the experimental data. Panels A, B, C, and D correspond to loads of 10, 50, 100, and 150 mmHg, respectively.

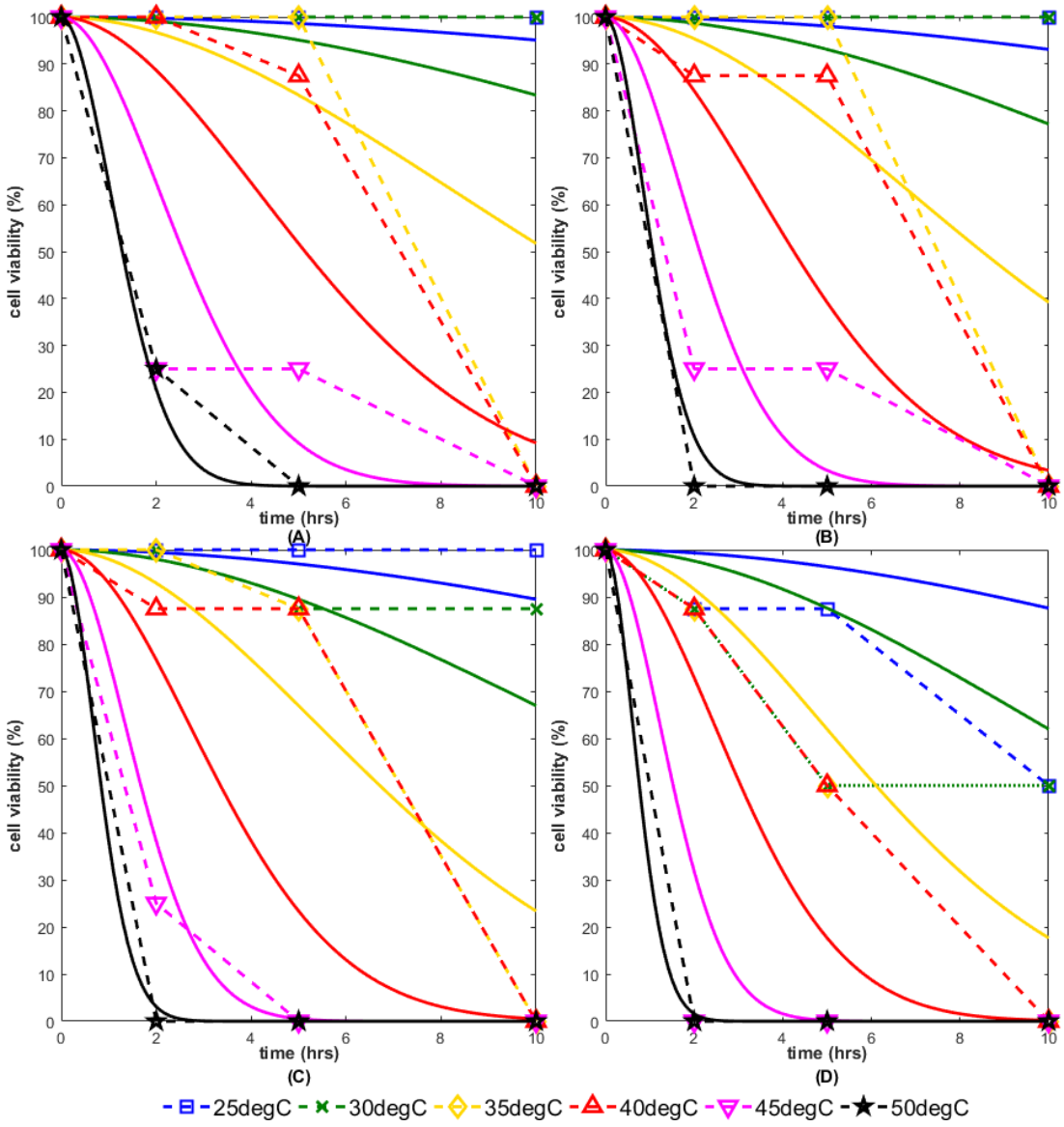

Fig. 2.4. Dermis injury model fit to the experimental data from publication [9]. Solid lines denote the model predictions, while the dotted lines are a linear interpolation of the experimental data. Panels A, B, C, and D correspond to loads of 10, 50, 100, and 150 mmHg, respectively.

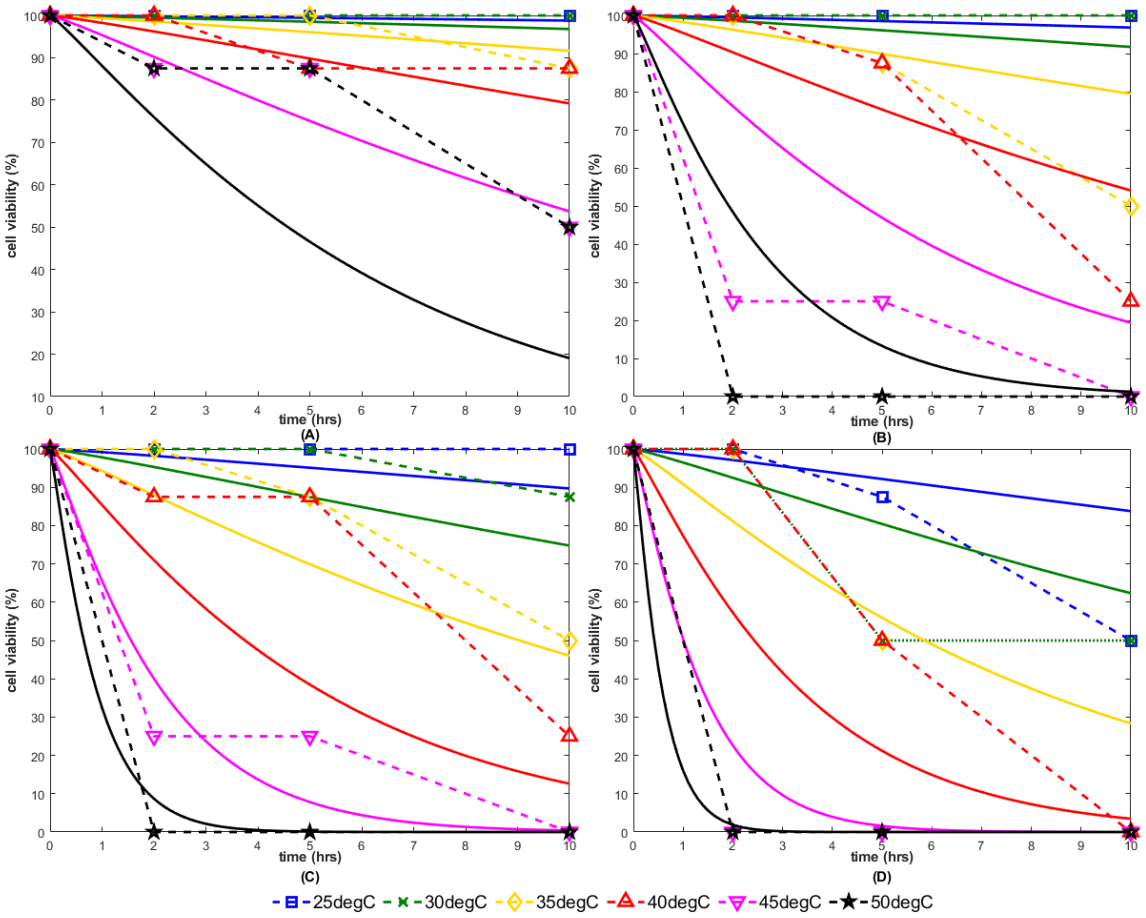

Fig. 2.5. Fat injury model fit to the experimental data from publication [9]. Solid lines denote the model predictions, while the dotted lines are a linear interpolation of the experimental data. Panels A, B, C, and D correspond to loads of 10, 50, 100, and 150 mmHg, respectively.

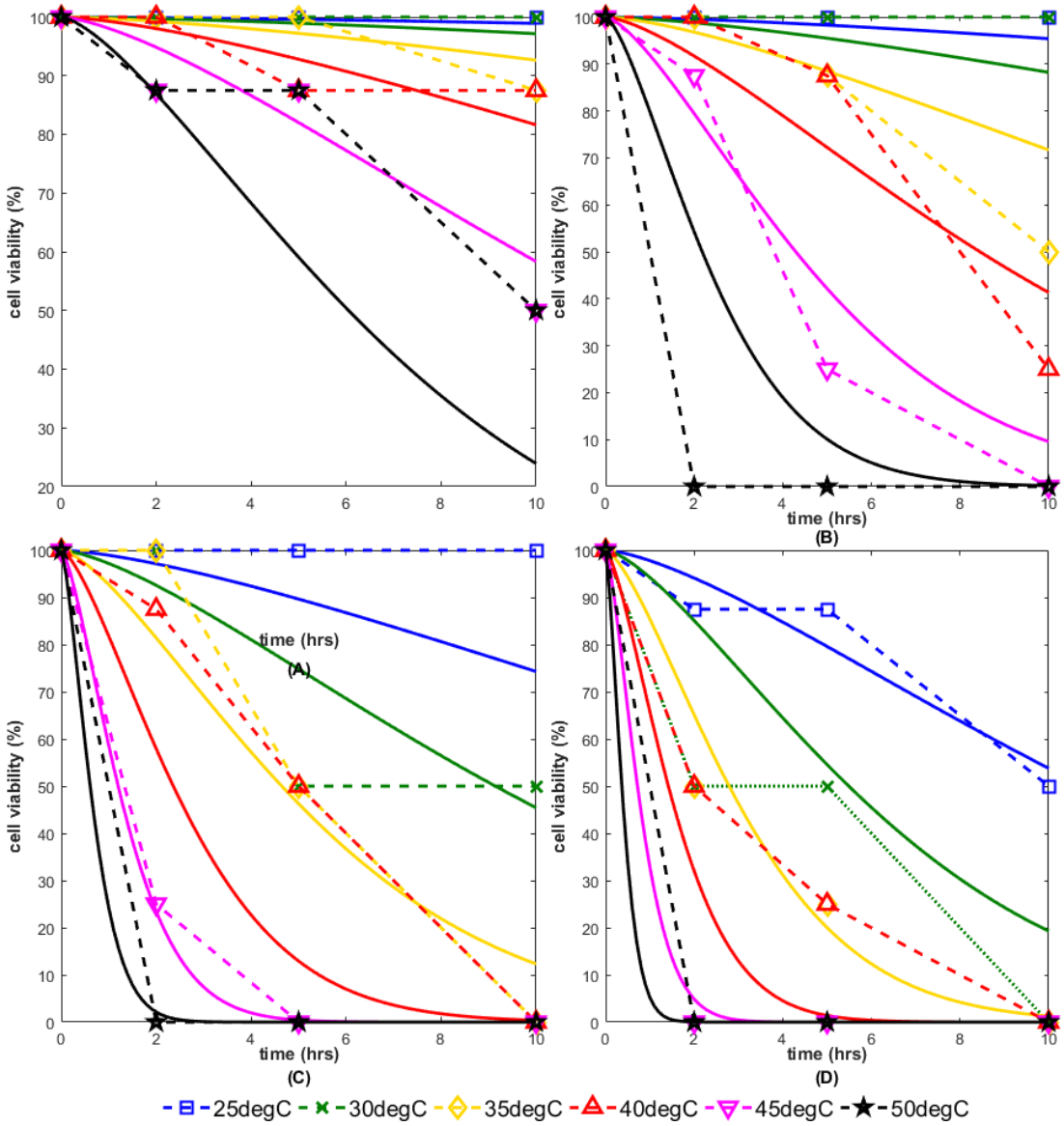

Fig. 2.6. Muscle injury model fit to the experimental data from publication [9]. Solid lines denote the model predictions, while the dotted lines are a linear interpolation of the experimental data. Panels A, B, C, and D correspond to loads of 10, 50, 100, and 150 mmHg, respectively.

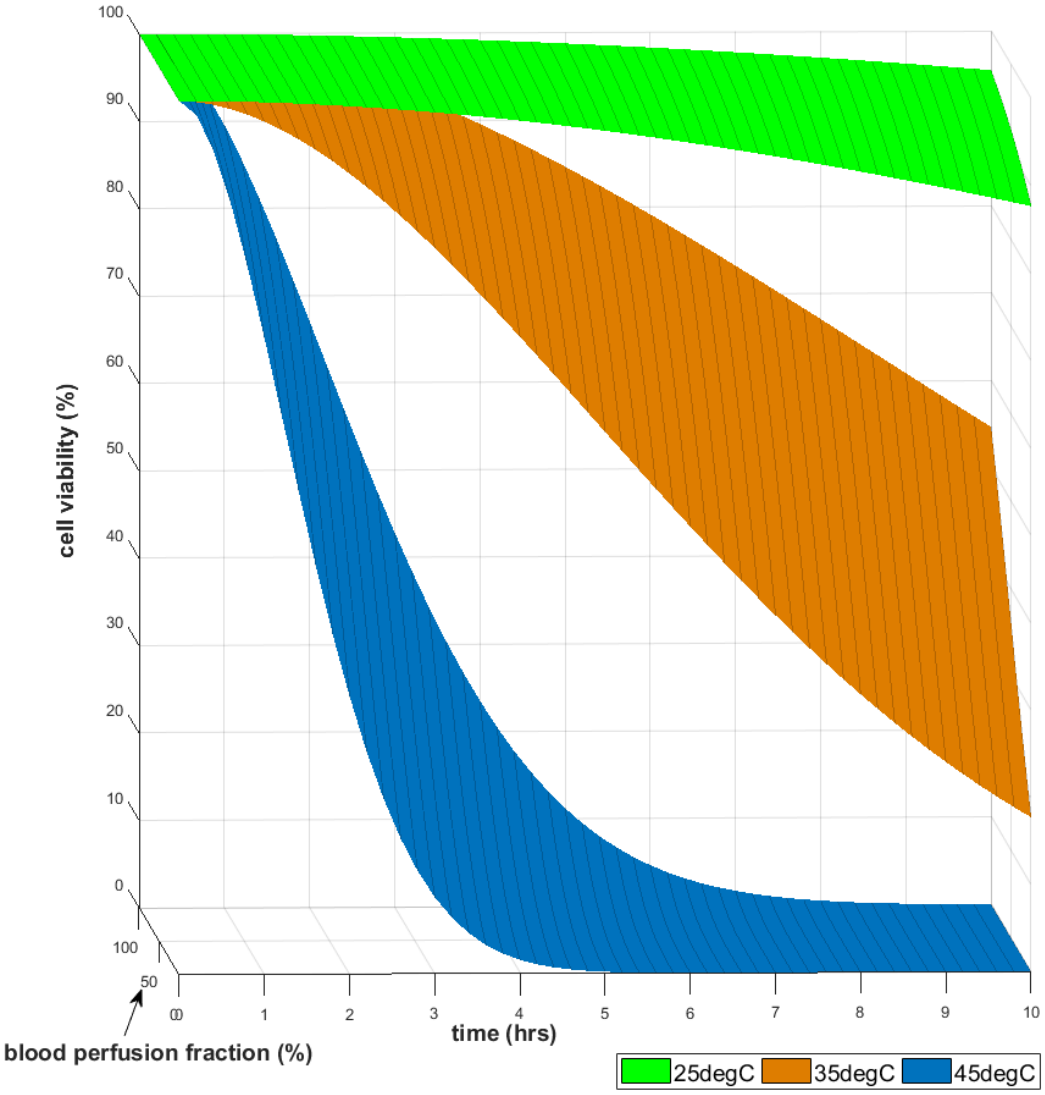

Fig. 2.7. The effect of surface pressure and time on cell viability for constant surface temperature response at the specified temperature. The isothermal surfaces in this figure are modeled from Eq. 9.

Fig. 8 illustrates that the simultaneous development of injury in the epidermis, dermis, fat, and muscle for imposed boundary conditions of 100 mmHg and 40°C. Interestingly, for these combined intermediate levels of thermal and pressure stress, the

injury at all four tissue depths develops at approximately the same rate. This outcome is influenced by the assumption that temperature and stress are uniform across all tissue domains which will dampen natural gradients that develop with increasing depth.

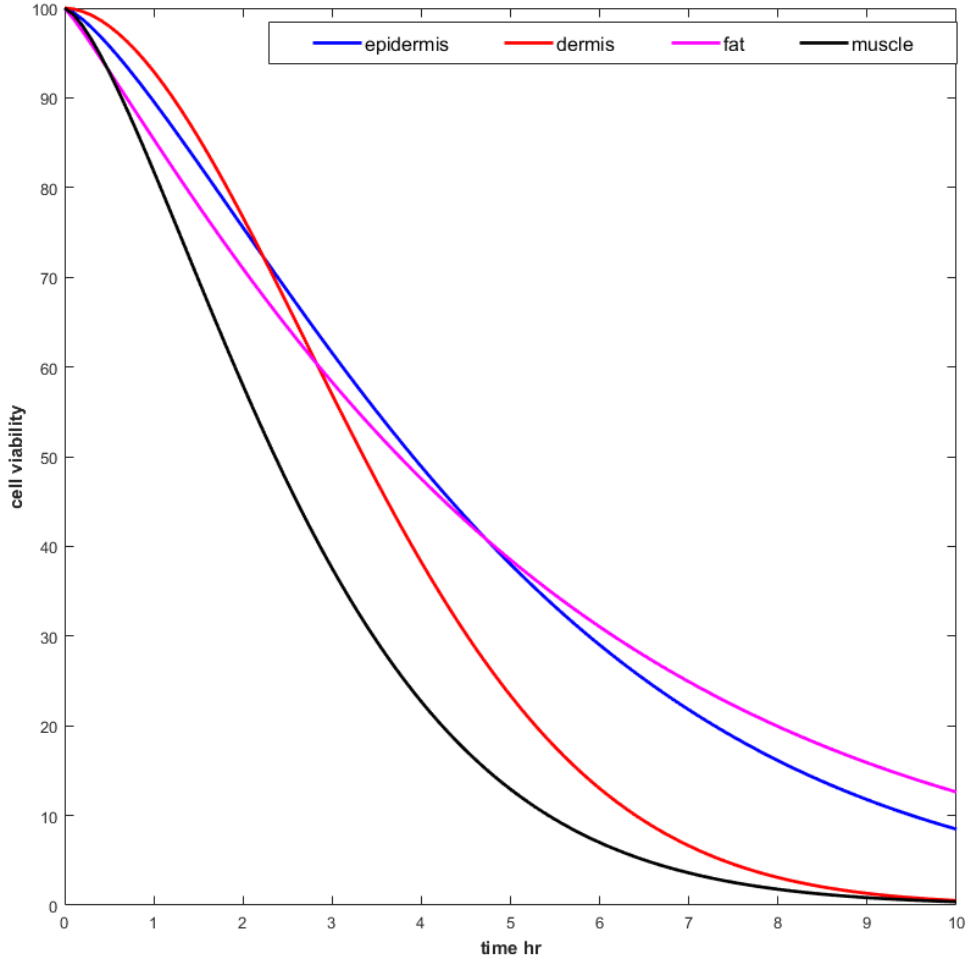

Fig. 2.8. Comparing cell viability of tissue layers verses time at constant temperature and pressure of 40°C and 100 mmHg. At this particular combination of temperature and pressure, the likely result of an injury related to tissue depth is relatively equal.

Fig. 9 shows the bivariate marginal likelihood functions for every possible pair of coefficients and reveals that each model coefficient plays a distinct role in describing the viability. This is demonstrated by the fact that the contours of the likelihood functions are mostly ellipsoidal, with major and minor axes that are approximately aligned with the axes

of the coefficient space. In other words, the probable true values for each coefficient do not depend highly on the values of other coefficients. The one possible exception is the covariance between the exponent coefficient k and the temperature coefficient β_T (note the uniquely diagonal shape of the likely regime, which indicates that the roles of these two coefficients are partly redundant in the model, from an error minimization perspective). Fig. 10 shows the corresponding univariate likelihood functions for each coefficient, thus demonstrating the overall uncertainty in the optimal coefficient estimates. Note that from a Bayesian perspective, the likelihood function is directly proportional to the posterior probability distribution of the coefficient set, under the assumption of a non-informative (i.e., uniform in $\mathbb{R}^4$) prior distribution.

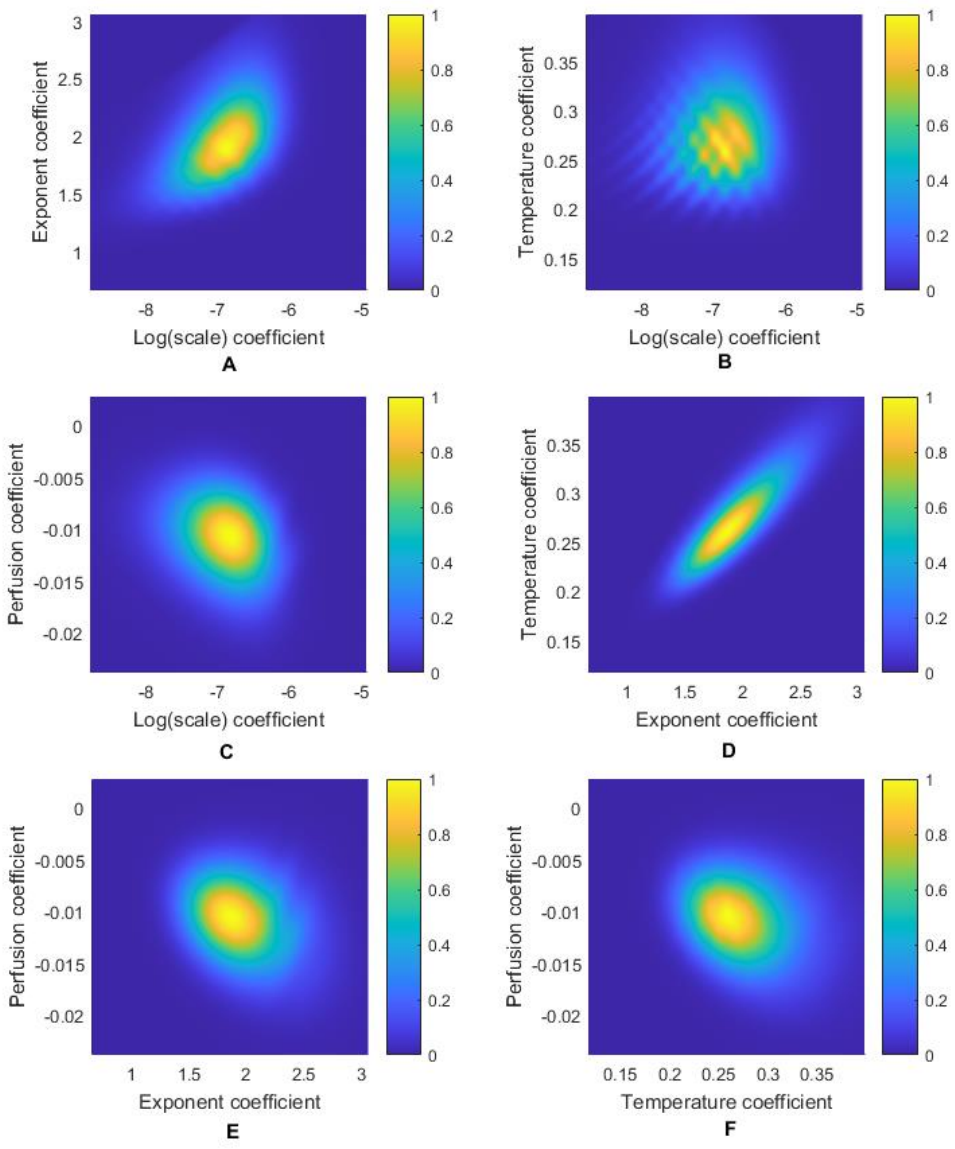

Fig. 2.9. Bivariate marginal likelihood functions for every possible pair of coefficients, shown here for epidermis as an example. Note that, with the exception of (D), the contours of the likelihood functions are mostly ellipsoidal, with major and minor axes that are approximately aligned with the axes of the coefficient space. In other words, the probable "true" values for each coefficient do not depend highly on the values of other coefficients. This result demonstrates how each model coefficient plays a distinct role in describing the time-dependent viability.

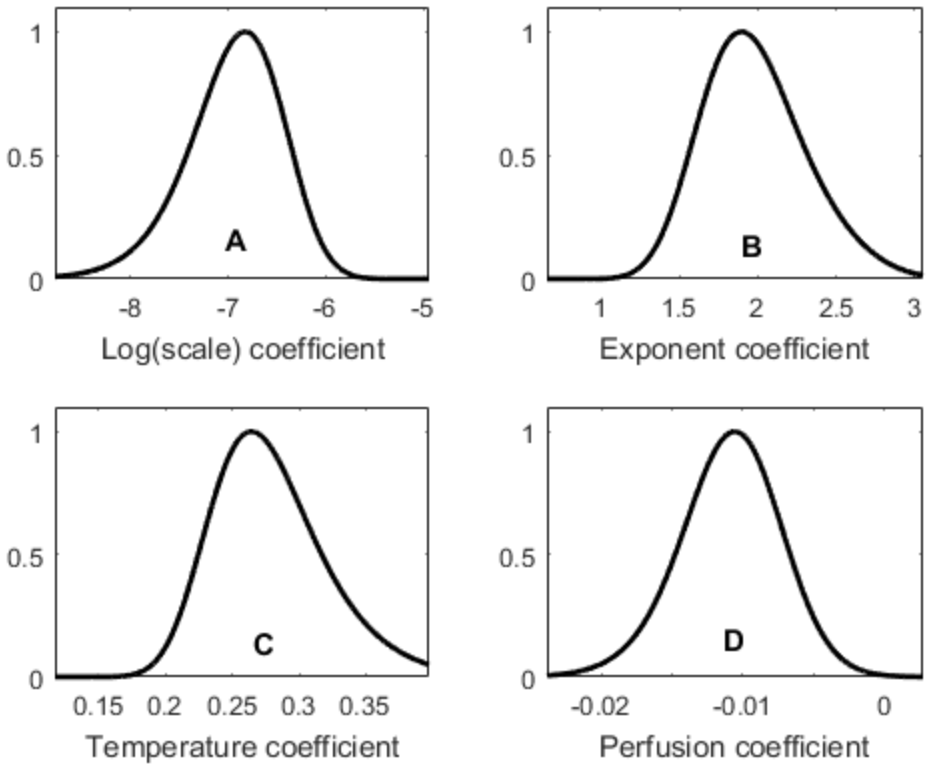

Fig. 2.10. Univariate marginal likelihood functions for every model coefficient, normalized by their maximum value, shown here for epidermis as an example. Note that from a Bayesian perspective, the likelihood function is directly proportional to the posterior probability distribution of the coefficient set, under the assumption of a non-informative (i.e. uniform in $\mathbb{R}^{\mathbf{4}}$) prior distribution. These results illustrate that the true value of each coefficient has an associated uncertainty (as is always the case in model fitting), but that the probability density is concentrated around a most likely value, with mild skewness and excess kurtosis.

DISCUSSION

Performance and broader context of the model.

The R^2 value for model prediction and experimental data for all tissue types is displayed in Table 2, along with the optimized values for the model coefficients and their corresponding posterior standard deviations. The predicted damage compared to the

experimental data shows a close match from start to finish of the testing protocol across the many cases evaluated (Figs. 3-6). Moreover, coefficient likelihood analysis suggests that the optimal model coefficients lie within an identifiable and mildly covariant regime (Figs. 9 and 10). In addition to quantifying uncertainty in the model coefficients, the likelihood analysis provides valuable information about the relative roles of the model coefficients. Interestingly, the bivariate marginal likelihood of the exponent coefficient k and the temperature coefficient β_T revealed moderate but notable positive correlation between these coefficients (Fig. 9D); this suggests that the two coefficients affect the model response (i.e., predicted viability) in similar ways. Importantly, in small or noisy data sets, model coefficients that correlate are generally harder to identify, since their roles in decreasing the error of the fit are partly redundant—taking an extreme example to illustrate this concept, if linearly related data (X, Y) were modeled using $y = abx + c$, the coefficients a and b, which are linearly dependent and thus exactly redundant, would be completely unidentifiable (although their product ab would be identifiable). Likelihood analysis and subsequent inspection of coefficient correlations, as we have performed herein, can thus be of critical importance to ensure the credibility of reported coefficient values. In the present study, the coefficient correlations were not sufficient to severely impact the identifiability of k and β_T, which both have standard errors < 20% of their optimal value for all tissue depths (Fig. 10; Table 2). Together, these results demonstrate that our proposed modeling approach can capture the diverse time progressions of viability across a wide array of applied temperatures and pressures, and for a variety of tissue depths, with

high fidelity and relatively low coefficient uncertainties. Our work thus provides an important extension upon the seminal work by Iaizzo et al. [8–11].

The swine model experiment of Iaizzo was designed to investigate the temperature modulation of PUs. Thus, their experiments were intended to show the extent of soft tissue damage as a function of defined combinations of pressure and temperature loading applied against an underlying skeletal structure straddling the flanks. The physiological outcome was assessed with low spatial and temporal resolution and quantified in terms of a simple damage score of zero, one, or two. This is a coarse damage scale that provides only minimal information regarding gradation in the progressive development of injury in the four-layered tissue model. However, it would have been prohibitively expensive and challenging to dedicate a sufficient number of animals, experimenter time, and project expense to provide a more complete data set, as well as ethical considerations in using so many animals. The trials that were run represent a tremendous commitment to this investigation, as is. Thus, for this subsequent modeling study based on the experimental data, an objective has been to derive as much useful information as possible from a sparse data matrix to inform the understanding of thermally modulated pressure ulcer formation.

The damage score was determined by a histologist who evaluated the biopsy tissue while blinded to individual testing parameters and assigning a graded injury score with a resolution of 0, 1, or 2. The injury scores were then averaged across all similar experiments. This constraint on injury resolution limits the ability to derive model coefficient values by optimally fitting it to the data. Burns are likewise ranked in severity with a coarse

macroscopic classification as first, second, and third-degree injuries with the same limitation.

Our lab has previously performed a microscopic scale analysis of thermal stress effects on populations of disaggregated cells, enabling injury to be evaluated as a continuous function of exposure temperature and time [26,31,32]. Subsequently, Pearce has fit a hybrid Arrhenius Time Delay thermal injury model to this data to obtain an elegantly matched description of the injury process progression, deriving unique model constitutive coefficients for specific cell types [18]. The Pearce model adds the time delay for relatively low temperature thermal insults that require a long exposure period for injury to accrue to account for the self-repair function of heat shock proteins (HSP)[33]. Fig. 11 shows measurements for cell viability and the Pearce model fit to the microscopic data for thermal injury. Viability was assessed for cell populations using supravital dyes as determined by microscopic examination. Thus, the resolution for determining the extent of injury caused by exposure to specific thermal stress was able to be finer than for the data derived from the Iaizzo study, as seen in the continuity of response curves in the data plots. To our knowledge, there is not similar resolution microscopic scale data for mechanical injury available that could be adopted for the current model of coupled temperature and pressure insult. Thus, our injury model coefficients were determined by optimized fitting only to the available macroscopic data set using state-of-the-art numerical optimization methods.

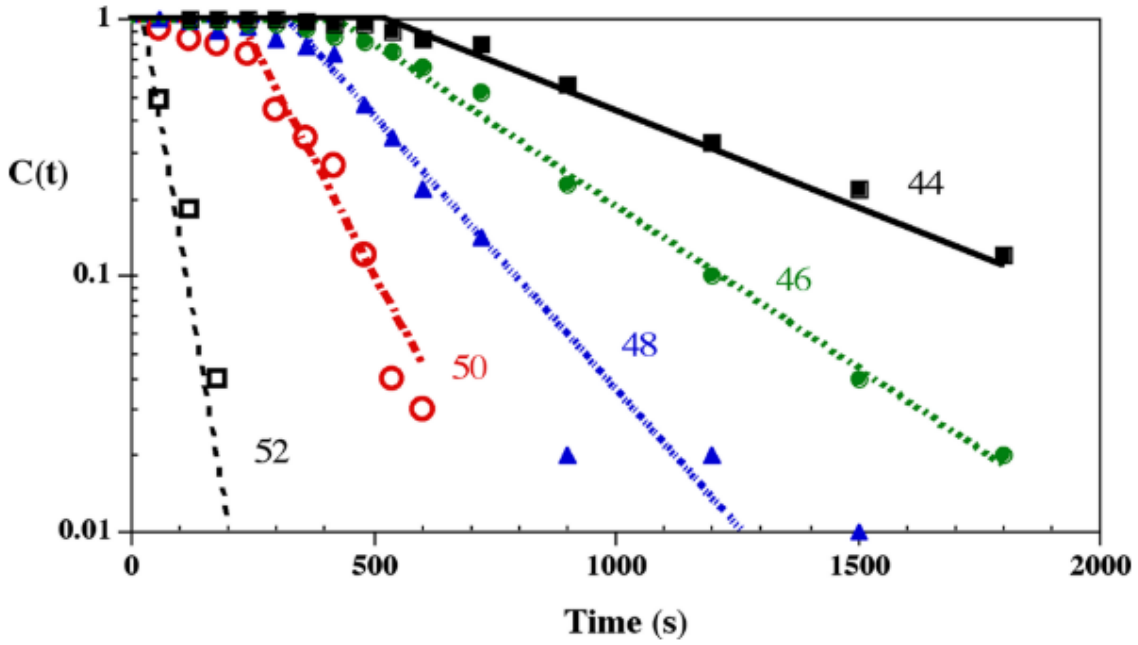

Fig. 2.11. Replication of Pearce's time delayed Arrhenius equation for thermal injuries. Note that C(t) is plotted on a logarithmic scale.

The starting hypothesis for this study was that cell viability associated with PU formation would follow a similar mathematical trend as do pure thermal injuries. However, the ability to compare the model with the source data to evaluated goodness of fit is compromised by the limited resolution in viability (injury). For example, some of the data indicates that at 10 hours, cell viability is 50% (Iaizzo damage score of 1), but the actual value may have been considerably higher or lower without discrimination. The conversion process from damage score to estimate cell viability has a large factor of uncertainty, but this effect has been accommodated in the model fitting process.

By performing simple comparisons of Pearce's modified Arrhenius equation that includes an added time delay with literature papers on burns, the current model does not

predict burns accurately based only on the Iaizzo et al. data set. This is most likely associated with either uncertainty in recorded experiment data, translation of data to the format used in this analysis, shortcomings due to assumptions in the model, or missing data points. The authors take responsibility for limitations of the current analysis and are in no way implying deficiencies with the original data set.

The model underpredicts cell damage at higher temperatures in comparison with the experimental data. The assumption of isothermal and isobaric conditions in the tissue that match the surface boundary values are particularly compromised for fat and muscle which are deeper within the system and less rigorously governed by the imposed temperature and pressure loads.

The original experimental data sets had incomplete coverage of the conditions needed for burn injury simulations. First, there is no data for thermal loads and zero pressure, which is how most burns occur. Second, there are not sufficient data points for short times that are usually most critical for burn injury causation to capture the cell damage process accurately. Thermal damage to cells can happen within seconds or minutes, depending on the temperature and cell type (compare the time scale in Fig. 11, which is less than 30 minutes total, to the time resolution of the Iaizzo data, which is several hours) [6,17,18]. As shown in Fig. 11, the Pearce time-delay model for PC3 prostate cancer cells predicts about 2% cell viability after half an hour exposure at 45°C. In contrast, the smallest time sample in the Iaizzo data is at two hours of constant temperature/pressure application.

For higher temperatures, shorter times become more important for capturing the physical progression of PU and burn causation. Given the accelerated rate of injury at

elevated temperatures, the time resolution of two hours is insufficient to observe the occurrence of injury. To illustrate, 0% cell viability might occur in 15 minutes at 50°C and in 60 mins at 45°C, but both are recorded as 0% cell viability only after two hours with no sense of differentiation between the two very different insult conditions. To further validate our model against direct measurements of cell viability over this crucial initial time span, we fit the model to the shorter time data from Rylander's PC3 cell viability study, which had much greater time resolution compared to the main porcine data set [26,31,32]. Fitting of the data points from this paper yielded an improved R^2 value of 0.95 (Fig. 12). Thus, with better time-resolved data, the current model can simulate thermal injuries.

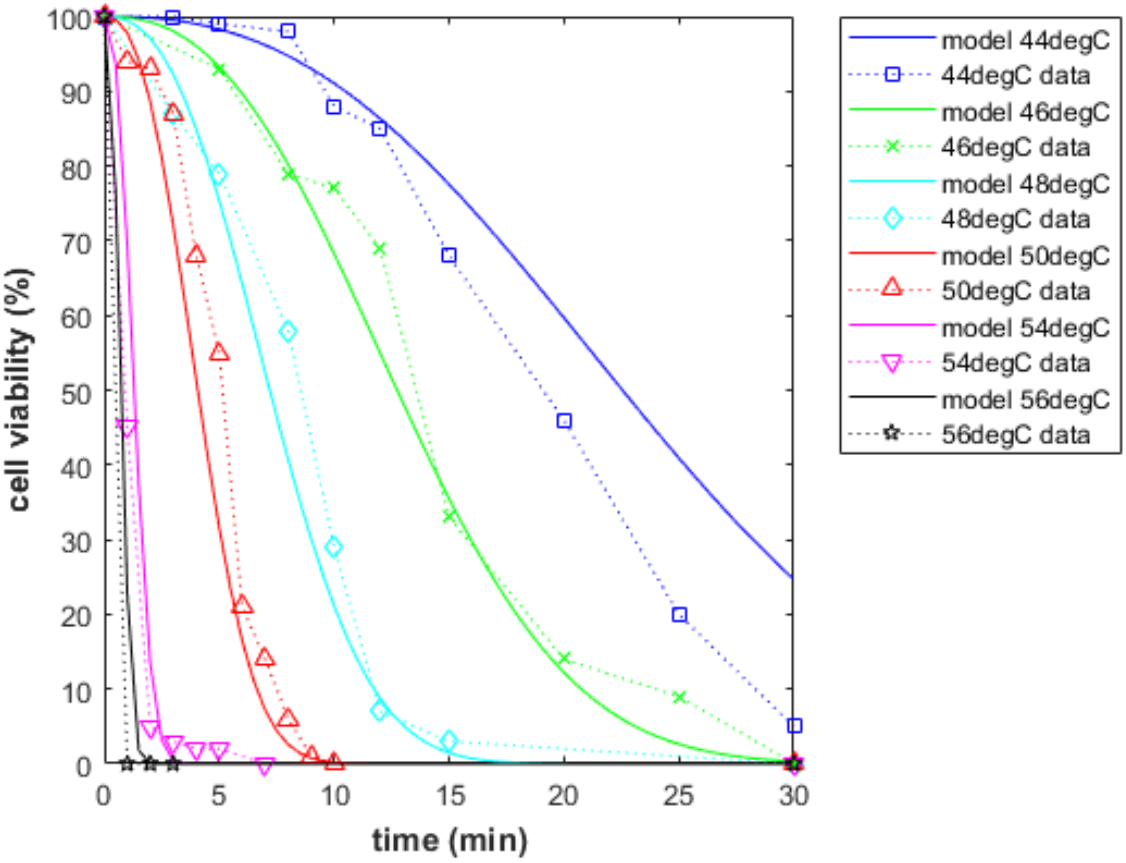

Fig. 2.12. Validation of the injury model against viability data for PC3 cells under thermal injury (data previously reported by Pearce [ref], and modeled using a time-delayed Arrhenius equation). The regression achieved $R^2 = 0.95$, demonstrating that the proposed model can be used to effectively model thermal injury.

Interpreting the Model Coefficients.

The constitutive coefficients for the injury model equation are defined in Eq (7) and reported in Table 2 after being identified in the optimization routine. Given that this set of optimized values result in a good fit of the model to the data, it is important to consider what the physiological interpretation is for these coefficients. However, there is not

currently an explicit physiological interpretation for the coefficients λ^*, k, β_T, β_ω. Although the coefficients currently do not have a physiological explanation, they do have a mathematical representation in terms of the shape of the model. The coefficient λ represents the overall scale of the injury development curve. The coefficient k defines the shape of the curve. The coefficients β_T and β_ω weigh the effects that temperature and blood perfusion have on injury development.

Our initial intention was to avoid using a numerical black-box approach to develop a model that fit the available experimental data. The 3D shape of the model was inspired by the physical data, and mathematical techniques used to describe such curves are not coincidental. The injury model is tissue-specific and is intended to be implemented within a 2D or 3D finite element analysis (FEA), wherein spatial and temporal variances, biological properties, and inflammation are the key governing parameters.

Deformation/Perfusion term.

Gefen has provided elegant insights into the etiology of PU development[4,5,14], and this view of the injury process has had a strong influence on our work. Our initial modeling efforts were focused on correlating the PU occurrence solely with ischemia, and in the model presented in this paper, the physical loading on the tissue is expressed in terms of blood perfusion. In actuality, the initial precipitating factor is macroscopic deformation of tissue that translates to microscopic stress at the cellular level, followed by inflammation, and eventually leading to ischemia. Collectively, these serial events constitute a complex etiology leading to the manifestation of PUs. Although ischemia is an important factor in PU formation, it is not the leading component. However, the entire

process sequence is more sophisticated and complex than can be accommodated in this current model. Thus, our analysis is represented with mechanical loading simply translated to a diminution in blood flow, but in the absence of adequate attention given to the initial degree of mechanical deformation. It is also important to realize that when mechanical loading is applied to soft tissue, there will be differing time constants for injury processes associated with cell deformation, inflammation, and ischemia, with each stage having a progressively longer time constant. Gefen has described this total process in detail [4,34], which is beyond the scope of the present analysis. In the present study, the mechanical loading effects are described only in terms of a single phenomenon, ischemia. However, this model could be directly modified to include the time progression of mechanically induced events that lead to PU formation via the introduction of adequate constitutive data, properties and time constants.

The mechanical injury term in the model is a function of local loading (stress) that directly causes ischemia. Tissue deformation can be adjusted to include such more comprehensive insights to give the model added capability for representing the complex process of PU formation beyond being simply dependent on only a single state variable. The injury term has the flexibility to include the combined effects of both ischemia and local deformation or to be evaluated independently. One option not employed in the present study is to represent the loading term as a function of strain energy as related to the formation of pressure injuries, as shown in another publication [29]. The strain energy translates directly to the degree of tissue deformation from which initial damage and local blood could be derived [29].

Future Directions.

The intention in creating this model was to provide a platform to understand the interaction between combined pressure and thermal stress in causing soft tissue injuries. The model uniquely combines the cross-coupling among events in the mechanical, thermal, and fluid flow domains as translate to injury processes. Although we believe this model presents an important advance in addressing a complex physiological phenomenon, there remain many opportunities to build on it to gain further useful insights.

The porcine data from which the model was derived are unique but also sparse, particularly as relating to pure thermal injures, while providing valuable insights into the thermal modulation of PU occurrence. Further, in vivo animal experiments could be designed to fill gaps in the existing data, although they would require advanced expertise and be expensive to conduct. Alternatively, there has already been a sophisticated level of examination of PUs in rodents [35,36], from which data could be adopted for modeling purposes.

The current form for the loading (perfusion/deformation) term was dependent only on ischemia. Although the loading term is expressed in terms of perfusion, it is actually a function of local stress and strain. This format presents the possibility of testing different theories and experimental data for other mechanisms of injury prediction. The loading term has the capacity to be linear or nonlinear as a function of multiple physical factors, such as combinations of strain, stress, strain energy, and ischemia. Modifications can be added to describe specific biomolecular or mechanobiological processes.

The mathematical model for the injury process can be applied independently within the context of accounting for the internal gradients in temperature and pressure that occur commonly. But, due to the inherent complexity of the model and the nonlinearity of the tissue systems, the model must be solved via numerical means such as the FEA. We have performed this more complete analysis for other processes, see Fig. 13. Within the FEA simulation, physical and anatomical properties of tissue can be accounted for in the context of applied mechanical and thermal stresses and the coupled internal modification of blood flow.

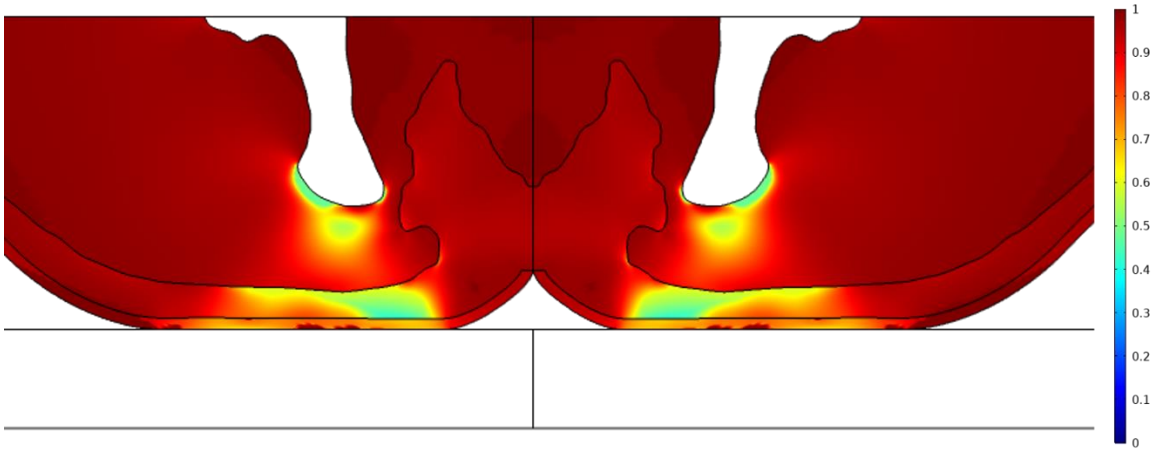

Fig. 2.13. The early stages of applying the injury model to a cross-section of an adult male's pelvis. The cross-section represents a man in a standard seated position on a hard chair that is heated to 50 °C, while wearing 1.5 mm of cotton clothing. Note the color scale from 1 to 0, with 1 indicating 100% cell viability and 0 indicating complete cellular necrosis. Any values below 0.5 would represent irreversible damage according to the model. At a temperature of 50°C, the skin is expected to be thermally damaged but there is deeper tissue damage under the ischial tuberosity from time under load. Areas where high stress and deformations such as near the sharp protrusions of the bones are the most likely areas a deep tissue pressure injury will form. Areas near the skin are strongly influenced by the temperature and loading time.

FEA software allows for a parametric approach with regard to model implementation. Under different physical conditions, variations of the model can be used to define cell damage. If tissue temperature and load are below a defined threshold, no damage is accrued. If the temperature is above 43°C thermal injury will dominate; thus, a different variation of the model is activated, similar to what is seen in Fig. 12. The simulation accounts for all damage types over the specified time domain and produces a

spatially varying map of cell viability (Fig. 13). Since the simulation parameters are time-dependent, the Eq. 8 variation of the model is used.

The best use of the current form of the model is not for patient-specific prediction of injury but for general understanding of injury processes. Human anatomy is complex and highly variable from person to person. Accounting for specific variations associated with genetics, age, disease, etc., it is unrealistic to develop a model that can accommodate all behaviors across a population. Instead, it is better to use a range of physiological conditions and anatomy and show the causes and effects for specific scenarios.

This model is able to address well many scenarios of interest in PU occurrence. The adaptability built into the model structure makes it well-suited for diverse applications as they are encountered.

SUMMARY

The pressure and thermal injury model presented in this paper simulates cell viability as a function of local soft tissue deformation/ischemia, applied surface temperature, and time. The combination of applied temperature and physical loading was used in a nonlinear multi-physics model to predict the time-dependent development of injury in soft tissue composed of multiple layers with unique properties. The constitutive coefficients of the model were determined by fitting to a unique set of porcine experimental data for the development of PUs under prescribed conditions of temperature and pressure loading, resulting in an optimal set of model coefficients. FEA was used to solve the model equations and make a prediction of injury under defined conditions of stress. The model

provides an enhanced understanding of the relative roles of thermal and pressure insults in soft tissue injury formation and progression.

The current form of the model is effective in predicting injury formation under complex loading conditions. A unique aspect of the model is that it extends continuously across the insult domains typically attributed individually to pressure injury and thermal injury. 44°C is the traditional threshold above which thermal injury is distinguished, and typical burn injury models have been invoked only for processes above this threshold. However, the porcine data of Iaizzo has demonstrated that applied pressure and temperature act in concert both above and below 43°C and that a continuous spectrum of injury conditions exists. The present model uniquely covers the entire mechanical and thermal loading domain from 10 to 150 mmHg and from 25 to 50°C, respectively. The model is extendable to cell damage outside of pressure injuries, as shown in Fig. 12 for pure thermal injury. This allows for alternative applications in investigations with additional damage parameters.

ACKNOWLEDGEMENTS

This was conducted with the generous support of the Robert and Prudie Leibrock Professorship in Engineering at the University of Texas at Austin. We thank the current Iaizzo lab for providing archival data from their original experiments, which was crucial in our effort to build and validate our injury model.

REFERENCES

[1] 2015, “The Agency for Healthcare Research and Quality’s (AHRQ)” [Online]. Available: https://www.ahrq.gov/topics/pressure-ulcers.html. [Accessed: 02-Apr-2020].

[2] 2017, “Centers for Disease Control and Prevention, National Center for Injury Prevention and Control. Web-Based Injury Statistics Query and Reporting System (WISQARS)” [Online]. Available: www.cdc.gov/injury/wisqars. [Accessed: 02-Apr-2020].

[3] NPUAP, 2016, “NPUAP Pressure Injury Stages,” NPUAP 2016 Staging Consens. Conf., pp. 1–2.

[4] Amit Gefen, 2018, “The Future of Pressure Ulcer Prevention Is Here: Detecting and Targeting Inflammation Early,” EWMA J., 19(2), pp. 7–13.

[5] Coleman, S., Nixon, J., Keen, J., Wilson, L., Mcginnis, E., Dealey, C., Stubbs, N., Farrin, A., Dowding, D., Schols, J. M. G. A., Cuddigan, J., Berlowitz, D., Jude, E., Vowden, P., Schoonhoven, L., Bader, D. L., Gefen, A., Oomens, C. W. J., and Nelson, E. A., 2014, “A New Pressure Ulcer Conceptual Framework,” J. Adv. Nurs., 70(10), pp. 2222–2234.

[6] Moritz, a. R., and Henriques, F. C., 1947, “STUDIES OF THERMAL INJURY II. The Relative Importance of Time and Surface Temperature in the Causation of Cutaneous Burns.,” Am J Pathol, 23, pp. 695–720.

[7] Moritz, A. R., 1947, “STUDIES OF THERMAL INJURY III. The Pathology and Pathogenesis of Cutaneous Burns An Experimental Study,” Am. J. Pathol., 13(6), pp. 915–941.

[8] Iaizzo, P. A., Kveen, G. L., Kokate, J. Y., Leland, K. J., Hansen, G. L., and Sparrow, 1995, “Prevention of Pressure Ulcers by Focal Cooling: Histological Assessment in a Porcine Model.,” Wounds A Compend. Clin. Res. Pract., 7(5), pp. 161–169.

[9] Kokate, J. Y., Leland, K. J., Sparrow, E. M., and Iaizzo, P. A., 1997, “Critical Thresholds for Pressure Ulcer Formation in a Porcine Model,” Wounds, 9(4), pp. 111–121.

[10] Hansen, G. L., Sparrow, E. M., Kokate, J. Y., Leland, K. J., and Iaizzo, P. A., 1997, “Wound Status Evaluation Using Color Image Processing,” IEEE Trans. Med. Imaging, 16(1), pp. 78–86.

[11] Kokate, J. Y., Leland, K. J., Held, a M., Hansen, G. L., Kveen, G. L., Johnson, B. a, Wilke, M. S., Sparrow, E. M., and Iaizzo, P. a, 1995, “Temperature-Modulated Pressure Ulcers: A Porcine Model.,” Arch. Phys. Med. Rehabil., 76(7), pp. 666–673.

[12] Zeevi, T., Levy, A., Brauner, N., and Gefen, A., 2018, “Effects of Ambient Conditions on the Risk of Pressure Injuries in Bedridden Patients—Multi-Physics Modelling of Microclimate,” Int. Wound J., 15(3), pp. 402–416.

[13] Schwartz, D., Magen, Y. K., Levy, A., and Gefen, A., 2018, “Effects of Humidity on Skin Friction against Medical Textiles as Related to Prevention of Pressure Injuries,” Int. Wound J., 15(6), pp. 866–874.

[14] Kottner, J., Black, J., Call, E., Gefen, A., and Santamaria, N., 2018, "Microclimate: A Critical Review in the Context of Pressure Ulcer Prevention," Clin. Biomech., 59(September), pp. 62–70.

[15] European Pressure Ulcer Advisory Panel, National Pressure Injury Advisory Panel, and Pan Pacific Pressure Injury Alliance, 2019, Prevention and Treatment of Pressure Ulcers/Injuries: Clinical Practice Guideline, The International Guideline.

[16] Gefen, A., Alves, P., Ciprandi, G., Coyer, F., Milne, C. T., Ousey, K., Ohura, N., Waters, N., and Worsley, P., 2020, "Device-Related Pressure Ulcers: SECURE Prevention," J. Wound Care, 29(Sup2b), pp. S1–S52.

[17] Pearce, J. A., 2013, "Comparative Analysis of Mathematical Models of Cell Death and Thermal Damage Processes," Int. J. Hyperth., 29(4), pp. 262–280.

[18] Pearce, J. A., 2015, "Improving Accuracy in Arrhenius Models of Cell Death: Adding a Temperature-Dependent Time Delay," J. Biomech. Eng., 137(12), pp. 1–7.

[19] Pearce, J. A., 2009, "Relationship between Arrhenius Models of Thermal Damage and the CEM 43 Thermal Dose," Energy-based Treat. Tissue Assess. V, 7181(February 2009), p. 718104.

[20] He, X., and Bischof, J. C., 2003, "Quantification of Temperature and Injury Response in Thermal Therapy and Cryosurgery," Crit. Rev. Biomed. Eng., 31(5–6), pp. 355–422.

[21] STOLL, A. M., and GREENE, L. C., 1959, "Relationship between Pain and Tissue Damage Due to Thermal Radiation," J. Appl. Physiol., 14(3), pp. 373–382.

[22] Henriques, F. C., 1947, “STUDIES OF THERMAL INJURY V. The Predictability and the Signinficance of Thermally Induced Rate Processes Leading to Irreverible Epidermal Injury,” 43(5), pp. 489–502.

[23] Moritz, A. R., Henriques, F. C., Durtra, F. R., and Weisiger, J. R., 1947, “STUDIES OF THERMAL INJURY IV. An Exploration of the Casualty-Producing Attributes of Conflagrations; Local and Systemic Effects of General Cutaneous Exposure to Excessive Circumambient (Air) and Circumradiant Heat of Varying Duration and Intensity,” Arch. Pathol., 43(5), pp. 466–488.

[24] Henriques, F. C., and Moritz, A. R., 1947, “STUDIES OF THERMAL INJURY I. The Conduction of Heat to and through Skin and the Temperatures Attained Therein. A Theoretical and an Experimental Investigation.,” Am. J. Pathol., 23(4), pp. 530–549.

[25] O’Neill, D. P., Peng, T., Stiegler, P., Mayrhauser, U., Koestenbauer, S., Tscheliessnigg, K., and Payne, S. J., 2011, “A Three-State Mathematical Model of Hyperthermic Cell Death,” Ann. Biomed. Eng., 39(1), pp. 570–579.

[26] Feng, Y., Oden, J. T., and Rylander, M. N., 2008, “A Two-State Cell Damage Model under Hyperthermic Conditions: Theory and in Vitro Experiments,” J. Biomech. Eng., 130(4), pp. 1–10.

[27] Xue, C., Friedman, A., and Sen, C. K., 2009, “A Mathematical Model of Ischemic Cutaneous Wounds,” Proc. Natl. Acad. Sci. U. S. A., 106(39), pp. 16782–16787.

[28] Linder-Ganz, E., and Gefen, A., 2009, “Stress Analyses Coupled with Damage Laws to Determine Biomechanical Risk Factors for Deep Tissue Injury during Sitting,” J. Biomech. Eng., 131(1), pp. 1–13.

[29] Friedman, R., Shabshin, N., Payan, Y., and Gefen, A., 2019, “Heel Ulcers: Investigating Injurious Tissue Load Thresholds in Humans, Based on a Patient-Specific Computational Heel Model,” Innovations and Emerging Technologies in Wound Care, pp. 123–139.

[30] Cox, D. R., 1972, “Regression Models and Life-Tables Authors (s): D . R . Cox Source : Journal of the Royal Statistical Society . Series B (Methodological), Vol . 34 , No . 2 Published by : Wiley for the Royal Statistical Society Stable URL : Http://Www.Jstor.Org/Stable,” J. R. Stat. Soc., 34(2), pp. 187–220.

[31] Rylander, M. N., Feng, Y., Zimmermann, K., and Diller, K. R., 2010, “Measurement and Mathematical Modeling of Thermally Induced Injury and Heat Shock Protein Expression Kinetics in Normal and Cancerous Prostate Cells,” Int. J. Hyperth., 26(8), pp. 748–764.

[32] Rylander, M. N., Diller, K. R., Wang, S., and Aggarwal, S. J., 2005, “Correlation of HSP70 Expression and Cell Viability Following Thermal Stimulation of Bovine Aortic Endothelial Cells,” J. Biomech. Eng., 127(5), pp. 751–757.

[33] Wang, S., Xie, W., Rylander, M. N., Tucker, P., Aggarwal, S. J., and Diller, K. R., 2008, “HSP70 Kinetics Study by Continuous Observation of HSP–GFP Fusion Protein Expression on a Perfusion Heating Stage,” Biotechnol. Bioeng., 99(1), pp. 146–154.

[34] Schwartz, D., and Gefen, A., 2020, “An Integrated Experimental-Computational Study of the Microclimate under Dressings Applied to Intact Weight-Bearing Skin,” Int. Wound J., (December 2019), pp. 1–16.

[35] Linder-Ganz, E., and Gefen, A., 2004, “Mechanical Compression-Induced Pressure Sores in Rat Hindlimb: Muscle Stiffness, Histology, and Computational Models,” J. Appl. Physiol., 96(6), pp. 2034–2049.

[36] Loerakker, S., Manders, E., Strijkers, G. J., Nicolay, K., Baaijens, F. P. T., Bader, D. L., and Oomens, C. W. J., 2011, “The Effects of Deformation, Ischemia, and Reperfusion on the Development of Muscle Damage during Prolonged Loading,” J. Appl. Physiol., 111(4), pp. 1168–1177.

Chapter 3: Tissue Temperature and Pressure Injury Model for Predicting and Designing Seat Heater Safety and Efficacy

The work contained in this chapter has been submitted to the Journal Dental Research for publication[3].

Gary McGregor contributed to design of numerical experiments, developing code, development of finite element simulation, conceptualizing the Multiphysics framework and inflammatory response, optimizing candidate treatment protocols, data analysis, plotting of results, and drafting the manuscript.

[3] This is a slightly modified version of the article submitted for publication to align with the dissertation format.

ABSTRACT

This paper presents a finite element simulation model for the coupled interaction between pressure and temperature in creating the potential for soft tissue injury to an individual while sitting on a heated vehicle seat. The analysis is an outgrowth from years of work on the SAE technical committee to establish the standard "Recommendation for Acceptable Operating Parameters of Heated Automobile Seats in Order to Mitigate Occupant Injury, J3047-2015-10-21". Fundamental principles of pressure ulcer formation and burn injury causation are explained, and the mechanisms of interaction between applied pressure and temperature to exacerbate the injury process above that commonly anticipated by their individual actions are clarified. The model is applied to replicate the development of mechanical stress distributed within soft tissue of the buttocks while seated and how this stress acts to retard the local perfusion of blood that can lead to ischemic injury. The model is also applied to replicate the progressive development of temperature within the buttocks in response to elevated temperature on the seat surface. A novel injury model has been created based on experimental data from the Iaizzo lab at the University of Minnesota to predict the occurrence of injury as a function of temperature, pressure, and duration of exposure. The model is in alignment with limited available human data, although purposeful injury experiments will never be conducted to provide benchmarks. Recommendations are made for designing seat heater operational protocols to provide more satisfying thermal comfort for occupants while ensuring safety from the combined action of elevated tissue pressure and temperature in causing soft tissue injuries.

INTRODUCTION

Car seat heating and cooling offers improved comfort for drivers and passengers for a broad range of environmental conditions. Typically, the seat surface is warmed or cooled by a regulated thermal element located in its interior. A properly functional system must exhibit efficacy to achieve a comfortable temperature range and to do so in a reasonably short time after it is activated. However, in the case of heating, it is important that the seat surface temperature not overshoot a threshold safe value to avoid the potential for causing a thermal injury to an occupant. Considerations for how to design of a seat heater to have an acceptable balance between both safety and efficacy is the subject of this paper.

Analysis of Burn Injury Causation

Vehicle seat heater efficacy and safety have been of direct interest to the SAE for many years, and they have published a series of standards, the most recent being issued in 2015 and updated multiple times thereafter [1]. The prime focus of this SAE standard is avoidance of thermal injury causation to seat occupants. Its recommendations are based primarily on pioneering studies conducted by Moritz and Henriques [2-4] and by Stoll [5-7] that measured in human subjects the level of injury caused by exposure of the skin surface for specific combinations of temperature and time or heat flux and time. These experimental results in human subjects have been verified repeatedly over the past 70 years and are considered to be highly reliable. Thus, it is appropriate that they are the basis for safety standards.

The studies of Moritz and Henriques (M&H) were focused primarily on the threshold exposure time and temperature conditions that produce first and second-degree burns. Subsequently, Lawrence and Bull extended the scope of injuries to include third degree burns [8, 9]. First, second, and third degree burns are progressively more severe and hold greater physiological consequences. However, it has been many years (decades) since burn experiments have been conducted on human subjects owing to ethical considerations, and in more recent times animal experimentation has also been greatly restricted. Tissue surrogates can be used in some instances, but it is challenging to replicate the thermal response characteristics of blood perfused skin and subcutaneous tissue. As an alternative, mathematical modeling of the burn process has been developed to an advanced state and is applied quite widely for many purposes including design of personal protective equipment [10-13], determination of the safe touch temperature for heated surfaces [14, 15], and reconstruction of thermal injury accidents [16-18]. Indeed, early on Henriques recognized the desirability of being able to predict thermal injury using mathematical tools and develop a first model for heat transfer into the skin in response to an elevated surface temperature coupled with an injury process based on Arrhenius rate process kinetics [2]. Buettner [19] and Stoll [5] soon adopted numerical methods to model the burn process in a complex tissue system.

Prior to the studies by M&H in the mid-1940's there had been little quantitative analysis of the physical and biological processes that govern burn injury. However, World War II introduced the weaponized delivery of targeted heat energy, motivating a concentrated effort to discover and describe how burns occur in response to

environment thermal factors and their duration. The (M&H) group at Harvard Medical School took the lead in this effort, resulting in the post-war publication of an extensive series of papers that serve as the foundation for our current quantitative understanding burn etiology. The M&H group conducted experiments on both swine and humans (mostly themselves), in addition to developing and fitting an analytical heat transfer and injury model to their data. This work directly supports the SAE seat heater standard [1].

M&H classified the measured levels of injury according to the standard discrimination of first, second, and third degree wounds. Unfortunately, they lumped second and third degree together in their data tables although, in the text the distinction was described. The consequence has been that frequently second and third degree burns have been considered in a common category, even frequently in the medical literature, although clinically there is a huge difference in these traumas.

Burns can be evaluated according to the clinical macroscopic presentation and, alternatively, according to microscopic criteria at the cell and molecular level that integrate to produce the macroscopic manifestation. These criteria have been very well summarized in the literature as, for example, in [20, 21]. Briefly, first degree burns are the most mild and do not result in lasting cell damage. Their effects are confined to the epidermis and consist of hyperemia and reddening, often with associated transient pain. M&H described a first degree burn in terms of reversible epidermal injury [2, 4]. The effects of a second-degree project deeper inward into the dermis, inducing inflammation and extravasation of fluid from the vasculature. The result is fluid accumulation and swelling with blisters. A second-degree burn may be superficial, just barely causing blister

formation. A deeper second-degree wound will penetrate through the entirely of the dermis, causing massive local swelling. The fact that fluid extravasation occurs means that there remains active perfusion within the dermis, providing good prospects for self-healing, although a deep injury may require weeks to heal and leave visible scaring. A second-degree injury is alternatively described as being partial thickness, with sub-categories of superficial and deep as a function of the depth to which thermal injury effects occur. M&H categorized the next most severe injury beyond first degree as resulting from the minimum exposure resulting in complete epidermal necrosis. Thus, this was the threshold criteria for just causing a second degree injury in which a blister began to manifest [2, 4].

A key point regarding a second-degree burn is that live tissue remains within the skin providing a ground for regeneration. In contrast, a third-degree burn occurs when thermal insult results in complete necrosis of the dermis, with an important consequence that there is no remaining active blood flow. This type of burn is also called full thickness and typically requires grafting for healing with hypertrophic scaring [21]. Given the very large difference in thickness of the epidermis (approximately 50 - 75mm) and the dermis (approximately 1 – 2mm), although these values vary widely with region on the body surface [22, 23], with age [24], with gender [22, 25], and among individuals [25], physiologically and medically there is a huge dichotomy between full epidermal necrosis and full dermal necrosis. These two should not be confused, but unfortunately, they are often misrepresented from the M&H database. This mistake has been pointed out clearly in the subsequent literature [26, 27], but regrettably the promulgation and adoption of this misinformation persists. In fact, vehicle seat heater injuries have become a prime

venue for promoting misinformation about how full thickness burn injuries occur, and it is important to understand the scientific truth concerning this issue as it relates to the design and operation of seat heaters.

Are Thermal Burns the Most Probable Cause of Injury When Using a Seat Heater?

One paper has developed a prominent position in spreading misinformation about seat heater injuries appeared in 2003 [28]. The M&H data for the criteria for the conditions for causing a threshold second degree burn are misrepresented as applying to third degree injuries. This paper has been cited repeatedly with incorrect information being applied to seat heater function [29-31]. An follow-up paper was written by the present author to the publishing journal to clarify the misrepresentation of the M&H data [27], to which the authors responded with a defensive rebuttal [32]. Nonetheless, this reference continues to be cited as an authoritative source [33, 34]. The question then begs – how can it be explained that so many experienced clinicians write that seat heaters have caused (in most cases) full thickness injuries to heated seat occupants?

Combined Effects of Pressure and Temperature in Injury Causation

Fortunately, there is a rational explanation based on a more comprehensive scientific analysis about how full thickness injuries can occur associated with use of vehicle seat heaters. The key added information is that when a person is sitting on a heated seat, the soft tissue of the buttock experiences both heating and pressure loading. Elevated temperature and elevated tissue interstitial pressure when acting alone may cause injury,

typically classified as a burn or a pressure ulcer [35-38], respectively. However, when temperature and pressure are applied simultaneously, there is a coupled additive effect that can produce injury under conditions for which it may not be expected. This scenario has been explored in an elegant and insightful experimental study conducted in the Iaizzo lab at the University of Minnesota [39-41], the outcome of which can be applied directly to explain how full thickness injuries can develop when seated on a heated surface. The objective of this paper is to apply a newly developed engineering modeling tool for simulating via finite element analysis the coupling effects of applied temperature and mechanical loading on soft tissue. Data from the Iaizzo study have been applied to derive kinetic coefficients for development of soft tissue injury under combined temperature and pressure stress. Simulations from the completed model are presented to illustrate its use for designing seat heater operation for achieve desirable levels of comfort and safety.

Analysis of Pressure Ucer Causation

A pressure injury (PI) defined by the National Pressure Injury Advisory Panel (NPIAP) is defined as " localized damage to the skin and underlining tissue, as a result of pressure or pressure in combination with shear" [42]. PI etiology is complex and has long been the subject of intense study [43, 44]. Ischemia is acknowledged to be a primary cause of PI, and more recent findings from Gefen show compounding effects of direct tissue deformation translated to the cellular level and the inflammatory response to trauma [43]. The Iaizzo studies present compelling evidence that temperature can modulate the kinetics of PI formation [40]. Elevated temperature enhances the rate and sensitivity to PI formation, and depressed temperatures are prophylactic [40, 41]. The fundamental idea

is that temperature regulates the cellular metabolic rate increasing its need for oxygen and nutrients while increase waste produces and CO_2. If blood flow is compromised to the tissue due to increased interstitial pressure caused by mechanical deformation, the thermally driven increase or decrease in metabolic need will significantly affect tissue survival. Plus, temperature affects many of the other PI related processes. Prior modeling of the PI injury for predictive purposes has been based primarily empirically derived approaches with no one method in consensus adoption.

Thermal and pressure injuries present an interesting contrast in their physical progression. PI are generally thought to originate internally proximally to bony protuberances such as the ischial tuberosity [35] where the interstitial stress and pressure are greatest [45]. Thus, PIs tend to grow from the inside out [35, 46]. In contrast, a seat heater applies its thermal input to the skin surface, resulting in an inward temperature gradient. The heat flow is into the tissue and if a burn occurs it will start from the outside of the tissue and be propagated inward. A complicating factor in the temperature / pressure coupling is that while the pressure is highest inwardly and the temperature is highest outwardly, temperature will enhance the rate of development of PI. Thus, if the temperature is higher in a region of lower tissue stress, the accrued PI may be greater that in a region of higher stress but lower temperature. The origin of such an outcome can be nonintuitive and lead to an interpretation / diagnosis of a thermally enhanced pressure ulcer as being a full thickness burn. This study is designed to identify and quantify how this scenario can occur. Elderly or people suffering from a spinal cord injury (wheelchair bound) are at

greater risk of developing a PI [47-50]. Being aware of this will help ensure proper design and customer/user awareness of possible risks.

The current paper presents a model for the combined effects of both temperature and pressure in injury causation for prediction of the safe design of equipment and devices. A separate publication covers the mathematical and conceptual development of the injury model [51]. The purpose of this paper is to present a practical method of applying the injury model to real-world system simulation to support the safe design of the seat's thermal system.

It is important to make a clear distinction between a model intended for a medical diagnosis of a specific patient with many personalized physiological and injury characteristics and a model for generalized understanding. A model used to make medical decisions about the best treatment for a patient requires specific information about that individual. A generalized model is for seeing if treatments or device design will improve or worsen based on a set of conditions. The present model has been developed and is presented from the latter perspective.

METHODS

Geometry and Mesh for Finite Element Model

The physiological system to be analyzed is illustrated by the cartoon shown in Fig. 1. The weight of the upper body is carried via the skeletal structure and is supported by a horizontal surface on which a person is seated. Soft tissues consisting primarily of muscle, fat, and skin are intermediate between the surface and the skeleton and are compressed between the skeleton and seat. As the soft tissue is compressed, mechanical

stresses will develop internally as a function of the supported weight, the anatomy of the skeleton / tissue interface, the seating posture, and characteristics of the seating surface. The skeleton features bony protuberances in the region of most intense support, these being the ischial tuberosities indicated in blue shading in Fig. 1.

The system of interest is the soft tissue. Key characteristics include the distribution of blood perfusion, the elastic properties, and the morphologies of all component tissues. Of particular interest is the fact that certain medical conditions can compromise the properties of the tissue overlying the IT, increasing the susceptibility to PI. Of primary interest is persons who are paraplegic and who historically have constituted a disproportionate population that experience soft tissue injuries when using a heated vehicle seat.

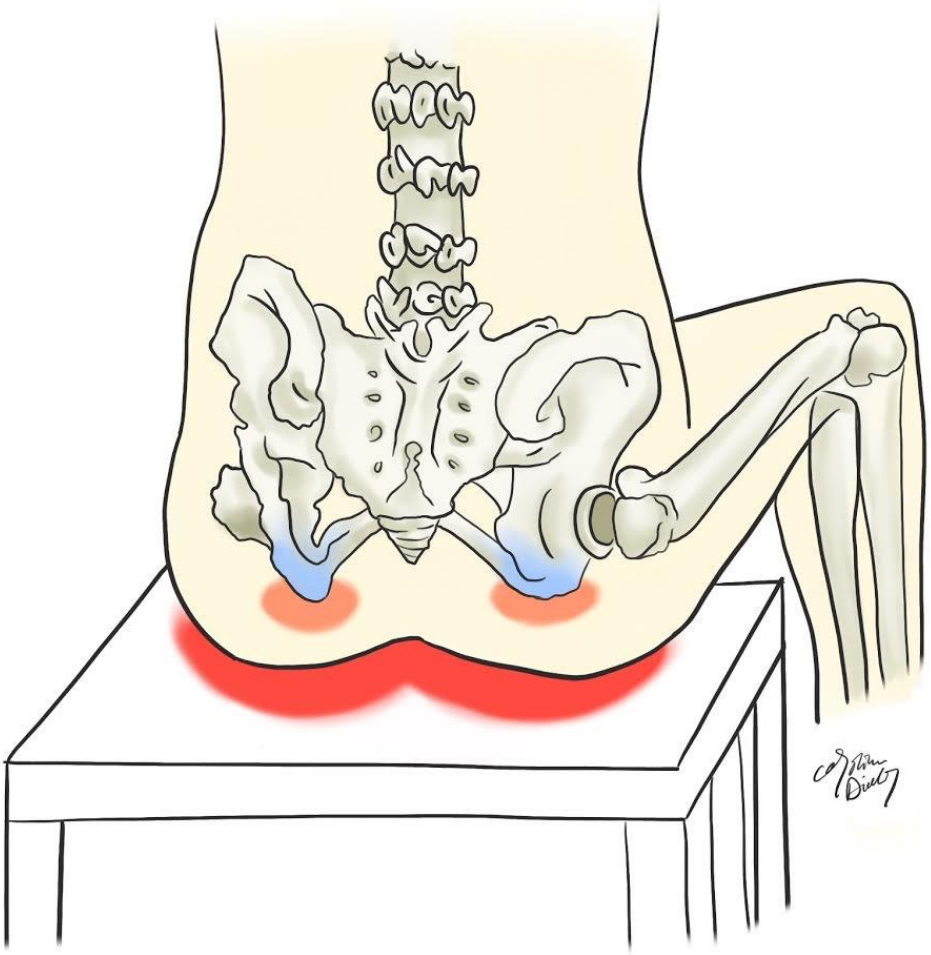

Figure 3.1. Cartoon of a person in the seated position. The upper body weight is carried in the skeletal structure and transferred for support via the Ischial tuberosities (IT) denoted in blue. Soft tissue underlying the IT distribute the weight load from the upper body while seated on a supporting surface, resulting in regions of high stress and internal pressure, as denoted in pink

Because of the composite nature and the complex three-dimensional geometry of the system, analysis of the stresses that develop in gluteal soft tissues when in the seated position is most efficaciously carried out vie finite element analysis (FEA). It is

necessary to define a geometric mesh to represent the physical system of interest. In this case, meshes have been built from original MRI data files for 2 male subjects obtained in a study and furnished by Brienza [49]. One subject served as a normal control, and the second had long-term spinal cord injuries (SI) and was wheelchair-bound. The original study provides a detailed description of how the images were collected [49].

To eventually evaluate the injury model using FEA, a 2D coronal cross-section in the loaded and unloaded conditions was selected to best represent a seated person. Loaded condition images were obtained with subjected seated on a test cushion. Unloaded images were taken with the subject supine with the hips and knees flexed at 90° and the calves supported in an elevated but horizontal position parallel to the back. The unloaded condition images were used as the basis for defining the system geometry as shown in Figs. 2A and 3A. The loaded condition images (Figs. 2B and 3B) were used for comparing the simulation results and adjusting model parameters. The MRI data can also be applied to develop a 3D model with appropriate interplane interpolation [49].

The MRI images were supplied digitally in dicom format by Professor Brienza [49] and were loaded into RadiAnt™ software to be measured, scaled, converted to jpeg files, and then processed with AutoDesk Inventor™ CAD software. Symmetry is assumed about a center vertical axis, so only one side of the images was analyzed. Tissues above the waist (upper aspect of the ischial tuberosity) were accounted for in the boundary conditions. The images were scaled in the XY plane, and segmented into individual tissue domains. The boundaries of the four tissue types of bone, fat, muscle, and skin were manually traced using 2D drawing tools. Figs. 4 and 5 show the areas of the images

occupied by the four tissues for the two subjects. The 2D drawings are converted to .dxf file format and loaded into COMSOL Multiphysics software [52] for FE meshing and modeling.

It should be noted that there are open source and commercial programs are available to convert diacom files to CAD compatible geometry, such as theScan-IP module of Simpleware® Ltd (Synopsis, Mountain View, CA). The method applied herein demonstrates directly building the geometry for a 2D image without requiring dedicated software. Drawbacks to this approach are that it depends on tedious manual input operations, and it is not adaptable for 3D geometry development.

An alternative to using original MRI data is to purchase prebuilt models which have undergone detailed validation. An example of this is Sim4Life® [53] which uses greatly detailed human models made from high-resolution MRI scans. They offer a library of human anatomical models covering a broad demographic of the population. The software allows the user to arrange the model in any variety of positions.

Figs. 2 and 3 show the digitized MRI images of the undeformed and deformed tissues for the non-SI and SI subjects, respectively. In plate A, a manually traced boundary is overlayed as a green line on the image at the outer edge of the skin, and the IT is presented in a solid green color. The most important region of interest (ROI) is the soft tissue between the ischial tuberosity (IT) and a seating surface (Fig. 1).

The digital MRI image data base was used to construct a vector from the bottom of the IT to the skin surface as shown by a lightweight green line in Figs. 2A and 3A. This vector provides a measure of the distance across the soft tissue in the ROI and

how much the tissue is compressed when a subject is seated, and it can be used as an imposed mechanical boundary condition.

Plate B in Figs. 2 and 3 shows MRI images after the subject was seated, thereby compressing the soft tissue underlaying the IT. It is important to note that the undeformed and deformed images were acquired when the subject was in different physical orientations, so there is no guarantee that these images represent the same anatomical cross section, limiting the ability to make accurate, direct comparisons of changes caused by sitting. The deformed images in Plate B or Figs. 2 and 3 also have a superimposed line along the bottom edge of the tissue. Unlike the green line in Plates

A, the red and yellow line in Plates B were generated from the computer simulation of deformation during sitting, as explained in the following section. The simulation was run with an imposed boundary condition of the extent of tissue compression of the soft tissue at ROI centered on the vector from the IT. Red indicates minimum deviation between the simulation and MRI data, and the transition to yellow shows progressively larger differences. The red and yellow lines is the soft tissue displacement predicted by the model. An important source of difference between the model and MRI displacements is that the model assumed a rigid planar seating surface, whereas the MRI image were obtained with the subjects seated on a deformable cushion. This difference is more apparent peripherally to the ROI. Nonetheless, there is very good match in extent of deformation centrally within the ROI.

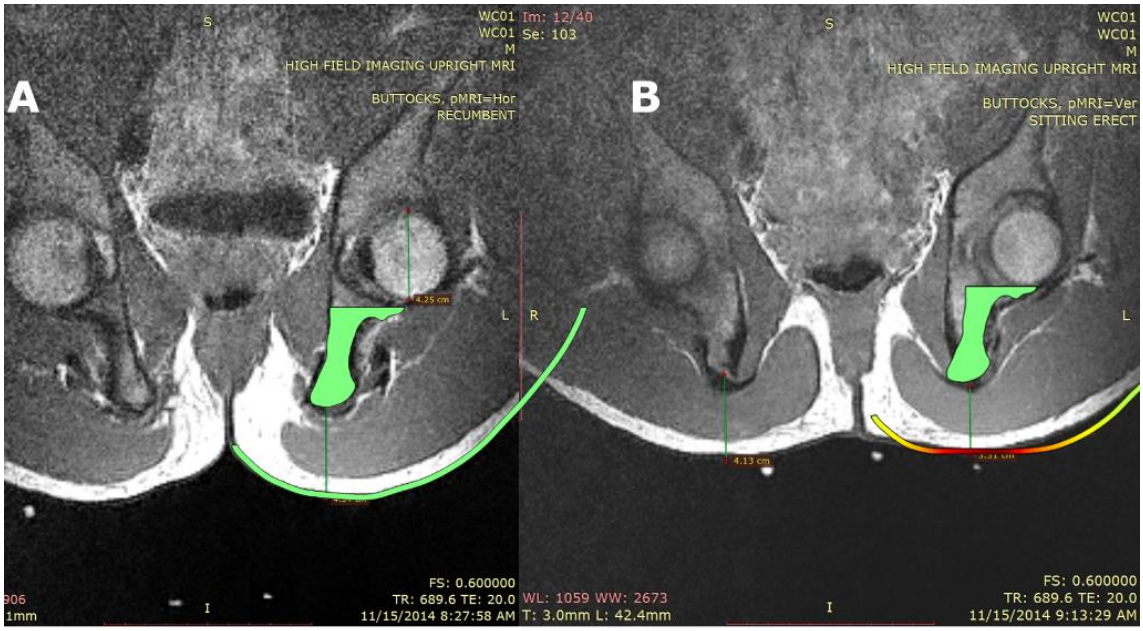

Figure 3.2. MRI imiages of non-SI subject. Plate A is undeformed prior to sitting. The green line was manually input at the surface of the skin. Plate B is deformed in a seated position. The red and yellow line was grnerated with the FEM simulation, showing the predicted deformation during sitting. Red indicated minimal difference between model and MRI image, transitioning progressively to yellow for larger differences.

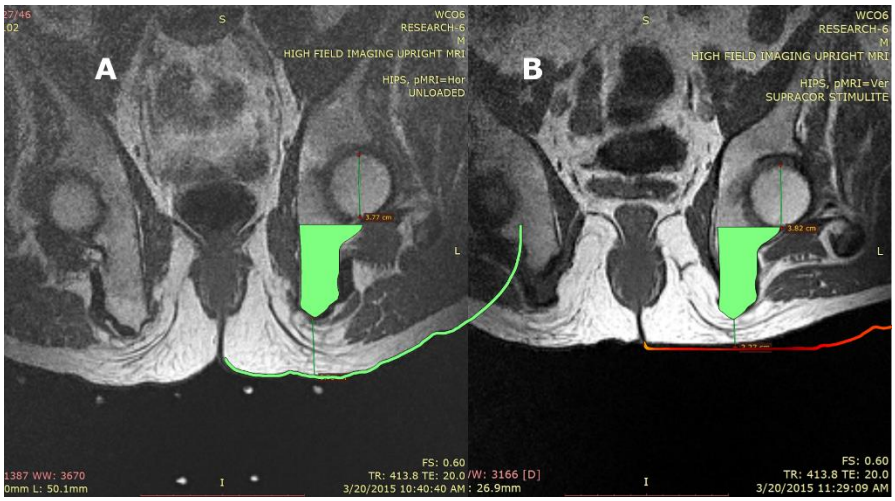

Figure 3.3. MRI imiagse of SI subject. Plate A is undeformed prior to sitting. The green line was manually input at the surface of the skin. Plate B is deformed in a seated position. The red and yellow line was grnerated with the FEM simulation, showing the predicted deformation during sitting. Red indicated minimal difference between model and MRI image, transitioning progressively to yellow for larger differences.

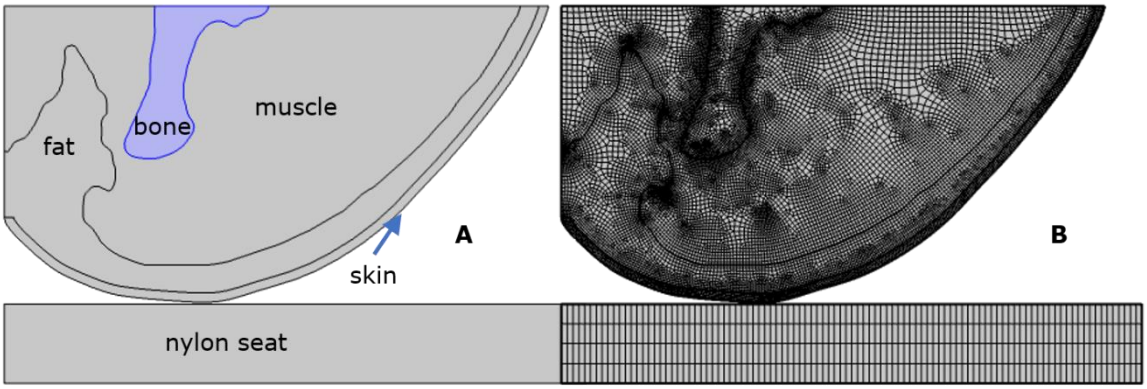

Figure 3.4. Plate A shows the four tissue regions as segmented manually from the MRI image for the non-SI subject. Plate B shows the quadrahedral meshed tissue domains. Total mesh elements are 16956

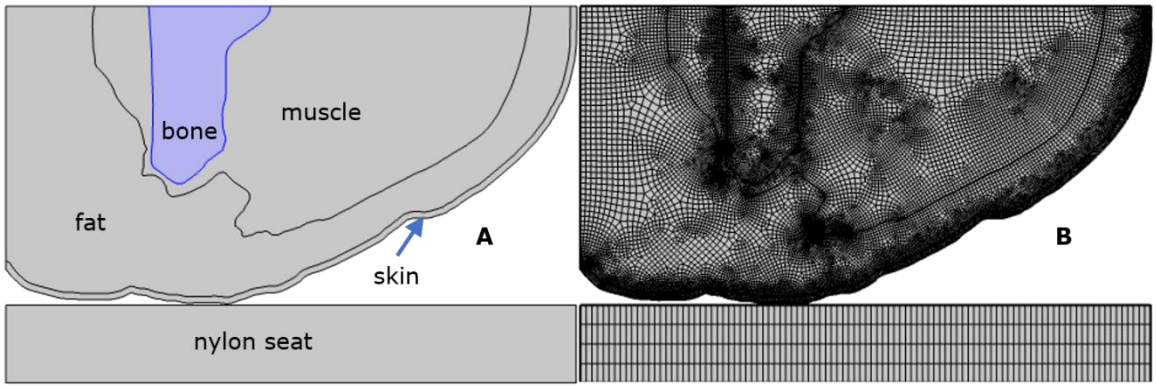

Figure 3.5. Plate A shows the four tissue regions as segmented manually from the MRI image for the SI subject. Plate B shows the quadrahedral meshed tissue domains. Total mesh elements are 20,982

FE Modeling

Comsol version 5.6 was selected for FE meshing and modeling due to its ease at adding and modifying equations and combining multiple physics domains under a single simulation environment. The Comsol software allows coupled analyses of nonlinear solid mechanics with heat transfer and the custom injury model we have developed [51] in a single program with two add-on modules for nonlinear solid mechanics and heat transfer. A summary of the mechanical properties and mesh density for the four tissue types if given in Table 1. A mesh sensitivity test [54] shows less than 1% change in results when doubling the number of elements in the model. The physical deformation of the system was assumed to be independent of the thermal loading of the tissue. The time constant for the propagation of mechanical stress throughout the tissue is orders of magnitude shorter than the time constant for propagation of thermal stress, justifying this assumption. Thus, the coupling between thermal and mechanical behavior is only in one direction, from mechanical to thermal. The mechanical loading has a direct effect on blood perfusion, which plays a key role in the internal convection within tissue. Trial solutions with the model set up for full bi-directional coupling show that there is no effect on the simulation results. Since full coupling requires more extended run times, the model was run with coupling from mechanical to thermal domains.

Nonlinear biomechanical model.

The NeoHookean, Hartmann-Neff volumetric strain energy nonlinear hyperelastic material model as described in Eq. (1) was selected to represent the skin, fat, and muscle

[55]. The bone is assumed separately to be linear elastic with negligible displacement, and the seat is a rigid body made of nylon. All materials are assumed isotropic. Material properties used are shown in Table 1. They are assumed to be constant throughout the simulation, including being independent of temperature. The presence of clothing is accounted for only in the heat transfer portion of the model.

Hyperelastic materials were given a large bulk modulus value to make them behave as being essentially incompressible to aid with numerical convergence and stability during computation. Others have had success using a fully incompressible model [55]. The NeoHookean model is expressed as

$$W = \frac{1}{2}\mu(I_1 - 3) + \frac{1}{50}\kappa(J^5 + J^{-5} - 2) \qquad (1)$$

W is strain energy density (kJ/m^3 or kPa)

μ Lamė parameter (kPa)

I_1 is first invariant of the right Cauchy-Green deformation tensor

κ is bulk modulus (kPa)

J is the determinant of the deformation gradient tensor

Material	μ [kPa]	K [kPa]	ν	E [kPa]	# of mesh elements
Skin non-SI[a]	39.1	666.67	0.494	-	2198
Fat non-SI[a]	39.1	66.67	0.494	-	4297
Muscle non-SI[a]	8.5	37.5	0.494	-	8679
Bone non-SI[a]	-	-	0.3	7e6	1782
Skin SI[b]	9.775	666.67	0.494	-	2328
Fat SI[b]	9.775	66.67	0.494	-	9284
Muscle SI[b]	2.125	37.5	0.494	-	6926
Bone SI[c]	-	-	0.3	7e6	2444
Nylon Plate[c]	-	-	-	-	400

Table 1 Mechanical properaty values and FE mesh densities used in biomechanical model

[a]data adopted from [48, 55]]

[b]data adopted from litature and modified using pressure map [38, 49, 56]

[c]Assummed to be a rigid solid with no deformation, with elastic properties not needed.

A rigid plastic surface was selected for the model seat to represent the worst-case scenario of induced tissue stress and strain for someone in a seated position. A prior modeling publication addressed the effect of a seat cushion, which could easily be adapted to this model [49].

All solid mechanics is assumed to take place instantly, so A steady-state solver was used to simulate mechanical displacement of the soft tissue since it was assumed (correctly) to occur at a rate orders of magnitude more rapidly that do other governing processes associated with sitting on a heated seat. The transient time is negligible for

someone sitting in a seat, especially compared to the larger time domains of the bioheat transfer and injury. No further movement or expansion is assumed for the remainder of the simulation. Once this phase of the model is finished, the stress and strain are static for heat transfer and injury calculations.

Boundary conditions are depicted in Fig. 6. One of the challenges of implementing a nonlinear model to describe large deformations between two objects is to characterize the moving contact surface. This portion of the simulation is solved first to avoid complications with coupling to other physical domains. The no lateral loading is assumed between the skin and plate. A displacement boundary condition a applied to the plate / tissue interface y-direction, with the skeleton fixed in the coordinate space. Incremental displacement is added in the model until a force load equivalent to the person's weight in the sitting position is reached. Deformation is checked against the MRI images and pressure map for verification.

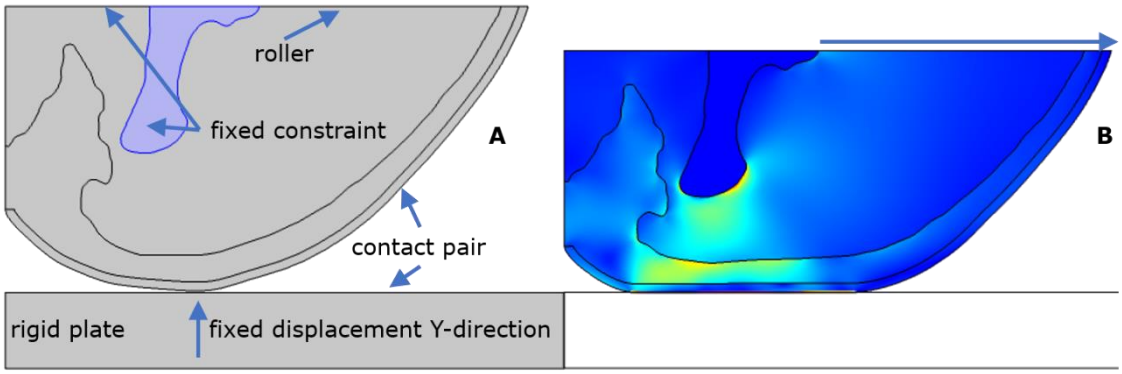

Figure 3.6. Plate A shows the applied mechanical boundary conditions for sitting of a flat surface. Plate. B is a map of Von Mises stress that develops within the system tissues for the applied boundard conditions, plus the geometric deformation from the surface to the interior of the soft tissues..

Bioheat transfer model.

The governing equation for bioheat transfer is the conservation of energy [57]. In living tissue it is important to account for internal convective heat transfer associated with blood perfusion and metabolic heat production, as described in the Pennes bioheat transfer equation [58].

$$\rho C \frac{\partial T}{\partial t} = \nabla \cdot (k \nabla T) + Q_{met} + \rho_b C_b \omega_f \omega_b (T_b - T) \quad (2)$$

$$\omega_f = 1 - \frac{\sigma}{120 mmHg} \quad (3)$$

ρ is the density of tissue (kg/m^3)

C is the heat capacity at constant pressure in the tissue (J/(kg·K))

T is the absolute temperature of the tissue

k is the thermal conductivity (W/(m·K))

Q_{met} is the metabolic heat generation of the tissue (W/m^3)

ρ_b is the density of blood (kg/m^3)

C_b is the heat capacity at constant pressure in the blood (J/(kg·K))

ω_b is the blood perfusion rate (1/s)

ω_f is the blood perfusion fraction as a function of internal stress state (1/s)

T_b is the arterial blood temperature (K)

Q_r is the energy deposited by the radiative beam - light/laser source ((W/m^3))

Material	ρ [kg/m^3]	C [J/kg·K]	k [W/(m·K)]	ρ_b [kg/m^3]	C_b [J/kg·K]	ω_b [1/s]	T_{ref} [°K]	T_b [°K]	Q_{met} [W/m^3]
Skin[a]	1109	3391	0.37	1050	3617	0.001959	310	310	368
Fat[a]	911	2348	0.21	1050	3617	0.000672	310	310	58
Muscle[a]	1090	3421	0.49	1050	3617	0.000672	310	310	684
Bone[a]	1908	1313	0.32	-	-	-	-	-	-
Nylon[b]	1150	1700	0.26	-	-	-	-	-	-
Clothing[c]	-	-	0.04	-	-	-	-	-	-

Table 3.2 Constitutive property values for materials and tissues in bioheat transfer model
[a]adpted from [57, 59]]

[b]supplied in Comsol material model [52]
[c]adpted from [59]

The property values used in the Pennes equation are held constant throughout the simulation with the exception of the perfusion factor term as described in Eq. (3). Owing to the application of physical pressure to the soft tissue, blood perfusion decreases with the development of interstitial stress during tissue deformation. This effect provides a direct coupling between the mechanical and thermal domains with

significant consequences. First, blood perfusion is modulated based on local stress and deformation, compromising the local tissue's ability to remove heat conducted in from a seat heater. Second, this relationship provides a direct link to the development of ischemia that is a critical element in modeling pressure ulcer causation. The linear function of Eq. (3) serves as a simple placeholder for possible more complex and complete formulations should further data become available.

The thermal boundary conditions for the bioheat transfer model are illustrated in Fig. 7. The seat occupant is assumed to be wearing a cotton clothing ensemble with a total thickness of 1.5mm. Prior to being seated, in panel 7A with tissue is not deformed, and the thermal boundary condition is natural convection heat transfer with a representative coefficient of 20 ($W/m^2.K$). More complex convection models may be justified, as by Gefen [56]. Air temperature is assumed to be 20°C. After the occupant is seated, the body weight against the rigid seat surface causes the deformation seen in panel 7B. Convection is physically blocked, and the boundary condition is changed to conduction. In one heating scenario, the seat temperature is maintained continuously constant at one of six selected temperatures (40, 42, 44, 46, 48, and 50°C). A second two-step protocol starts with a higher seat temperature of 55°C for 5 minutes and then drops to

42.5°C for the remainder of the time to simulate providing an initial boost in heating to provide occupant comfort as quickly as possible in cold environment followed by lowering the heating rate to minimize the risk of thermal injury. The upper boundary is held at 37°C to nominally match core temperature. The center spine is geometrically and thermally symmetric so there is no heat flow.

Once seated the boundary condition between the seat surface and the occupant is equivalent to contact between two semi-infinite media, although the occupant comprises a geometrically complex composite. The thermal response between the seat and occupant is governed by the property product $k\rho C$ for both materials that is known as the thermal inertia [57]. For most seating materials, the interface temperature between the seat and the occupant is biased toward the seat, but there are anticipated differences between leather and cloth as a function of their unique thermal inertias.

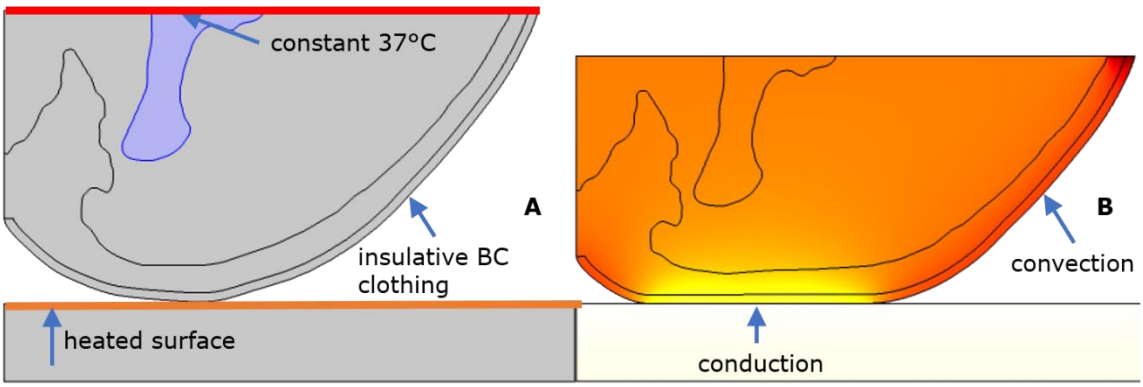

Figure 3.7. Change in the thermal boundary conditions from unseated (Plate A) to seated (Plate B) state..

Injury model for pressure and thermal injuries.

The injury model was adopted from McGregor and Diller [51] for the combined action of pressure and temperature on soft tissue injury causation. Pressure and temperature injuries have two different mechanisms of action and therefore are usually modeled separately. However, Iaizzo has conducted an elegant and comprehensive series of experiments that document the coupling interaction that can occur when temperature and pressure stresses are applied simultaneously [39-41]. This is exactly the situation that exists when a person sits on a heated seat resulting in compression of soft tissue underlaying the IT and an inward heat flow driven by an elevated seat surface temperature. Based on the Iaizzo data, a new coupled temperature / pressure injury model was developed to predict the progressive development of tissue damage as a function of time, temperature, and blood perfusion, which is directly coupled to applied pressure via Eq. (3). The model is described by Eq. (4).

$$\Omega(t,T,\omega) = e^{-\int_0^t \left[\left(e^{\lambda^*}\right)^k k \cdot e^{\beta_T \cdot T(\tau) + \beta_\omega \cdot \omega(\tau)} \cdot \tau^{k-1}\right] d\tau} \qquad (4)$$

λ^* is scale term, simplified, overall impact physiological variables have on injury term

k is shape term, simplified, once injury occurs how suddenly will cell viability change

β_T weighs the effect temperature has on injury development outside of homeostasis

β_ω weighs the effect blood profusion has on injury development outside of homeostasis

ω is the blood profusion in the tissue

τ & t are time (s)

Material	λ	k	B_T	B_ω
Skin Pressure Injury	-6.8595	1.8554	0.2573	-0.0105
Fat Pressure Injury	-8.2467	1.1168	0.1963	-0.0291
Muscle Pressure Injury	-6.0199	1.4420	0.1953	-0.0441
Pure Thermal Injury	-12.6210	2.9298	0.8880	0

Table 3.3. Values for the injury model coefficients in Eq. (4) for specific soft tissue types as determined by fitting to the Iaizzo experimental data set of combined temperature and pressure induced injury [51].

Figure 8 shows a three-dimensional depiction of injury level as predicted by Eq. (4). The model output is the percentage of cell viability on a continuous scale from 100% being no injury to zero being no survival. Since patient-specific data for sensitivity to injury is not available for individuals, the model is used to develop a heuristic understanding of the potential consequences of a person's interaction with the environment. The model is a significant step forward for capturing the complex behavior of injury formation under multiple interactive variables.

The simulation applies the model in two different contexts. First, it can predict a pressure injury with thermal modulation. If the internal stress exceeds 10 mmHg of mercury, the pressure injury version of the model is executed. Second, if the temperature exceeds 44 °C, pure thermal injury becomes the dominant driver. Eq. (4) can be applied with a coefficient derived specifically for burns, as shown in Table 3.

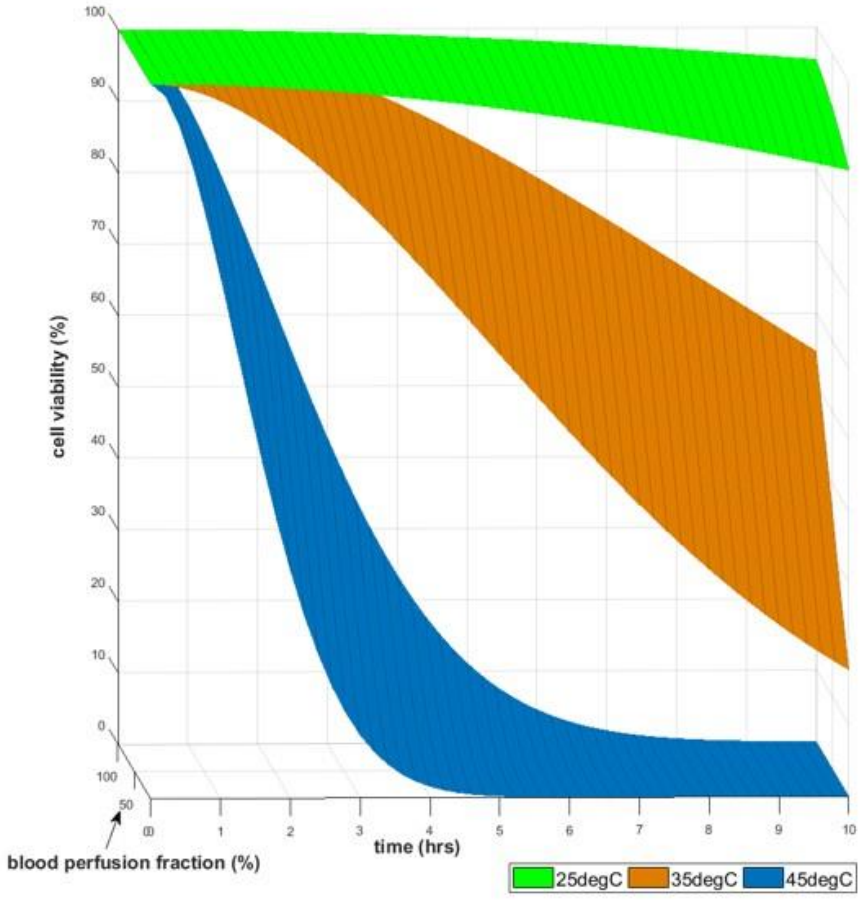

Figure 3.8. Predicted level of injury by Eq. 4 when solved with coefficient values in Table 3 across continuous ranges of time, surface temperature and perfusion. Temperature is held constant for the entire simulation duration. .

RESULTS

The results of the analysis are expressed as maps of stress, strain, temperature, and cell viability for simulations based on data from normal and spinal cord injured subjects. The maps are presented in two spatial dimensions in the soft tissue that underlays the IT and show the effects of specific combinations of temperature and pressure

applied at the skin surface in conjunction with sitting on a heated vehicle seat. Seated time is also a key independent variable.

Analysis of subjects in the seated posture means that the MRI images from Figs. 2B and 3B were selected for analysis with a focus on the ROI in soft tissue underlaying the IT where the probability of injury is greatest. Fig. 9 shows the calculated peak stress concentration and area of elevated stress are substantially higher in subjects with spinal cord injuries (SI). It is understood that the bony protrusion extending from the IT is likely a contributing factor to the difference. However, three other factors are also relevant. First, the tissue stiffness had to be reduced by a factor of four from the experimental pressure maps to enable alignment of the simulation fit to the data, meaning the tissue properties of muscle, fat, and skin are more pliable than those of the non-SI subject. Second, the total displacement from an undeformed to deformed shape for the SI subject is greater, as shown in Fig. 10 by measurement of the strain energy. Third, the atrophy of muscle directly under the IT reduces the cushioning compression length to the seated surface. Therefore, a person suffering from a SI has a greater overstress potential than does a no-SI subject. Table 4 compares the deformed and undeformed distances derived from the MRI images between the bottom of the IT and the contact surface of the seat.

Subject Type	Undeformed Distance [mm]	Compression Distance [mm]	*Finial Distance* [mm]
non-SI	46	15	31
SI	39	19	20

Table 3.4. Comparison of tissue thickness from the bottom of the IT to the outter surface of the skin.The SI subject has less underformed distance from IT to skin due to lower muscle mass. The compression distance is higher due less stiff material properties. The SI subject has a 35.4% smaller distance from the IT to the skin surface.

Both seated subjects show raised stress levels exceeding 10 mmHg (1.3 kPa). The peak stress in non-SI is 30[kPa] compared with 45-60[kPa] for SI. In both cases, peak stress occurs at or near the IT, causing it to be the most concern for PI occurrence. Strain energy is another indicator of PI potential formation [43]. Skin exhibits high stress and strain on the SI subject due to the more extensive stretching from the deformation. The results align with what we understand about tissue mechanics under boney protrusions under load.

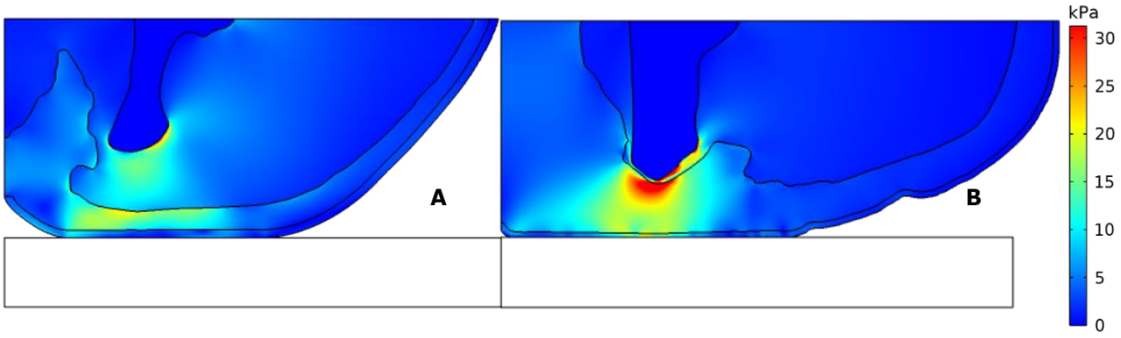

Figure 3.9. Von Misies stress distrubtion. Plate A shows a non-SI subject and Plate B a SI subject. Higher peak stress is seen in the SI subject due to the higher deformation of tissue, greater elastic material properties, less muscle mass, and sharper bony protrusion.

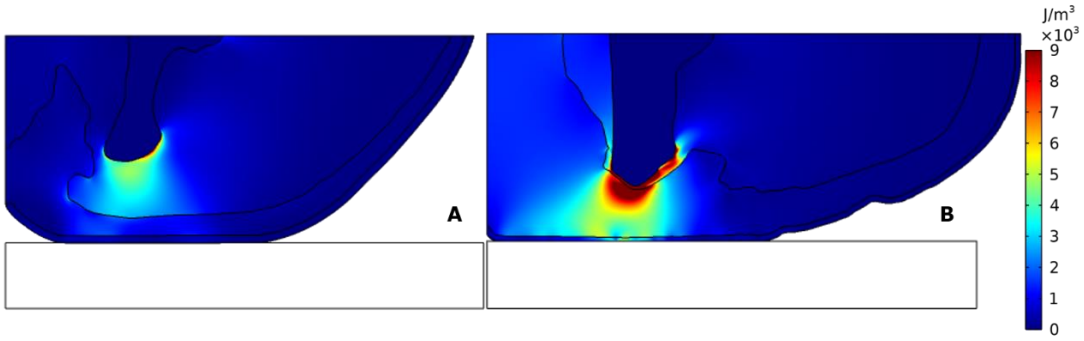

Figure 3.10. Calculated strain energy distrbution. Plate A is non-SI subject and Plate B is SI subject. Accourding to Gefen et a [60],l strain energy is usful indicator of the potential locations of PI formation.

The tissue temperature distributions for SI and non-SI occupants sitting on a seat surface maintained at 50°C are shown in Fig. 11. Clothing acts as a thermal resistance between the seat and skin, reducing the temperatures, and blood flow cools the tissue internally. The temperature decreases progressively with depth into the tissue, away from the heating source on the skin surface. Fig. 12 presents a plot of the temperature histories in the dermis for the array of seat temperatures modeled. The highest tissue temperatures occur in the dermis. The heater was activated at t = 0, after which there was approximately a 45 min rise time to maximum temperature for each seat value.

A complementary experiment was conducted by the senior author in testing the dynamic thermal operation of an actual vehicle seat. The trial was conducted inside a large, heated warehouse after both the vehicle and subject had been acclimated to an

interior air temperature of about 25°C. Exemplary clothing consisting of cotton under shorts and blue jeans were worn. Instrumentation consisted of Cu/Co 1mm thermocouples affixed in immediately adjacent locations on the outer surface of the blue jeans and the skin, both directly underlaying the right IT. A plot of both sensor outputs is in Fig. 13. The seat heater was actively shortly after the subject was seated. Note that the rise time is approximately 45 min, as predicted by the model. The temperature drop across the clothing was slightly less than 3°C. This drop is consistent with the model given that the temperatures plotted in Fig. 12 are interior to the dermis which must be cooler than the skin surface.

The peak dermal temperatures are about 2°C lower in the non-SI model predictions than in the SI. This differential is anticipated as described previously. The predicted dermal temperature for the non-SI subject never exceeds 43.8°C, which is below the threshold for causation of any level of thermal injury at 44°C [2, 4]. The two highest seat temperatures at 48 and 50°C resulted in dermal temperatures for the SI subject reached the injury threshold at 44 and 46°C, respectively The SI tissue exceed 44°C for the two highest seat temperatures. However, as is discussed subsequently, the sub-threshold temperatures are sufficient to enhance the formation of pressure ulcers.

A design protocol was modeled for an initial higher heating of the seat temperature to 46°C for 10 min followed by a drop to 41°C for the duration of the trial. This set of initial and steady state temperatures are simply exemplary to illustrated how this type of protocol can be evaluated, and many other combinations of initial temperature and time could be modeled. This particular trial shows that the dermal temperature is far

below the threshold for causing thermal burn injury, and the initial higher heating time is far short of the period necessary for causing a pressure ulcer. The conclusion is that it should be safe to operate a seat heater at a higher initial temperature should be not be maintained for a long duration, but that would provide an occupant a more rapid sensation of thermal comfort in a cold environment. Combinations of initial temperature and time will be a function of environmental conditions and tolerance of occupants for thermal and pressure injuries. Further used of the model to more broadly explore the design of this heated seat operational scenario is warranted.

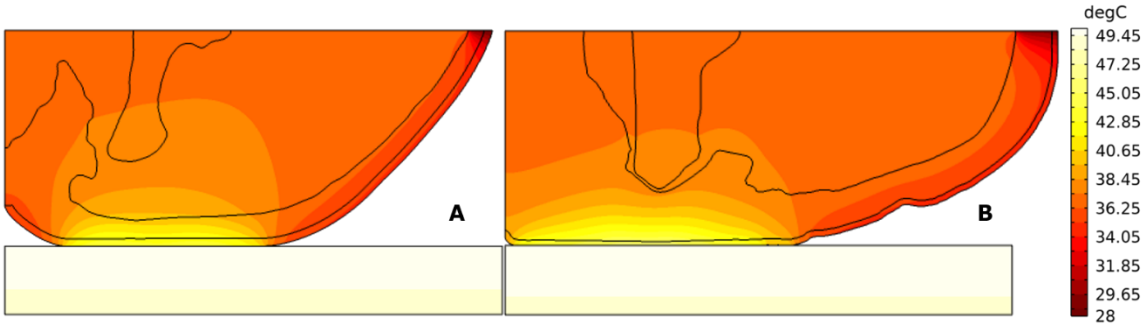

Figure 3.11. Tissue temperature distributions for Plate A non-SI and Plate B SI for a seat surface of 50°C.

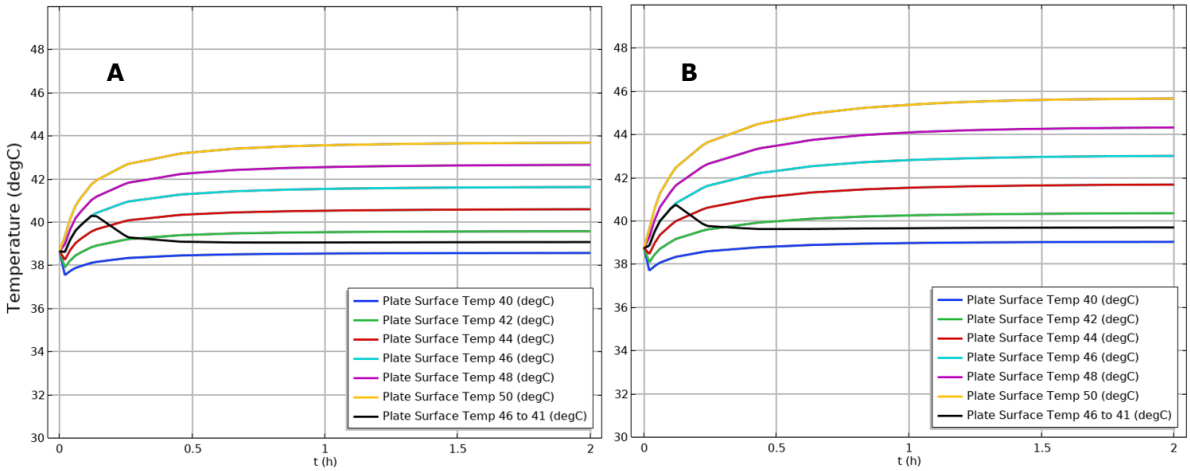

Figure 3.12. Peak tissue temperatures over time. Plate A is for non-SI and Plate B is SI. Regaurdless of surface temperature, the non-SI peak temp never exceeds 44°C due to the insulation from clothing and the heat removel from blood flow. The SI subject has two conditions above 44°C. The higher temperatrures are mostly due to greater contact area with the seat and lower blood flow from increased local stress. Accourding to the pioneering burn studies of Mortiz and Henriques [2, 4], for two hours of exposure, temperatures must approach 46°C to produce even the lowest level of irreversible injury.

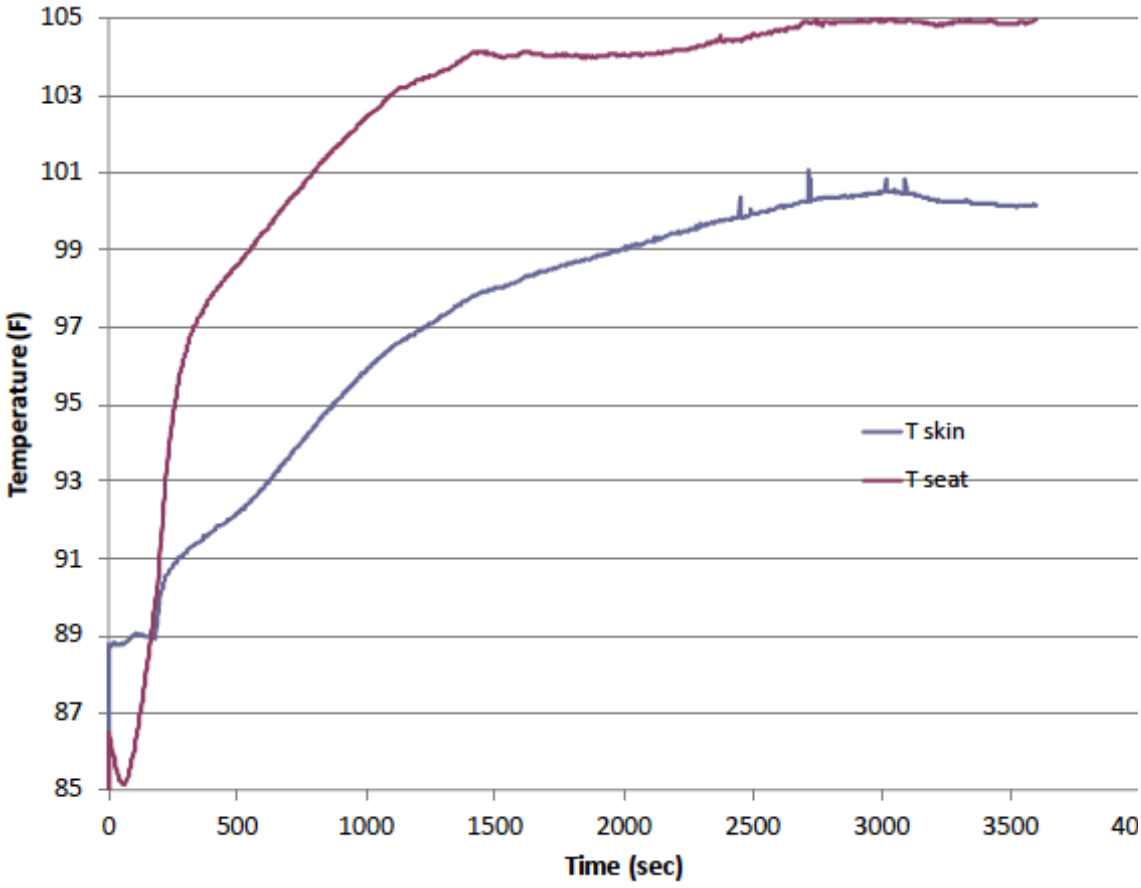

Figure 3.13. Temperature histories recorded during prior testing of a vehicle seat heater by the senior author. The clothing ensemble worn consisted for cotton undershorts and blue jeans. Copper constantan thermocouples were positioned immediately adjacent to each other on the outer surface of the blue jeans and on the skin, both directly underlaying the IT. Temperatures were recorded in the common US consumer scale in (°F). 100°F converts to about 37.8°C; 105°F to about 40.6°C; a maximum temperature difference of about 5°F to about 2.8°C.

Figs. 14 and 15 show the injury effect on non-SI subject at the 1 and 2 hours seated mark for the selected seat surface temperatures. The simulation produces results from 1 to 0, with one representing 100% cell viability and zero equaling 0% viability. From the simulation standpoint, the model predicts when the viability value falls below the 50%

range that can be considered as a threshold for concern representing irreversible damage to extensive tissue in the ROI. Figs. 16 and 17 display injury using a binary color system with red highlighting tissues regions with potentially irreversible damage values below this 50% threshold and blue being injury free. For Fig 16, at the 1-hour mark, all the results are the same regardless of the seat surface temperature which is why only one image frame is presented. Although some damage could potentially occur, the simulation points to it being reversible. In Fig 17 at the 2-hour mark, regardless of temperature challenge all cases exhibit the same classic PI form near the bony regions where the stress and strain concentrations are the highest. Fig 17 D, E, F subdermal irreversible damage occurs in the fat tissue where the combination of stress and higher temperature create a thermally enhanced pressure injury. The peak stress for fat ranges from 15-21.5 kPa from fat large deformation gradient. The peak temperature range between 40-42°C, which is still below the threshold for causing a burn injury. Increasing seat temperature raises the severity of the thermally induced PI. Fig. 18 A represents the total image area (mm^2) of tissue below 50% over the 2-hour time period. All of image A represents either pure or thermally enhanced PI and does not manifest until 1.5 hours. In Fig. 18 B the total irreversible damaged area over time shows a significant increase for the SI subject compared to non-SI.

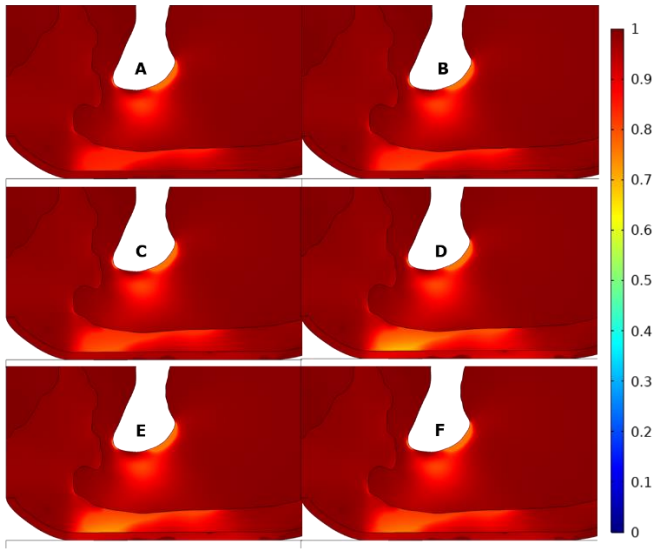

Figure 3.14. Cell viability for the non-SI subject sitting for 1 hour. A, B, C, D, E, F correspond to seat surface temperatures of 40, 42, 44, 46, 48, 50°C. Cell viability below 50% is equivalent to irreversible damge.

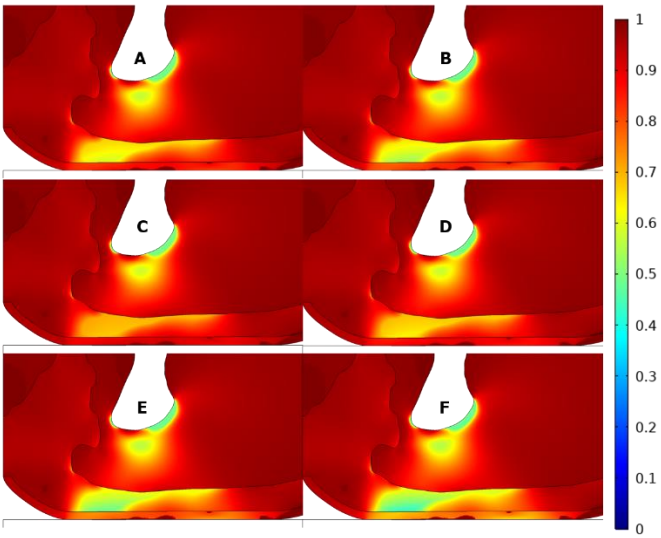

Figure 3.15. Cell viability for the non-SI subject sitting for 2 hours. A, B, C, D, E, F correspond to seat surface temperatures of 40, 42, 44, 46, 48, 50°C. Cell viability below 50% is equivalent to irreversible damge.

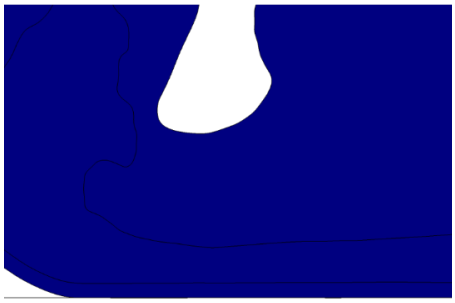

Figure 3.16. Cell viability for the non-SI subject sitting for 1 hour. Images were filtered so that viabilities higher than 50% are blue, and lower are red.. A, B, C, D, E, F corrispond to seat surface temperatures of 40, 42, 44, 46, 48, 50°C. No irreversible damage was predicted for any of the modeled conditions..

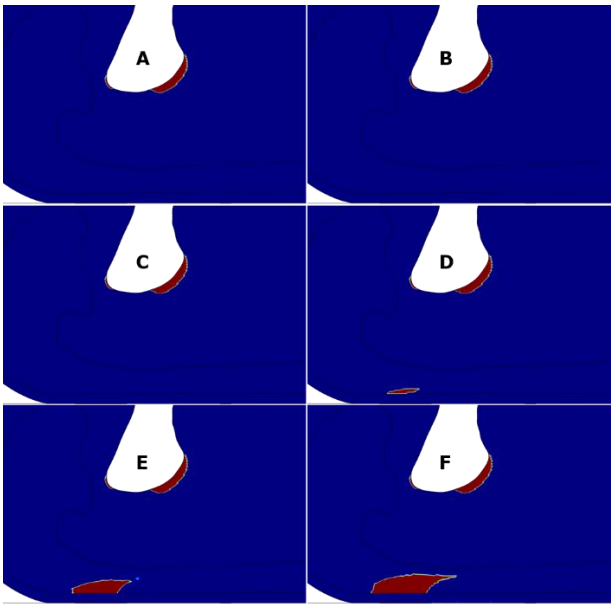

Figure 3.17. Cell viability for the non-SI subject sitting for 2 hours. Images were filtered so that viabilities higher than 50% are blue, and lower are red.. A, B, C, D, E, F corrispond to seat surface temperatures of 40, 42, 44, 46, 48, 50°C. All images exhibit the classic pressure injury to deep tissue next to the bone where peak stress exisit, but there is minimum influence of temperature. D, E & F show injury in the subcutanious region where thermal influence is more prominent.The combination of stress and temperature within the fat alows for the development of a thermally induced pressure injury.

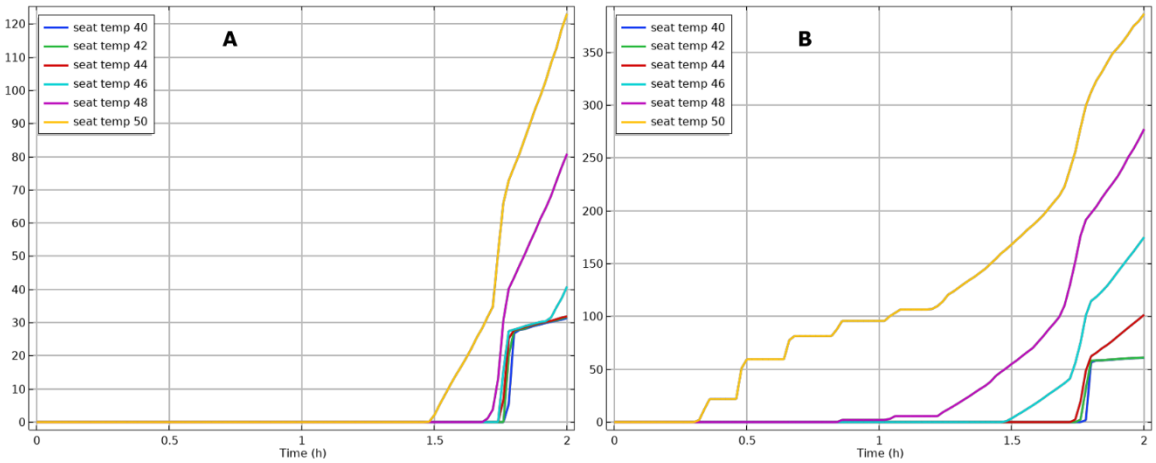

Figure 3.18. Timewise development of irrevesible tissue injury over a 2 hour time duration of heating at the indicated temperatures, expressed as total image area affected (mm^2). Plate A is a non-SI subject and Plate B a SI subject. All of graph A is pure PI or thermally enhanced and does not start till the 1.5 hours. B the volume starts as early as 0.3 hours with a combination of pure thermal, pure pressure, and thermally enhanced PI.

Figs. 19 and 20 show the injury effect on the SI subject at the 1 and 2 hours seated mark for the selected seat surface temperatures. As with the non-SI subject, output values are between 1 to 0, with one representing 100% cell viability and zero equaling 0% viability. Due to a reduced tissue stiffness and spatial distribution of tissue, the SI subject is at a higher risk of forming a PI. The nature of SI subjects experiencing classic PI is widely known and studied [61, 62]. Figs. 21 and 22 highlights in red areas where cell vitality will be below 50% indicating irreversible damage. In Fig. 21, after one hour A, B, C, D, E show no sign of tissue damage. In Fig. 21 F which has the highest temperature, damage is isolated in the cutaneous region proximal to the seat. From the previously discussed thermal analysis, the SI subject experiences higher temperature from increased contact surface and lower blood flow. According to Moritz et al., the time and temperature

exposure falls within the conditions for causing a first-degree or second-degree burn, but in the present analysis, there will be further complication from elevated pressure stresses. In Fig. 22, at 2 hours A, B, C, D, E, F show classic pressure injury present around the IT, where stress and strain are most concentrated. Fig. 22 C and D show thermally induced PI forms cutaneous and subcutaneously. For both C or D the tissue temperature never exceeds 43°C, which is still below the burn threshold. This dictates that both cases are strictly thermal enhanced pressure injuries. Fig. 22 E max tissue temperature is 44°C at 2 hours. This condition is not long enough to cause a pure thermal injury at this temperature, but it is well within an advanced PI range. Fig. 22 F presents a combination of pure and thermally enhanced PI in the cutaneous and subcutaneous regions.

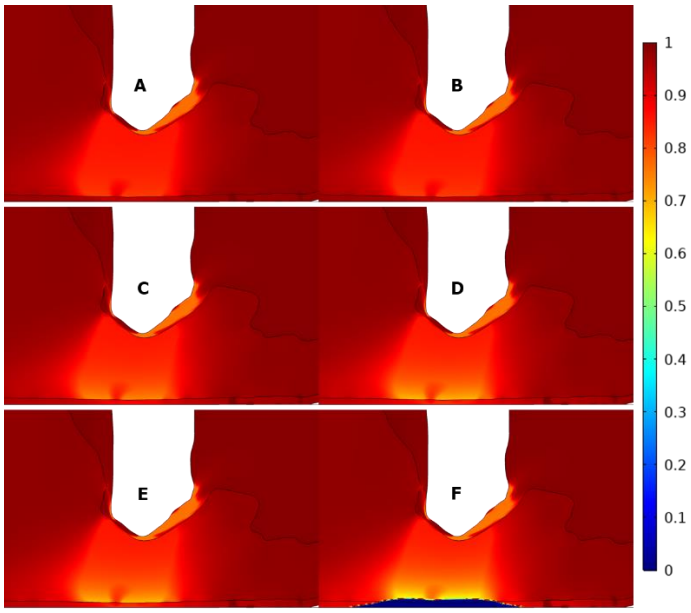

Figure 3.19. Cell viability for the SI subject sitting for 1 hour. A, B, C, D, E, F correspond to seat surface temperatures of 40, 42, 44, 46, 48, 50°C. Cell viability below 50% is equivalent to irreversible damge.

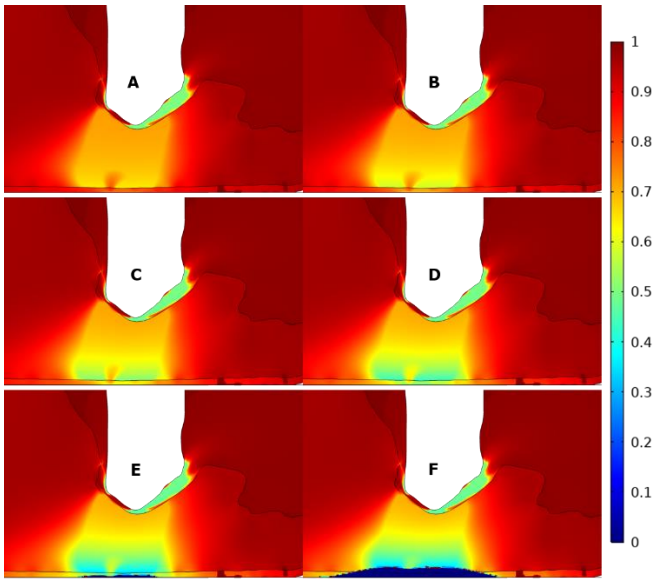

Figure 3.20. Cell viability for the SI subject sitting for 2 hours. A, B, C, D, E, F correspond to seatsurface temperatures of 40, 42, 44, 46, 48, 50°C. Cell viability below 50% is equivalent to irreversible damge.

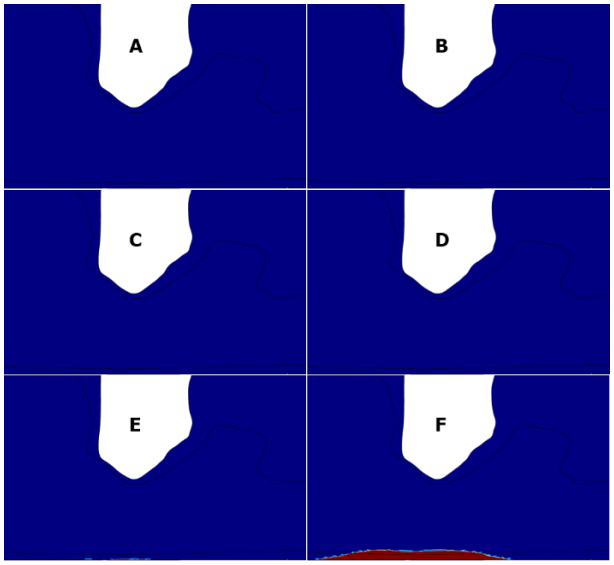

Figure 3.21. Cell viability of SI subject sitting for 1 hour. Images were filtered so that viabilities higher than 50% are blue, and lower are red.. A, B, C, D, E, F corrispond to seat surface temperatures of 40, 42, 44, 46, 48, 50°C. A, B, C, D & E show no irreversible damage. F shows thermal damage in the cutanious region proximal to the seat.

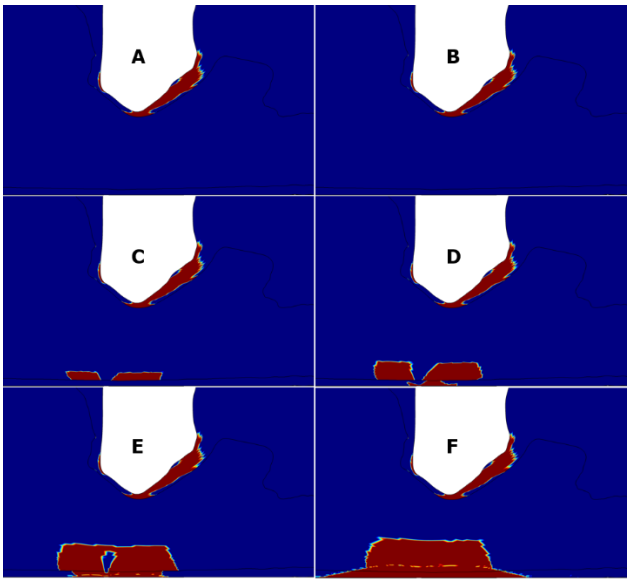

Figure 3.22. Cell viability of the SI subject sitting for 2 hours. Images were filtered so that viabilities higher than 50% are blue, and lower are red.. A, B, C, D, E, F corrispond to seat surface temperatures of 40, 42, 44, 46, 48, 50°C. All images exhibit classic of a pressure injury in the deep tissue next to the bone where peak stress exisit and thermal effects are minimal. C, D, E & F show damage in the subcutanious and cutanious regions that are proximal to the seat.

DISCUSSION

This paper demonstrates that a computer simulation can replicate the combined actions of temperature and pressure in creating soft tissue injuries when using a heated vehicle seat. Heating can cause creation of a pressure ulcer at temperatures below the threshold for a pure thermal injury, leading to a misinterpretation of injury causation as being a burn under conditions for which it is physically impossible, even with a seat heater activated. The computer model can be applied to screen heating and injury scenarios as a

design tool to optimize the tradeoffs between efficacy and safety in specifying operating domains for a seat heater.

One limitation of the assumptions embodied in the current model is that the seat is 100% rigid. With the exception of extreme cases for which seat heaters are unlikely to be encountered, heated seats will have elastic properties designed for comfort and will result in the creation of lower interstitial pressures. From this perspective, the injury conditions presented herein can be viewed as worst case scenarios.

Regardless of the existence of a spinal cord injury, if a subject sits for a prolonged time on a hard seat with no adjustments, pressure injuries will result in as little as 2 hours or less [63]. Typically, both normal and SI personals adjust their sitting posture periodically to relieve interstitial pressure as prophylactic to PI formation, often without conscious intention [64-66].

At lower seat temperatures, PI formation for both subject types start near the boney region of the IT, where stress and strain are the highest, creating a deep muscle injury that emanates from the inside out. With increasing seat temperature, the thermal gradient is progressively stronger from the outside inward, resulting greater thermal enhancement of PI formation closer to the surface, resulting in the damage development moving more superficially to within the fat and skin tissues. Since this injury is manifested near the skin, it may potentially lead to a misdiagnosis as a burn due to the dermal and subdermal locations [27]. The temperature, in most cases, never exceeded the minimum threshold for causing a pure thermal injury. Preheating the seat surface to 46°C and reducing it to 42°C produced similar results as a constant seat temperature of 42°C. The SI

subject experienced a higher peak temperature owing to an increased surface contact area and reduced convective blood cooling owing to tissue interstitial stress.

Physiological factors dictated the impact of the injury for both subject types. SI forecast the highest potential for injury within a smaller time window due to: having less tissue between the bottom of the IT and the outer surface of the skin; the tissue properties being more elastic; and greater atrophy of muscle mass. The consequence was an overall increase in local stress and strain than for the non-SI subject and increased surface area for heat transfer. For this simulation, initial blood flow to the tissue was set to be identical for both subjects. Lower blood flow to the local tissue will increase the potential for PI formation.

Seat cushions are anticipated lower the internal peak stress and increase the stationary seated time by distributing the load over a larger area. They are typically used for this purpose for paraplegics [49]. but heating and microclimate can still lead to deep and subdermal injuries [56]. Future iterations of this model can readily include refinements such as 3D physiology and seat cushions. The current form of the model can be increased in complexity by enhancing the structure of the boundary condition, as seen in other SI injury papers [56, 67].

SUMMARY

A new simulation model has been built to predict the occurrence of soft tissue injury that may result from occupying a heated vehicle seat. The primary governing factors are the seat surface temperature and time of occupancy, that must be considered in combination with the fact the sitting posture imposes an interstitial pressure within the soft

tissue that can also contribute to injury causation. An elevated temperature contributes to a more rapid development of a pressure ulcer in soft tissue adjacent to the ischial tuberosity. The model shows that a short initial period of higher temperature to more quickly provide thermal comfort to an occupant can be designed to be both effective and safe for the general population. Occupants such as paraplegics who have compromised lower limb sensation are at risk when seated for an extended time while unaware that a seat heater is activated.

ACKNOWLEDGEMENTS

This research was conducted with the support of the Robert and Prudie Leibrock Professorship in Engineering at the University of Texas at Austin. We thank the current Iaizzo lab for providing archival data from their original experiments to apply in building and verifying our injury model. We thank the Brienza lab for generously providing their experimental data and MRI images for the development of the FEA simulation.

REFERENCES

[1] SAE, 2015, "Recommendation for Acceptable Operating Parameters of Heated Automobile Seats in Order to Mitigate Occupant Injury, J3047-2015-10-21."

[2] Henriques, F. C., 1947, "Studies of Thermal Injury. V. The Predictability and the Significance of Thermally Induced Rate Processes Leading to irreversible Epidermal Injury," Archives of Pathology, 43, pp. 489-502.

[3] Moritz, A. R., 1947, "Studies of Thermal Injury. III. The Pathology and Pathogenesis of Cutaneous Burns. An Experimental Study," American Journal of Pathology, 23(6), pp. 915-941.

[4] Moritz, A. R., and Henriques, F. C., 1947, "Studies of Thermal Injury. II. The Relative Importance of Time and Surface Temperature in the Causation of Cutaneous Burns," American Journal of Pathology, 23(5), pp. 695-720.

[5] Stoll, A. M., 1960, "A Computer Solution for Determination of Thermal Tissue Damage Integrals from Experimental Data," IRE Transactions on Medical Electronics, ME-7(4), pp. 355-358.

[6] Stoll, A. M., 1967, "Heat Transfer in Bioethcnology," Advances in Heat Transfer, 4, pp. 65-141.

[7] Stoll, A. M., and Greene, L. C., 1959, "Relationship Between Pain and Tissue Damage Due to Thermal Radiation," Journal of Applied Physiology, 14(3), pp. 373-382.

[8] Bull, J. P., and Lawrence, J. C., 1979, "Thermal Conditions to Produce Skin Burns," Fire and Materials, 3(2), pp. 100-105.

[9] Lawrence, J. C., and Bull, J. P., 1976, "Thermal Conditions Which Cause Skin Burns," J. Inst. Mech. Eng. Engineering in Medicine, 5(1), pp. 61-63.

[10] Log, T., 2017, "Modeling Skin Injury from Hot Spills on Clothing," Int J Environ Res Public Health, 14(11).

[11] Stoll, A. M., and Chianta, M. A., 1968, "Burn Production and Prevention in Convective and Radiant Heat Transfer," Aerospace Medicine, 39, pp. 1097-1100.

[12] Stoll, A. M., and Chianta, M. A., 1969, "Method and Rating System for Evaluation of Thermal Protection," Aerospace Medicine, 40(11), pp. 1232-1237.

[13] Stoll, A. M., Chianta, M. A., and Munroe, L. R., 1964, "Contact Flame Studies," JOURNAL OF HEAT TRANSFER-TRANSACTIONS OF THE ASME, 86(3), pp. 449-456.

[14] Chato, J. C., and Subramanian, B., 1998, "Safe Touch Temperatures for Hot Plates," Journal of Biomechanical Engineering, 120(6), pp. 727-736

.

[15] Stoll, A. M., Chianta, M. A., and Piergallini, J. R., 1979, "Thermal Conduction Effects in Human Skin," Aviation space Environmental Medicine, 50(8), pp. 778-787.

[16] Diller, K. R., 1985, "Analysis of Skin Burns," Heat Transfer in Medicine and Biology: Analysis and Applications, A. Shitzer, and R. C. Eberhart, eds., Plenum Publishing Co., New York, pp. 85-134.

[17] Diller, K. R., 1991, "Analysis of Burns Caused by Long-Term Exposure to a Heating Pad," Journal of Burn Care & Rehabilitation, 12, pp. 214-217.

[18] Diller, K. R., 1998, "Modeling Thermal skin Burns on a Personal Computer," Journal of Burn Care and Rehabilitation(19).

[19] Buettner, K., 1952, "Effects of Extreme Heat and Cold on Human Skin. III. Numberical Analysis and Pilot Experiments on Penetrating Flash Radiation Effects," Journal of Applied Physiology, 5(5), pp. 207-220.

[20] Abraham, J. P., Plourde, B. D., Vallez, L. J., Nelson-Cheeseman, B. B., Stark, J. R., Sparrow, E. M., and Gorman, J. M., 2018, "Skin Burns," Theory and Applications of Heat Transfer in Humans, D. Shrivastava, ed., John Wiley & Sons, New York, pp. 723-739.

[21] Orgill, D. P., Porter, S. A., and Taylor, H. O., 2005, "Heat injury to cells in perfused systems," Ann N Y Acad Sci, 1066, pp. 106-118.

[22] Southwood, W. F. W., 1955, "The Thickness of the Skin," Plastic and Reconstructive Surgery, 15, pp. 423-429.

[23] Leider, M., and Buncke, C. M., 1954, "Physical Dimensions of the Skin," AMA Archives of Dermatology and Syphilology, 69, pp. 563-569.

[24] de Rigal, J., Excoffier, C., Querleux, B., Faivre, B., Agache, P., and Leveque, J.-L., 1989, "Asssessment of Aging of the Human Skin by In Vivo Ultrasonic Imaging," Journal of Investigative Dermatology, 93, pp. 621-625.

[25] Whitton, J. R., and Everall, J. D., 1973, "The Thickness of the Epidermis," British Journal of Dermatology, 89, pp. 467-476.

[26] Abraham, J. P., Plourde, B. D., Vallez, L. J., and Nelson-Cheeseman, B. B., 2016, "Correcting a prevalent misunderstanding of burns," Burns, 42(4), pp. 715-716.

[27] Diller, K. R., 2011, "Car Seat Heaters As a Potential Burn Hazard: a Clarification," J Burn Care Res, 32(2), pp. e33-34; author reply e35-36.

[28] Maguiña, P., Palmieri, T. L., and Greenhalgh, D. G., 2003, "Car Seat Heaters: A Potential Hazard for Burns," Journal of Burn Care & Rehabilitation, 24(5), pp. 315-316.

[29] Benjamin, C., Gittler, M., and Lee, R., 2011, "Burn from car seat heater in a man with paraplegia: case report," J Spinal Cord Medicine, 34(3), pp. 332-334.

[30] Demir, E., O'Dey, D. M., Fuchs, P. C., Block, F., and Pallua, N., 2006, "[Heated car seats--a potential burn risk for paraplegics]," Nervenarzt, 77(2), pp. 201-203.

[31] Sever, C., Kulahci, Y., Uygur, F., and Oksuz, S., 2010, "An Unusual Burn Caused by Heated Car Seat," Eplasty, 10(e28), pp. 231-232.

[32] Greenhalgh, D. G., Maguina, P., and Palmieri, T. L., 2011, "In Response: Car Seat Heaters as a Potential Burn Hazard: A Clarification," Journal of Burn Care & Research, 32(2), pp. e35-e36.

[33] Ketterer, A. R., and Hogrefe, C. P., 2019, "Gluteal Burns from a Car Seat Heater in a Neurologically Intact Patient: A Case Report," J Emerg Med, 56(6), pp. e107-e109.

[34] Yon, J. R., Fredericks, C., Mentzer, C., Kubasiak, J. C., and Poulakidas, S., 2021, "The end of the assembly line: Shifting patterns of automotive burns," Burns, 47(3), pp. 728-732.

[35] Bouten, C. V., Oomens, C. W., Baaijens, F. P., and Bader, D. L., 2003, "The etiology of pressure ulcers: skin deep or muscle bound?," Archives of Physical Medicine and Rehabilitation, 84(4), pp. 616-619.

[36] Gefen, A., 2008, "How Much Time Does it Take to Get a Pressure Ulcer? Integrated Evidence from Human, Animal, and In Vitro Studies," Ostomy Wound Management, 54(10), pp. 26-35.

[37] Gefen, A., 2019, "Prevention and Treatment of Pressure Ulcers/Injuries: Clinical Practice Guideline."

[38] Oomens, C. W., Bader, D. L., Loerakker, S., and Baaijens, F., 2015, "Pressure induced deep tissue injury explained," Annals of Biomedical Engineering, 43(2), pp. 297-305.

[39] Iaizzo, P. A., Kveen, G., Kokate, J. Y., Leland, K. j., Hansen, G. L., and Sparrow, E. M., 1995, "Prevention of Pressure Ulcers by Focal Cooling: Histological Assessment in a Porcine Model," Wounds, 7(5), pp. 161-169.

[40] Kokate, J. Y., Leland, K. J., Held, A. M., Hansen, G. L., Kveen, G. L., Johnson, B. A., Wilke, M. S., Sparrow, E. M., and Iaizzo, P. A., 1995, "Temperature-modulated Pressure Ulcers: A Porcine Model," Archives of Physical Medicine and Rehabilitation, 76, pp. 666-673.

[41] Kokate, J. Y., Leland, K. J., Sparrow, E. M., and Iaizzo, P. A., 1997, "Critical Threshold for Pressure Ulcer Formaion in a Porcine Model," Wounds, 9(4), pp. 111-121.

[42] Council, N. P. I. A., 2012, Pressure Ulcers: Prevalence, Incidence and Implcations for the Future.

[43] Gefen, A., 2019, "How medical engineering has changed our understanding of chronic wounds and future prospects," Med Eng Phys, 72, pp. 13-18.

[44] Gefen, A., Beienza, D., Edsberg, L., Milton, W., Murphy, C., Oomens, C. W. J., Perry, L., and Sari, Y., 2019, The Etiology of Pressure Injuries, Prevention and Treatment of Pressure Ulcers/Injuries: Clinical Practice Guideline. 3rd Ed., European Pressure Ulcer Advisory Panel (EPUAP), National Pressure Injury Advisory Panel (NPIAP), and Pan Pacific Pressure Injury Alliance (PPPIA).

[45] Zhang, J. D., Mak, A. F. T., and Huang, L. D., 1997, "A Large Deformation Biomechanical Model for Pressure Ulcers," Journal of Biomechanical Engineering, 99(4), pp. 406-408.

[46] Agam, L., and Gefen, A., 2007, "Pressure Ulcers and Deep Tissue Injury: a Bioengineering Perspective," Journal of Wound Care, 16(8), pp. 336-342.

[47] Linder-Ganz, E., Shabshin, N., Itzchak, Y., Yizhar, Z., Siev-Ner, I., and Gefen, A., 2008, "Strains and stresses in sub-dermal tissues of the buttocks are greater in paraplegics than in healthy during sitting," J Biomech, 41(3), pp. 567-580.

[48] Linder-Ganz, E., Yarnitzky, G., Yizhar, Z., Siev-Ner, I., and Gefen, A., 2009, "Real-time finite element monitoring of sub-dermal tissue stresses in individuals with spinal cord injury: toward prevention of pressure ulcers," Ann Biomed Eng, 37(2), pp. 387-400.

[49] Brienza, D., Vallely, J., Karg, P., Akins, J., and Gefen, A., 2018, "An MRI investigation of the effects of user anatomy and wheelchair cushion type on tissue deformation," J Tissue Viability, 27(1), pp. 42-53.

[50] Sae-Sia, W., Wipke-Tevis, D. D., and Williams, D. A., 2005, "Elevated sacral skin temperature (T(s)): a risk factor for pressure ulcer development in hospitalized neurologically impaired Thai patients," Appl Nurs Res, 18(1), pp. 29-35.

[51] McGregor, G., and Diller, K. R., 2021, "Modeling and Simulation of Coupled Pressure and Thermal Injury," Journal of Heat Transfer, in review.

[52] "COMSOL Multiphysics," COMSOL, Inc, Burlington, MA 01803.

[53] "Sim4Life," ZMT Aurich MedTech AG, Zurich, Switzerland.

[54] Espino, D. M., Shepherd, D. E., and Hukins, D. W., 2013, "Development of a transient large strain contact method for biological heart valve simulations," Comput Methods Biomech Biomed Engin, 16(4), pp. 413-424.

[55] Levy, A., Kopplin, K., and Gefen, A., 2014, "An air-cell-based cushion for pressure ulcer protection remarkably reduces tissue stresses in the seated buttocks with respect to foams: finite element studies," J Tissue Viability, 23(1), pp. 13-23.

[56] Zeevi, T., Levy, A., Brauner, N., and Gefen, A., 2018, "Effects of ambient conditions on the risk of pressure injuries in bedridden patients-multi-physics modelling of microclimate," Intl Wound J, 15(3), pp. 402-416.

[57] Roselli, R. J., and Diller, K. R., 2011, Biotransport: Principles and Applications, Springer, New York.

[58] Pennes, H. H., 1948, "Analysis of Tissue and Arterial Blood Temperatures in the Resting Human Forearm," Journal of Applied Physiology, 1(2), pp. 93-122.

[59] Fanger, P. O., 1970, "Conditions for Thermal Comfort. Introduction of a General Comfort Equation," Physiological and Behavioral Temperature Regulation, J. D. Hardy, A. P. Gagge, and J. A. J. Stolwijk, eds., Charles C Thomas, Springfield, pp. 152-176.

[60] Schwartz, D., and Gefen, A., 2020, "An integrated experimental-computational study of the microclimate under dressings applied to intact weight-bearing skin," Int Wound J, 17(3), pp. 562-577.

[61] Olney, C. M., Simone, A., Hanowski, K., Rector, T. S., Goldish, G. D., Hansen, A. H., and Ferguson, J. E., 2018, "Microclimate evaluation of strap-based wheelchair seating systems for persons with spinal cord injury: A pilot study," J Tissue Viability, 27(3), pp. 181-187.

[62] Swaine, J. M., Moe, A., Breidahl, W., Bader, D. L., Oomens, C. W. J., Lester, L., O'Loughlin, E., Santamaria, N., and Stacey, M. C., 2018, "Adaptation of a MR imaging protocol into a real-time clinical biometric ultrasound protocol for persons with spinal cord injury at risk for deep tissue injury: A reliability study," J Tissue Viability, 27(1), pp. 32-41.

[63] Lustig, M., Levy, A., Kopplin, K., Ovadia-Blechman, Z., and Gefen, A., 2018, "Beware of the toilet: The risk for a deep tissue injury during toilet sitting," J Tissue Viability, 27(1), pp. 23-31.

[64] Gefen, A., 2007, "The Biomechanics of Sitting-Acquired Pressure Ulcers in Patients with Spinal Cord Injury or Lesions," International Wound Journal, 4(3), pp. 222-231.

[65] Linder-Ganz, E., Scheinowitz, M., Yizhar, Z., Margulles, S. S., and Gefen, A., 2005, "Frequency and Extent of Spontaneous Motion to Relief Tissue Loads in Normal Individuals Seated in a Wheelchair," 2005 Summer Bioengineering Conference, ASME, Vail, CO.

[66] Yang, Y. S., Chang, G. L., Hsu, M. J., and Chang, J. J., 2009, "Remote monitoring of sitting behaviors for community-dwelling manual wheelchair users with spinal cord injury," Spinal Cord, 47(1), pp. 67-71.

[67] Gefen, A., Alves, P., Ciprandi, G., Coyer, F., Milne, C. T., Ousey, K., Ohura, N., Waters, N., Worsley, P., Black, J., Barakat-Johnson, M., Beeckman, D., Fletcher, J., Kirkland-Kyhn, H., Lahmann, N. A., Moore, Z., Payan, Y., and Schluer, A. B., 2020,

"Device-related pressure ulcers: SECURE prevention," J Wound Care, 29(Sup2a), pp. S1-S52.

Chapter 4: Combined Actions of H_2O_2 Diffusion, Laser Heating, Internal Stresses, Blood Perfusion, and Pulp Inflammation During Tooth Whitening Procedures

The work contained in this chapter has been submitted to the Journal Dental Research for publication[3].

Gary McGregor contributed to design of numerical experiments, developing code, development of finite element simulation, conceptualizing the Multiphysics framework and inflammatory response, optimizing candidate treatment protocols, data analysis, plotting of results, and drafting the manuscript.

[3] This is a slightly modified version of the article submitted for publication to align with the dissertation format.

ABSTRACT

Tooth whitening is widely practiced in both clinical and home settings. The mechanism of action is via bleaching of discoloration by hydrogen peroxide introduced at the tooth surface. Laser light may be applied to augment the bleaching phenomenon. The design of bleaching protocols requires an appreciation for the action and interaction of multiple processes for which a general, rigorous quantitative understanding is yet to be developed. Prime elements of a whitening procedure include applied hydrogen peroxide concentration and exposure time, laser light wavelength, illumination intensity, pattern, and duration, and morphology and dimensions of target teeth. Undesirable side effects may result, such as pain, inflammation of the pulp, and cell necrosis. The whitening process, viewed from a wholistic perspective, is complex, with coupling effects occurring among many simultaneous processes, making a comprehensive understanding challenging. This paper presents an overview of a new computer simulation model that embodies the diverse physical and physiological processes involved during whitening. The analysis model is implemented via the finite element method that is particularly suited to describing the complex morphologies and composite materials structure of teeth. Individual properties of enamel, dentin, and pulp are applied for molecular diffusion of hydrogen peroxide, wavelength-specific optical properties, stress/strain relationships, tissue blood perfusion, laser heating absorption, development of inflammation, and cell injury. The model provides a design tool that can be used as a guide for developing whitening procedures that combine efficacy with safety from risk of injury.

Keywords: tooth whitening, hydrogen peroxide, finite element model, inflammation, laser heating, molecular diffusion

INTRODUCTION

Tooth whitening has become a widely adopted practice for aesthetic purposes in both clinical and home settings [1]. Bleaching devices are available to individuals on an over-the-counter basis and therefore may be used in the absence of oversight by health care professionals, making the safety of the user a primary concern [1]. Many technologies make use of hydrogen peroxide (H_2O_2) as a bleaching agent to remove discoloration from teeth based on its powerful oxidizing properties [2]. Chemical reaction of free radicals released by the peroxide with pigments or chromophores in the extracellular matrix of the tooth constitutes the basis for tooth whitening [3,4]. However, there is a risk that H_2O_2 may induce inflammation to the pulp with undesired consequences [5].

The application of H_2O_2 embedded in a gel to the surface of a tooth initiates a complex cascade of physical events [1]. All of the structural elements of a tooth are permeable to H_2O_2, enabling its progressive diffusion from enamel through dentin and into the pulp, each with a differential conductivity [1,6]. The concentration of H_2O_2 and time of exposure have a direct effect on both the efficacy of whitening and the risk of injury [2]. The presence of H_2O_2 as a noxious chemical stimulant causes the neurological release of inflammatory mediators leading to vasodilation and molecular extravasation with a concomitant increase in pulpal tissue pressure[7,8].

In addition, it has been demonstrated that laser-assisted bleaching can be used to enhance the kinetics of the release of free radicals from within a gel applied to the surface of a tooth to decrease the time required to achieve a whitening effect[9]. However, a cautionary approach must be used when augmenting H_2O_2 with light activation since an

optical source is inherently energy-dissipative, leading to a local temperature rise. If the temperature reaches a threshold level, irreversible thermal injury to tissue may occur[10–12].

The aggregate phenomena that govern tooth whitening can be described briefly along with their known domains of operation. A brief qualitative description of the multiple coupled processes during laser enhanced tooth whitening includes the following components.

- When a strip of tooth whitening gel is placed onto the surface of a tooth, H_2O_2 diffuses progressively into the enamel, then into the dentin, then into the pulp if the concentration and time of application are sufficient. Each of the tooth materials has a unique coefficient of diffusion for H_2O_2 that determines the rate at which the active agent is delivered into the body of the tooth [13]. H_2O_2 bleaches discoloration in proportion to its local concentration and time of action [1].
- Laser light may be applied at the tooth surface in conjunction with the use of H_2O_2 to enhance its bleaching action [1,9]. The light is absorbed differentially in the enamel, dentin, and pulp as a function of the coefficient of absorptivity for the laser wavelength and the incident flux that has penetrated to a given depth within the tooth [14–16]. As the light is absorbed, it is converted to energy that will raise the local temperature proportionately [17–20]. In general, the absorption and heating pattern will occur in a three-dimensional pattern.

- Blood perfusion occurs continuously through the pulp and is a nonlinear function of temperature [21–26]. With a moderate elevation of temperature above physiological baseline, perfusion will increase. Above a threshold, extravasation will begin to occur, resulting in elevated interstitial pressure, tissue deformation, and developing ischemia [7,8]. Since the enamel and dentin sheath is rigid, no swelling is possible, and over time cell necrosis may result [7,8]. Simultaneous pain will also be present.
- The rate at which injury may occur under these conditions is a complex physiological and physical function. The presence of H_2O_2 as a noxious chemical stimulant causes the neurological release of inflammatory mediators leading to vasodilation and molecular extravasation with a concomitant increase in pulpal tissue pressure[7,8]. The added pressure then reduces blood flow and causes cell deformation. The effects of ischemia are exacerbated at elevated temperature for which metabolic demands and the production of toxic byproducts are increased.
- There is a strong interplay among these various processes that are nonlinear and therefore very difficult to describe with a mathematical model that could serve as a design tool for optimizing application protocols, plus the inherent geometry of the teeth is highly irregular, making simulation and prediction problematic.

Each component of a model must be based on known physical and physiological phenomena that follow explicit laws of nature. These laws are given in Table 1, below.

Phenomenon	Governing Equation	Driving Force	Tissue property	Units
H_2O_2 diffusion	Fick's law	H_2O_2 concentration	Diffusion coefficient	m^2/sec
Laser heating	Beer's law	Light flux	Absorptivity	L/mol.cm
Blood perfusion	Poiseuille's law	Pressure gradient	Viscosity	Poiseuille
Tissue deformation	Hooke's law	Mechanical stress	Elastic modulus	Pa
Tissue injury and inflammation	Arrhenius law	Combined thermal & mechanical stresses	Activation energy	J/mol

Table 4.1. Summary of the physical laws and physiological processes that govern the response of teeth to application of a gel whitening strip to a tooth surface. The individual laws can be considered independently, but it is important to include interactions that occur across normally separated functional domains so that anticipated behavior may be modified.

The solution of these governing equations for the geometries of incisor and molar teeth and boundary conditions that describe tooth whitening with laser augmentation was carried out on a multi-physics finite element (FE) modeling platform using COMSOL software (COMSOL, Inc, Burlington, MA). The fundamentals of the analysis are outlined in the following section.

MATERIALS AND METHODS

Finite Element Model

The finite element method uses meshing to represent the geometry and material structure of a system for analysis. Figure 1 (a) and (b) show the meshes for incisor and molar teeth.

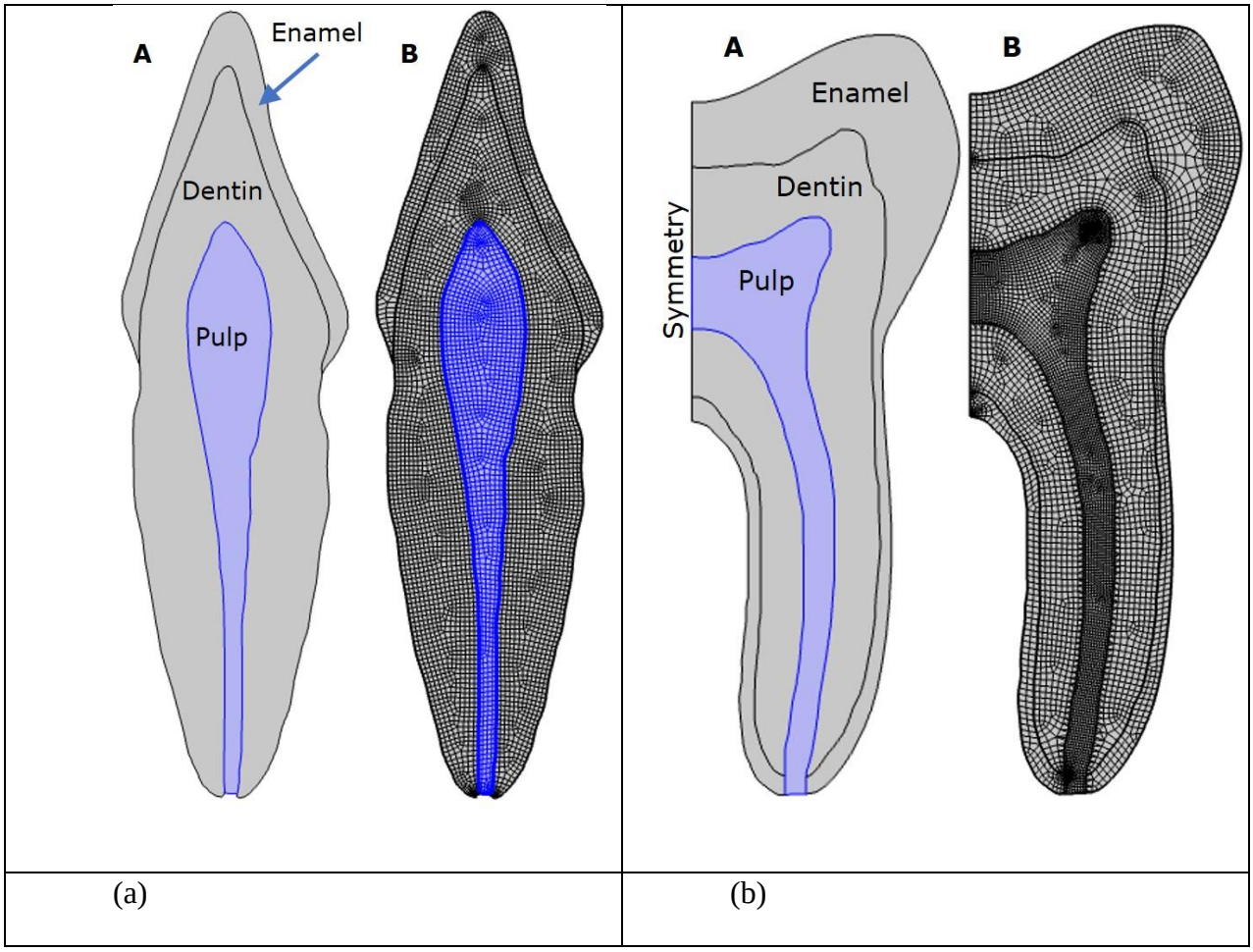

Figure 4.1. Two-dimensional finite element meshes of incisor (a) and molar (b) teeth. The physical models of the teeth with composite materials are shown in A, and the corresponding meshes in B. Spatial domains of enamel, dentin and pulp are denoted, each having unique diffusive, thermal, optical, mechanical, and prefusion properties. The grid geometry matches the anatomy of the teeth, with the element density greatest in regions in which gradients in properties are anticipated to be highest. The incisor model has 5810 quadrahedral mesh elements with 89,568 degrees of freedom. The molar model had 6992 quadrahedral mesh elements with 146,232 degrees of freedom.

All physical subdomains of heat and mass diffusion, light absorption, blood flow, and mechanical stress defined in the model are fully coupled together through co-dependent variables, properties, and time. A whitening process of 12 hours was used to

provide adequate time for manifestation of inflammatory injury mechanics to their completion, even though the actual physical treatment times were considerably shorter. The average computer run time for a single tooth model was 1.5 - 20 min depending on boundary conditions, using a parallel processing machine with 8 Intel I9 tenth generation processors with 64 GB RAM and Windows 10 Pro Multicore. Serial simulations were conducted with incremental values of the governing physical parameters to identify the sensitivity of the outcome to specific physical properties and protocol design.

Diffusion of H_2O_2

The movement of H_2O_2 through the incremental layers of the tooth occurs via molecular diffusion. The conservation of mass law (often called Fick's second law) can be applied throughout the entire tooth,

$$\frac{\partial c}{\partial t} + \nabla \cdot J = \dot{n} \tag{1}$$

where c is the concentration of diffusing species (kg/m^3), J is the flux (kg/m^2.sec) which must be expressed as a vector if movement is in more than a single direction as is the case during tooth whitening, and $\dot{n}$ is the rate of production or consumption of the species. Often there is another term in Eq. (1) to account for motion owing to net convection movement within the system, but the rigid structure of the tooth precludes this effect. Locally the diffusion flux is described in terms of Fick's first law.

$$J = -D\nabla c \tag{2}$$

where D is the diffusion coefficient (m^2/sec) that depends on the diffusing species and the substrate through which it is passing. It also may depend on temperature and pressure, which is relevant to consider during laser heating.

The concentration of H_2O_2 presented at the surface of the tooth is dictated by the composition of gel in a whitening strip and is described quantitatively as the boundary condition applied to solve Equation (1) for concentration as a function of position and time within the tooth.

Thermal Effects

Application of laser heating to the frontal surface of a tooth will result in absorption of energy in a pattern that depends on the optical and geometric properties of the tooth materials and the wavelength and intensity of irradiation. The transient temperature distribution that occurs in the composite tooth material is a result of the action of conservation of energy, as originally attributed to Pennes (1947) [27].

$$\rho C \frac{\partial T}{\partial t} = \nabla \cdot \left(k \nabla T \right) + \rho_b C_b \omega_b \left(T_b - T \right) + \dot{Q}_i \tag{3}$$

where ρ is tissue density (kg/m^3), C is tissue heat capacity (J/kg.K), T is temperature (K), with the subscripts $_b$ referring to blood properties, k is thermal conductivity (W/m.K), ω_b is blood perfusion through tissue (1/sec), and $\dot{Q}_i$ is the rate of heat generation from internal sources such as metabolism and absorption of laser energy (W/m^3). The boundary conditions vary around the periphery of the tooth from conduction with the cementum to convection with air in the oral cavity. It is important to note that blood perfusion occurs only in the pulp, and as inflammation may develop, resulting in

elevated interstitial pressure, the rate of perfusion will be reduced proportionately [24]. Since internal convection with flowing blood provides a cooling effect distributed throughout perfused tissue, heat transfer and temperature distribution will be affected directly by inflammation that generally reduces perfusion.

Inflammation in the Pulp

Normally, swelling of soft tissue occurs in conjunction with inflammation. Inflammatory mediators induce increased vascular permeability leading to fluid extravasation into the interstitial tissue and strain, which produces stress as the elastic properties of the tissue enable it to oppose swelling. Cell deformation occurs with swelling and is a leading cause of tissue injury. The elevation of internal stress opposes the perfusion of blood at local arteriolar pressure with the consequence that ischemia develops, which also contributes directly to cell necrosis. Notable exceptions to inflammatory-induced swelling occur when soft tissue is encased within a rigid structure, such as the brain within the skull and tooth pulp within dentin and enamel. The consequences of such physically constrained inflammation can be severe, and, in the case of traumatic brain injury, fatal.

To our awareness, there does not currently exist a quantitative model to describe the development of strain in soft tissue in conjunction with inflammation. Thus, we have constructed a model based on anticipated governing phenomena, including the accumulation of interstitial mass and the rate at which inflammatory injury may develop within tissue. This model is expressed in Equation (4).

$$e_{ifm} = \frac{K}{1 + e^{\left(-a\left(m_p - b\right)\right)}} \tag{4}$$

where ε_{ifm} is strain in the pulp resulting from inflammation, K is the maximum strain that can occur, a is related to the sensitivity of the pulp to being inflamed by H_2O_2 exposure (1/mg), b is a mass accumulation constant for the start of inflammation (mg), and m_p is accumulated mass of in the pulp chamber at any given time (mg). Since this representation of the development of inflammation in pulp is new, there are no existing data for the values of constitutive constants in Equation (4). Values were estimated by fitting the equation to data from the literature and are shown below [1,5,6,28].

Cell Damage Model

A possible outcome of the tooth whitening process is that it may progress to the point of cell injury or necrosis in the pulp. In general, this outcome may result from a combination of mechanical deformation of cells, ischemia, general inflammatory response, and thermal denaturation (Gefen, 2018). All of these injuries occur as rate processes over time, so that it is effective to describe them in terms of an Arrhenius style rate equation. A classic example is for burn injury in which the driving potential for molecular denaturation is temperature (Moritz and Henriques, 1947) [10,29–32]. Other injuries relevant to the current analysis are driven by mechanical strain of cell membranes and deprivation of O_2 and metabolites as well as accumulation of toxic metabolic waste products, both in conjunction with depressed local blood perfusion. The rate processes have a cumulative effect when integrated over time.

We have modified the Moritz and Henriques equation for thermal injury to include simultaneous ischemia and hyperthermia. Equation (5) contains new constitutive coefficients to account for the nonlinear coupling across multiple insult potential fields.

$$\Omega(T,w,t) = e^{-\int_0^t \left[\left(e^{l}\right)^{k} k \cdot e^{\left[g_T T(t)+g_w w(t)\right]} \cdot t^{(k-1)}\right] dt} \tag{5}$$

where previously undefined properties are: l is a scaling factor, k is a scaling factor, g_T is a weighting factor for the influence of temperature on injury development, and g_w is a weighting factor for the influence of blood perfusion on injury development. Estimates for these coefficients have been established based on matching with experimental data (Iaizzo, 1999) [33–36]. The values determined for these parameters are shown below.

RESULTS

The development of inflammation is with extravasation is assumed to reduce blood flow. Ischemia may act in concert with elevated temperature over time to cause a loss of cell viability. The interaction between these two factors as described by Equation (5) is illustrated in Figure 2.

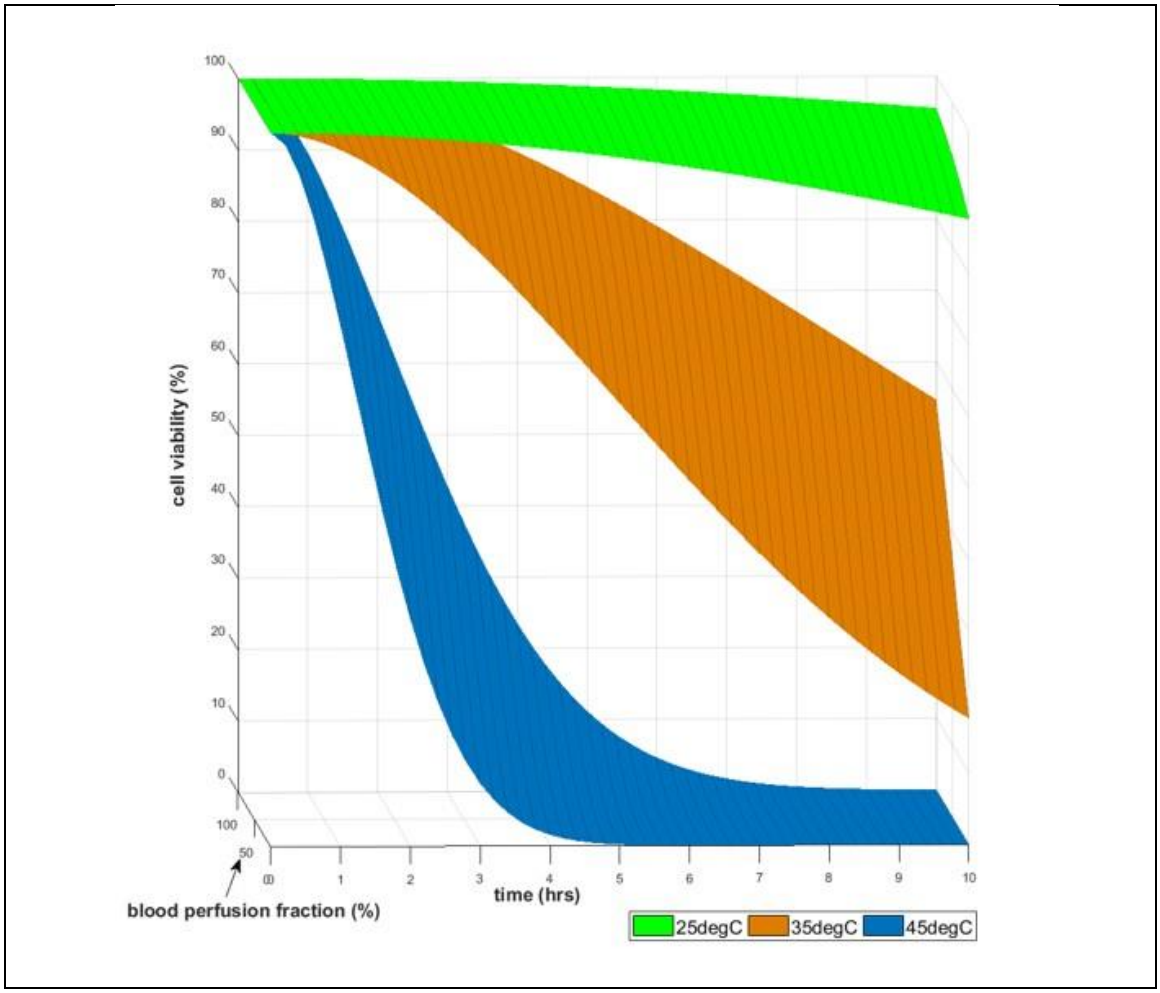

Figure 4.2. Combined actions of reduced blood flow and elevated temperature on accumulated cell injury over time. It is assumed that flow is reduced owing to applied mechanical stress and that the basal level of stress is high enough to elicit injury if continued for a sufficiently long time. Injury accumulates progressively overtime at a rate that increases significantly at higher temperatures that accelerate the action of ischemia. The finite element model predicts the occurrence of increased temperature and reduced blood flow in pulp as a function of applied whitening protocols. Adapted from data in Iaizzo () for combined effects of applied temperature and pressure on injury causation in soft tissue.

The response of teeth during whitening to both H_2O_2 and laser heating is dose-dependent. Higher H_2O_2 concentration results in more mass added, and higher irradiation

power produces greater temperatures. Plus, since both mass diffusion and heat transfer are transport processes, the shape of the tooth is important. Incisors have a much larger ratio of surface to volume than do molars so that they reach higher concentrations and temperatures for identical boundary conditions. This phenomenon is illustrated in Figure 3.

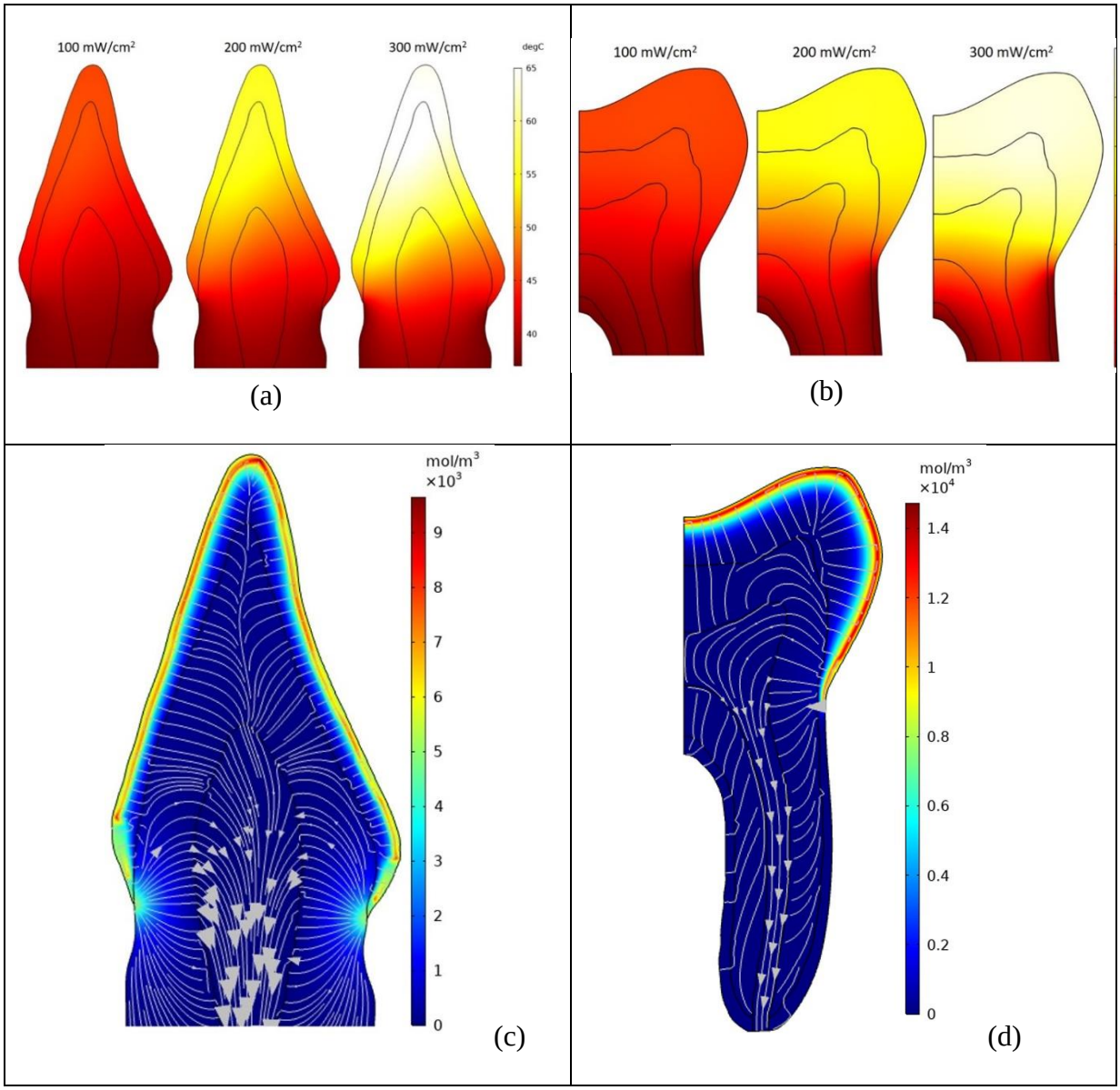
100 mW/cm²
200 mW/cm²
300 mW/cm²
degC
65
60
55
50
45
40
(a)
100 mW/cm²
200 mW/cm²
300 mW/cm²
(b)
mol/m³
×10³
9
8
7
6
5
4
3
2
1
0
(c)
mol/m³
×10⁴
1.4
1.2
1
0.8
0.6
0.4
0.2
0
(d)

Figure 4.3. Dose effect responses of both H_2O_2 diffusion and laser heating for incisor (a), (c) and molar (b), (d) teeth. Two-dimensional data are displayed as pseudocolor maps. (a) and (b) show steady-state temperatures reached after about 10 minutes of laser irradiation at the three power levels indicated. Note that the incisors rise to a much higher temperature that is caused by the larger surface-to-volume ratio enabling a greater amount of energy input per unit volume. The initial temperature was assumed to be 37ºC, and the innermost surface at the cementum is maintained at that value. A parallel response occurs for H_2O_2 diffusion in (c) and (d). Concentration profiles are indicated in pseudocolor, grid lines, and vector arrows showing the diffusion pathway. Concentrations are much higher in the incisor, meaning that the amount of material added is also greater, especially in the pulp that has the most susceptible as a site of inflammation.

Mechanical stresses may occur owing to a combination of temperature gradients causing differential displacement along with extravasation resulting from inflammation. Although mechanical stresses have been calculated for the enamel and dentin and may be important during laser heating, of greatest interest in this study is the pulpar stress that will arise from the dual action of thermal and inflammatory strains. Figure 4 shows these stresses.

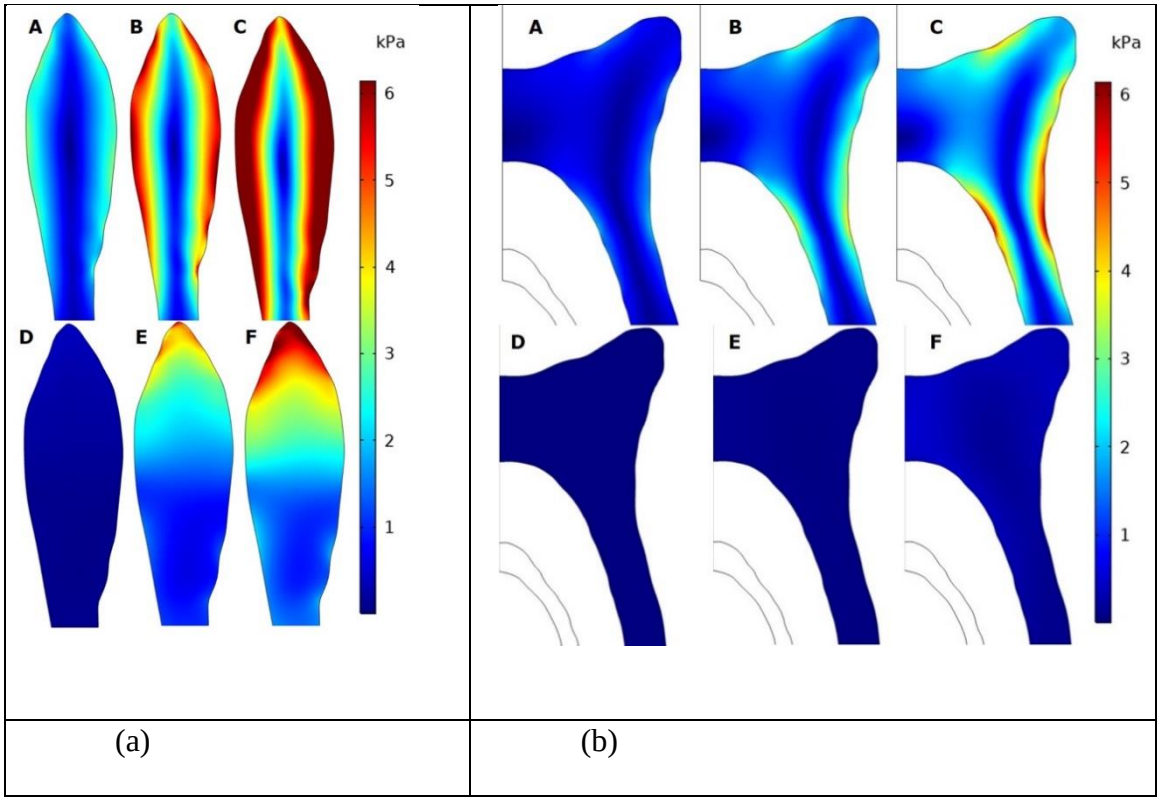

Figure 4.4. Stresses in incisors (a) and molar (b) at the completion of H_2O_2 diffusion and laser heating processes. A, B, and C are for laser heating at 100, 200, and 300 mW/cm^2, respectively. D, E, and F are for H_2O_2 diffusion at 15%, 30%, and 50% surface concentrations, respectively, applied for 30 minutes on the tooth surface. Note the very distinctive stress patterns resulting from the different insult processes emanating from the surface by radiation absorption and mass diffusion.

Finally, the model can be applied to predict differential injury to specific regions of the tooth for various whitening protocols defined in terms of H_2O_2 concentration and laser irradiation power density. Although we performed a very large array of parameter sweeps, space allows presentation of only a sample of the type of data obtained.

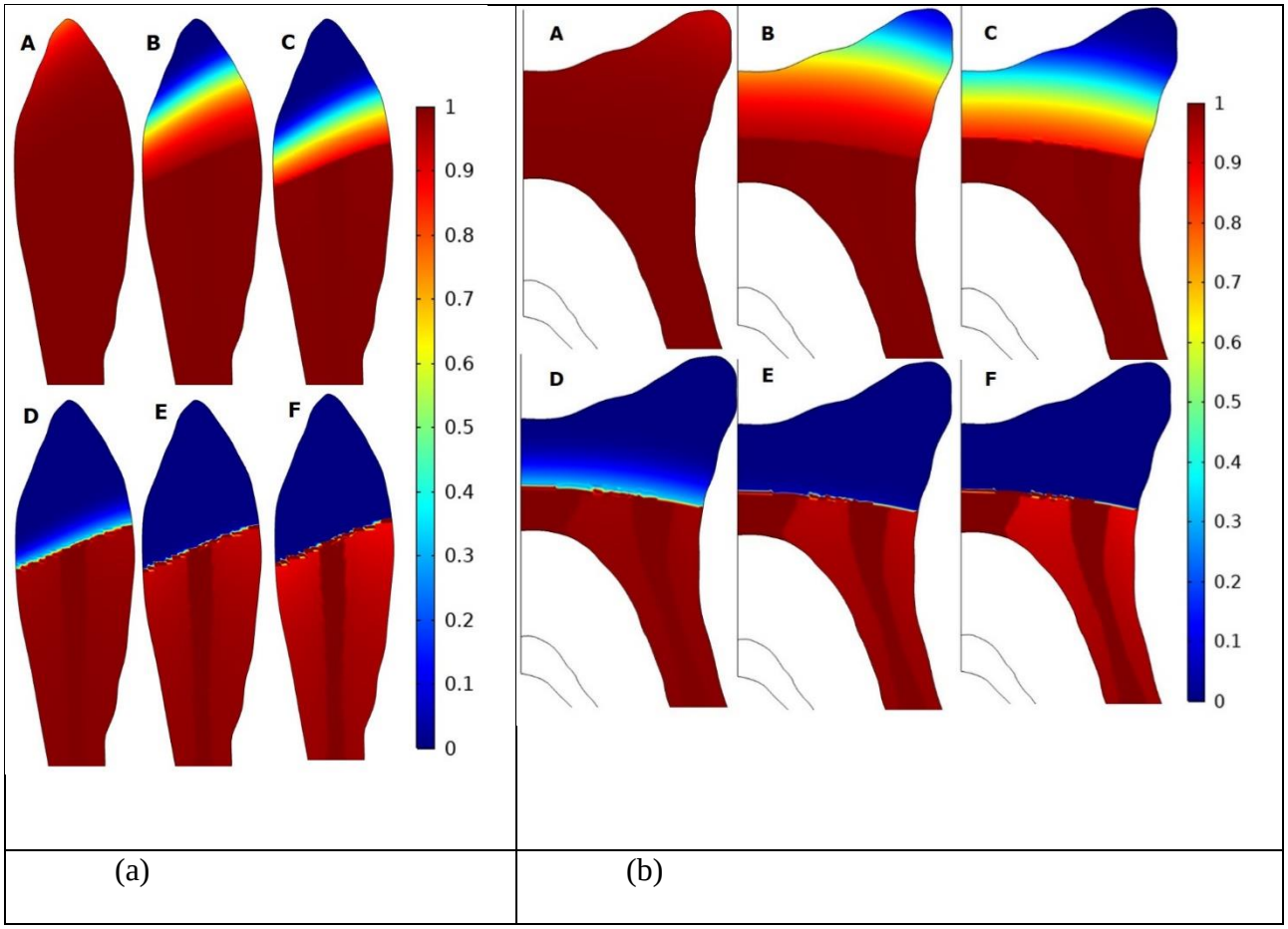

Figure 4.5. Distribution of damage to incisor (a) and molar (b) teeth from specific whitening protocols defined in terms of H_2O_2 concentration and application time and laser irradiation power density and application time. Cell Viability, 1 = 100%; less than 50%= irreversible damage

DISCUSSION

The process of whitening teeth with laser enhancement is highly complex to be able to describe quantitatively in terms of predictive models. Coupling across multiple analysis domains that are not typically addressed simultaneously presents a major challenge for developing a modeling tool that can be practically applied for designing protocols for

whitening procedures that are both effective and safe. This analysis demonstrates how the ability to screen the effects of applying different design protocols can be very useful.

This paper presents the background for development of a broad analysis tool for understanding the governing processes that define tooth whitening procedures. Much of the detail of the development is omitted owing to space limitations. However, specific optimization exercises will be executed for presentation and discussion in forthcoming papers.

CONCLUSION

In summary, we have successfully developed the first computer simulation model to describe the interactions between tooth whitening gel containing H_2O_2 as a bleaching agent, laser irradiation applied for enhancement of the bleaching effect, and the various physiological responses of various tooth tissues that may result in inflammation and injury. The model provides an effective tool for rapidly evaluating optimization procedures to design whitening protocols to balance the tradeoffs between improving outcome efficacy and limiting the risk of injury. Specific numerical examples are shown.

ACKNOWLEDGMENTS

This work was sponsored in part by the Robert and Prudie Leibrock Endowed Professorship in Engineering at the University of Texas and by a gift from The Proctor and Gamble Company to the Diller lab at UT.

REFERENCES

[1] Kwon, S. R., and Wertz, P. W., 2015, “Review of the Mechanism of Tooth Whitening,” J. Esthet. Restor. Dent., **27**(5), pp. 240–257.

[2] Rodrigues, F. T., Serro, A. P., Polido, M., Ramalho, A., and Figueiredo-Pina, C. G., 2017, “Effect of Bleaching Teeth with Hydrogen Peroxide on the Morphology, Hydrophilicity, and Mechanical and Tribological Properties of the Enamel,” Wear, **374**–**375**, pp. 21–28.

[3] Goldberg, M., Grootveld, M., and Lynch, E., 2010, “Undesirable and Adverse Effects of Tooth-Whitening Products: A Review,” Clin. Oral Investig., **14**(1), pp. 1–10.

[4] Silva-Costa RSG, Ribeiro AEL, Assunção IV, Araújo Júnior RF, Araújo AA, Guerra GCB, B. B., 2018, “In-Office Tooth Bleaching with 38 % Hydrogen Peroxide Promotes Moderate / Severe Pulp Inflammation FGF-2 and Osteocalcin in Rats Abstract,” J. Appl. Oral Sci., **26**(1), pp. 1–9.

[5] Colares, V. L. P., Lima, S. N. L., Sousa, N. C. F., Araújo, M. C., Pereira, D. M. S., Mendes, S. J. F., Teixeira, S. A., Monteiro, C. de A., Bandeca, M. C., Siqueira, W. L., Moffa, E. B., Muscará, M. N., and Fernandes, E. S., 2019, “Hydrogen Peroxide-Based Products Alter Inflammatory and Tissue Damage-Related Proteins in the Gingival Crevicular Fluid of Healthy Volunteers: A Randomized Trial,” Sci. Rep., **9**(1), pp. 1–11.

[6] Cohen, S. C., and Chase, C., 1979, “Human Pulpal Response to Bleaching Procedures on Vital Teeth,” J. Endod., **5**(5), pp. 134–138.

[7] Kim, S., 1985, “Microcirculation of the Dental Pulp in Health and Disease,” J. Endod., **11**(11).

[8] Kim, S., 1990, “Neurovascular Interactions in the Dental Pulp in Health and Inflammation,” J. Endod., **16**(2).

[9] Fekrazad, R., Alimazandarani, S., Kalhori, K. A. M., Assadian, H., and Mirmohammadi, S. M., 2017, “Comparison of Laser and Power Bleaching Techniques in Tooth Color Change,” J. Clin. Exp. Dent., **9**(4), pp. e511–e515.

[10] Henriques, F. C., 1947, “STUDIES OF THERMAL INJURY V. The Predictability and the Signinficance of Thermally Induced Rate Processes Leading to Irreverible Epidermal Injury,” **43**(5), pp. 489–502.

[11] STOLL, A. M., and GREENE, L. C., 1959, “Relationship between Pain and Tissue Damage Due to Thermal Radiation,” J. Appl. Physiol., **14**(3), pp. 373–382.

[12] He, X., and Bischof, J. C., 2003, “Quantification of Temperature and Injury Response in Thermal Therapy and Cryosurgery,” Crit. Rev. Biomed. Eng., **31**(5–6), pp. 355–422.

[13] Petersen, B. K., 2012, “Quantitative Analysis of the Diffusion of Hydrogen Peroxide through Teeth,” UCLA.

[14] Spitzer, D., and Ten Bosch, J. J., 1975, “The Absorption and Scattering of Light in Bovine and Human Dental Enamel,” Calcif. Tissue Res., **17**(2), pp. 129–137.

[15] Turrioni, A. P. S., De Oliveira, C. F., Basso, F. G., Moriyama, L. T., Kurachi, C., Hebling, J., Bagnato, V. S., and De Souza Costa, C. A., 2012, “Correlation between Light Transmission and Permeability of Human Dentin,” Lasers Med. Sci., **27**(1), pp. 191–196.

[16] Elgendy, H., Maia, R. R., Skiff, F., Denehy, G., and Qian, F., 2019, "Comparison of Light Propagation in Dental Tissues and Nano-Filled Resin-Based Composite," Clin. Oral Investig., **23**(1), pp. 423–433.

[17] Zach, L., and Cohen, G., 1965, "Pulp Response to Externally Applied Heat," Oral Surgery, Oral Med. Oral Pathol., **19**(4), pp. 515–530.

[18] Bouillaguet, S., Caillot, G., Forchelet, J., Cattani-Lorente, M., Wataha, J. C., and Krejci, I., 2005, "Thermal Risks from LED- and High-Intensity QTH-Curing Units during Polymerization of Dental Resins," J. Biomed. Mater. Res. - Part B Appl. Biomater., **72**(2), pp. 260–267.

[19] Sulieman, M., Addy, M., and Rees, J. S., 2005, "Surface and Intra-Pulpal Temperature Rises during Tooth Bleaching: An in Vitro Study," Br. Dent. J., **199**(1), pp. 37–40.

[20] Zezell, D. M., Ana, P. A., Pereira, T. M., Correa, P. R., and Velloso, W., 2011, "Heat Generation and Transfer on Biological Tissues Due to High-Intensity Laser Irradiation," *Developments in Heat Transfer*, BoD–Books on Demand, pp. 227–246.

[21] Kramer, I. R. H., 1960, "The Vascular Architecture of the Human Dental Pulp," Arch. Oral Biol., **2**(3).

[22] Van Hassel, H. J., 1971, "Physiology of the Human Dental Pulp," Oral Surgery, Oral Med. Oral Pathol., **32**(1), pp. 126–134.

[23] Matthews, B., and Andrew, D., 1995, "Microvascular Architecture and Exchange in Teeth," Microcirculation, **2**(4).

[24] Bragin, D. E., Statom, G. L., Yonas, H., Dai, X., and Nemoto, E. M., 2014, "Critical Cerebral Perfusion Pressure at High Intracranial Pressure Measured by Induced Cerebrovascular and Intracranial Pressure Reactivity," Crit. Care Med., **42**(12), pp. 2582–2590.

[25] Dick, S. K., Chistyakova, G. G., Terekh, A. S., Smirnov, A. V., Salimi Zadeh, M. M., and Barun, V. V., 2014, " Characterization of Blood Flow Rate in Dental Pulp by Speckle Patterns of Backscattered Light from an in Vivo Tooth ," J. Biomed. Opt., **19**(10), p. 106012.

[26] Meyer, M. W., 1993, "Pulpal Blood Flow: Use of Radio-labelled Microsoheres," Int. Endod. J., **26**(1).

[27] Pennes, H., 1948, "Analysis of Tissue and Arterial Blood Temperatures in the Resting Human Forearm," J. Appl. Physiol., pp. 5–34.

[28] Vaz, M. M., Lopes, L. G., Cardoso, P. C., de Souza, J. B., Batista, A. C., Costa, N. L., Torres, É. M., and Estrela, C., 2016, "Inflammatory Response of Human Dental Pulp to At-Home and in-Office Tooth Bleaching," J. Appl. Oral Sci., **24**(5), pp. 509–517.

[29] Moritz, a. R., and Henriques, F. C., 1947, "STUDIES OF THERMAL INJURY II. The Relative Importance of Time and Surface Temperature in the Causation of Cutaneous Burns.," Am J Pathol, **23**, pp. 695–720.

[30] Moritz, A. R., Henriques, F. C., Durtra, F. R., and Weisiger, J. R., 1947, "STUDIES OF THERMAL INJURY IV. An Exploration of the Casualty-Producing Attributes of Conflagrations; Local and Systemic Effects of General Cutaneous Exposure

to Excessive Circumambient (Air) and Circumradiant Heat of Varying Duration and Intensity," Arch. Pathol., **43**(5), pp. 466–488.

[31] Moritz, A. R., 1947, "STUDIES OF THERMAL INJURY III. The Pathology and Pathogenesis of Cutaneous Burns An Experimental Study," Am. J. Pathol., **13**(6), pp. 915–941.

[32] Henriques, F. C., and Moritz, A. R., 1947, "STUDIES OF THERMAL INJURY I. The Conduction of Heat to and through Skin and the Temperatures Attained Therein. A Theoretical and an Experimental Investigation.," Am. J. Pathol., **23**(4), pp. 530–549.

[33] Kokate, J. Y., Leland, K. J., Held, a M., Hansen, G. L., Kveen, G. L., Johnson, B. a, Wilke, M. S., Sparrow, E. M., and Iaizzo, P. a, 1995, "Temperature-Modulated Pressure Ulcers: A Porcine Model.," Arch. Phys. Med. Rehabil., **76**(7), pp. 666–673.

[34] Iaizzo, P. A., Kveen, G. L., Kokate, J. Y., Leland, K. J., Hansen, G. L., and Sparrow, 1995, "Prevention of Pressure Ulcers by Focal Cooling: Histological Assessment in a Porcine Model.," Wounds A Compend. Clin. Res. Pract., **7**(5), pp. 161–169.

[35] Hansen, G. L., Sparrow, E. M., Kokate, J. Y., Leland, K. J., and Iaizzo, P. A., 1997, "Wound Status Evaluation Using Color Image Processing," IEEE Trans. Med. Imaging, **16**(1), pp. 78–86.

[36] Kokate, J. Y., Leland, K. J., Sparrow, E. M., and Iaizzo, P. A., 1997, "Critical Thresholds for Pressure Ulcer Formation in a Porcine Model," Wounds, **9**(4), pp. 111–121.

Chapter 5: Conclusion

This research aimed to develop a functional injury model that could work in a finite element analysis (FEA) simulation to understand how products affect humans. I further wanted to develop a fully functional FEA model using commercial software with complex Multiphysics and the injury model to evaluate medical devices and consumer products.

Chapter 2 I present a new novel approach for mathematically modeling injury kinetics with two different types of wounds, pressure injuries PI and thermal injuries TI. The injuries have an overlapping condition under particular tissue loading, temperature, and time. The model goodness of fit is demonstrated against experimental data for both PI and TI with high agreeance. Even though the mathematical model is in the beginning stages of development, it meets or exceeds existing injury prediction methods for similar methods.

Chapter 3 I present a nonlinear simulation combining the injury model, tissue mechanics, and heat transfer for a person sitting on a seat. I compare two subject types, those with and without a spinal cord injury (SI). I demonstrate using available off-the-shelf tools and software that a simulation can be made to analyze the difference in how two different subject types interact physiologically with the seat under various conditions. The results align with the outcomes of other studies regarding how SI subjects are more susceptible to injury.

Chapter 4 I show how the injury model can be applied to a commercial tooth-whiting product. According to Proctor & Gamble, it is the most advanced tooth model to date. For this simulation, I demonstrate a new tissue inflammatory method by relating swelling to the amount of mass infiltrating the dental pulp. By combining effects of

laser/light, bioheat transfer, tissue mechanics, inflammation, mass diffusion of H_2O_2, and injury model, various types of device parameters can be tested for what kind of impact they will have on the dental pulp. It was revealed that it could take up to 6-8 hours after the application of H_2O_2 ended before peroxide stopped diffusing into the pulp chamber.

Appendix

Raw unedited data, tables, and figures from the dental model simulation for use in multiple manuscripts for dental journals.

Background

Tooth whitening has become a widely adopted practice for aesthetic purposes in both clinical and home settings. Bleaching devices are available to individuals on an over-the-counter basis and therefore may be used in the absence of oversight by health care professionals, making safety of the user a primary concern. Many technologies make use of hydrogen peroxide (H_2O_2) as a bleaching agent to remove discoloration from teeth based on its powerful oxidizing properties. Chemical reaction of free radicals released by the peroxide with pigments or chromophores in the extracellular matrix of the tooth constitutes the basis for tooth whitening[1].

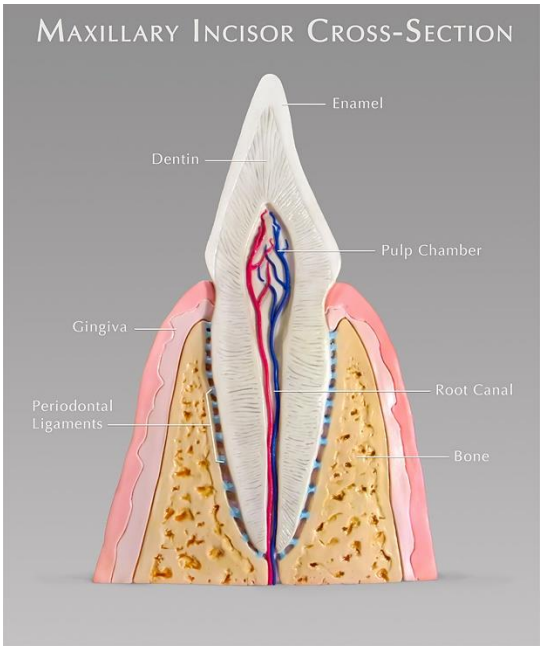

Figure 13 Cross-sectional view of the Maxillary Incisor. Photo provided by Stream Studios: Medical Illustration

A cartoon of tooth anatomy is shown in Fig. 1. Tooth whitening agents are typically applied to the surface of the enamel that is the target of their operation. Note that the pulp chamber in the innermost region of the tooth contains active blood perfusion through a network of larger supply veins and arteries that branches into a plexus of microvessels that provide the nutritional supply to the tooth.

It has been demonstrated that laser-assisted bleaching can be used to enhance the kinetics of the release of free radicals from within a gel applied to the surface of a tooth to decrease the time required to achieve a whitening effect[2]. However, a cautionary approach must be used when augmenting H_2O_2 with light activation since an optical source is by definition an energy-dissipative device that will cause of an accumulation of energy at a site of absorption leading to a local temperature rise. If the temperature reaches a threshold level, irreversible thermal injury to tissue may occur. This process has been very well defined for many years, and has been demonstrated innumerable times in a multitude of biological specimens[3–5].

On a different front, it is well known that the tooth whitening agent, H_2O_2, can cause inflammation to pulpal tissue as well as degrading the enamel and dentin[6–9]. Usually, tooth whitening can be conducted in a manner that minimizes the risk of damage while balancing the need to produce a whitening effect. H_2O_2 is able to diffuse to the pulp through the overlying enamel and dentin that is permeable to diverse molecules at rates based primarily on size and configuration[10]. The presence of H_2O_2 as a noxious chemical stimulant causes the neurological release of inflammatory mediators leading to vasodilation and molecular extravasation with a concomitant increase in pulpal tissue pressure[11,12].

The inflammatory response of dental pulp is highly dependent on its microvascular physiology and function that have been characterized in detail relevant to the present

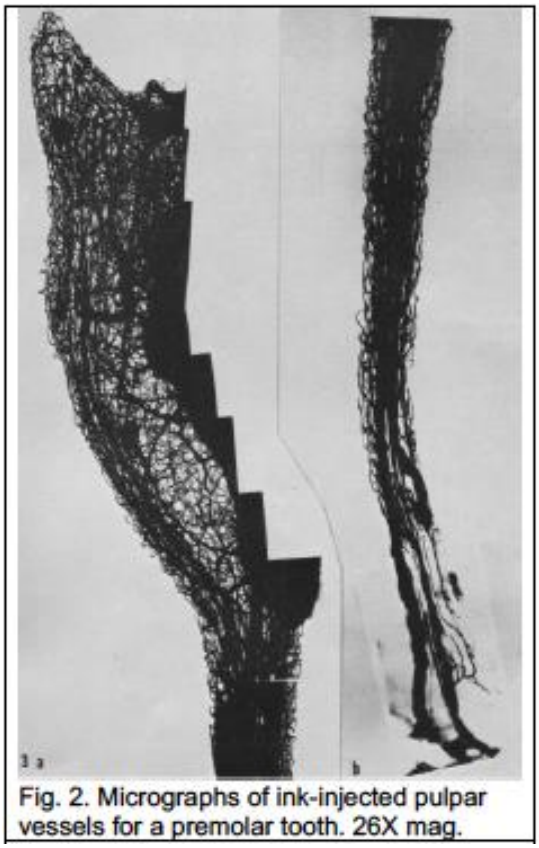

Figure 14 The is a republication of a photo from Kramer [ref] Photo of vacular casting of dental pulp tissue. The tissue is higly vacular.

analysis[11,13]. Fig. 2 shows an image of the pulpar vessels in an extracted premolar tooth after being injected with India ink[14]. Both images are from the same tooth. The left side image is of the pulp chamber and coronal aspect of the root canal. The right image is a continuation of the vasculature to the bottom of the root canal, where it meets the larger arterial and venous supply vessels. The ink has penetrated to the smallest size of vessels. Obviously, the pulp has a rich vascular network, and this vasculature plays a key role in maintaining the health of a tooth and in the inflammatory response to noxious insults.

When a H_2O_2 gel is applied on the surface of a tooth, it may reach the pulp cavity via diffusion through the enamel and dentin[15]. The diffusion properties of these tooth materials to specific molecular species have been studied and characterized[10,16]. The result is the buildup of the H_2O_2 concentration in the pulp that will issue inflammation. As the inflammation sequence progresses, one of the primary consequences is vascular permeability and fluid extravasation into the interstitial matrix. Ordinarily in soft tissue, these sequelae of events produce local swelling, perhaps with blister formation. However, the rigid, low compliance enclosure of the pulp formed by the dentin and enamel prevents

mechanical swelling, resulting in an increase in tissue pressure. This process may be considered analogous to the reaction to a traumatic brain injury (TBI) in which the highly perfused soft tissue of the brain is subjected to inflammation but is unable to swell owing to being enclosed within the rigid cavity of the skull[17]. TBI has been studied extensively, including the dynamics of the transient response of internal blood perfusion. This understanding will be extrapolated in the present study to the analysis of inflammation in the tooth pulp.

Inflammation-induced extravasation will cause the pulpal tissue pressure to rise, opposing the perfusion pressure of circulating blood and contributing progressively to a developing state of ischemia. The persistence of ischemia over time in combination with mechanical injury to cells because of elevated local pressure will lead to cell damage and tissue necrosis[18]. An associated phenomenon early in the process may be the pain that sometimes occurs with the use of whitening agents. However, the fact that tooth whitening technologies are widely practiced without inducing serious inflammatory side effects indicates that careful methodology can control this phenomenon.

Simple chemical-based whitening can be enhanced by augmentation with light-based activation. The tooth pulp is particularly at risk for suffering thermal injury during a light-enhanced tooth whitening procedure[19]. Temperatures in the pulpal cavity and on the surface of extracted teeth have been measured in vitro via an inserted thermocouple in response to irradiation by broad-spectrum light sources and a monochromatic laser (IR - λ=800nm at 3W power delivery)[20]. Laser irradiation lasted 30 sec. Both the surface and pulpal temperatures were considerably higher for the laser than for equivalent broad-

spectrum lights. The laser caused a pulpal temperature rise above ambient of 13.2±2.6°C averaged across six repeated trials in four different tooth types when the surface was uncovered[20]. When a tooth whitening gel was applied to the surface, the pulpal temperature rise was reduced to 7.9±0.8°C. Extrapolated to in vivo circumstances in which the initial pulpal temperature may be on the order of 37°C, the intra-pulpal temperature without gel for the same irradiation conditions could be expected to rise to as high 50±3°C. The long-standing data of Henriques shows that at this combination of exposure time and temperature, at least 30 sec for the worst condition (at 53°C) or for 1,300 sec for the least risky condition (at 47°C) is required to produce reversible thermal trauma, and 50 sec to 2,400 sec to produce the lowest level of irreversible injury[3]. Obviously, the thermal damage process is a highly nonlinear function of temperature in this range, making the prediction of injury problematic. Tooth restorative procedures have been demonstrated to cause similar rises in pulp temperature[21]. In another study, direct contact heating of the tooth surface with a high temperature (275°C) depended on pure conduction through the outer layers to reach the pulp. For exposure times ranging from 5 to 20 sec, the intrapulpal temperature rises varied from 4 – 30°F (2.2 – 16.7°C)[22]. Temperatures well into the mid to high 40's for exposures of 2 to 3 minutes did not give rise to pulpal injury. An important conclusion to take from this background information is that it is possible to use laser illumination for enhancement of H_2O_2 for tooth whitening without causing direct irreversible thermal injury of the pulpal tissue. However, the effect of elevated temperatures on the inflammation process in pulp may be an important consideration for the design of tooth whitening technologies.

The coupled interaction between H_2O_2 and temperature rise due to light irradiation is a consequence of the fact that the injury kinetics associated with H_2O_2 induced inflammation are strong functions of temperature. This type of phenomenon in which tissue temperature and pressure-induced inflammation have a combined synergistic effect on wound causation has been identified in limited contralateral scientific studies[23,24]. It has also been encountered in unexpected contexts such as vehicle seat heaters. When both thermal and pressure insults operate simultaneously, soft tissue injury may occur for elevation in temperature that is less than required to produce thermal injury based on molecular denaturation processes, i.e., a burn. Unfortunately, this pressure/temperature/blood flow coupling is frequently misunderstood, leading to medical opinions in which injury causation is interpreted incorrectly in terms of a purely thermal insult source[25]. This interpretation is misaligned with the actual science of how burns occur, leading to opinions and advice that are misleading and problematic[3,26]. Apart from an appreciation of the coupling among the mechanical/thermal/flow domains, it is difficult, if not impossible, to reconcile the governing scientific data with experiences derived from medical practice.

Hypothesis

The hypothesis of the present analysis is that during laser enhanced tooth whitening procedures coupled thermal and mechanical effects occur that govern blood perfusion to the pulp and and that dictate mechanisms of inflammatory injury. These coupled phenomena may be described in terms of established analytical methods and tools derived from biomedical engineering and applied to predict the response to specific whitening

protocols. This capability may be applied to guide the design of protocols to achieve a balance between whitening efficacy and risk of inflammatory injury. In the present study this hypothesis is explored and developed to the extent that its applicability to tooth whitening can be evaluated and provide a more mechanistic understanding of the events that govern the tissue response to application of chemical whitening agents enhanced by illumination with laser light.

This analysis approach falls within the domain of a more general problem that we have studied in other medical contexts. Common features of these phenomena include complexity of anatomical geometry, composite materials structures, cross coupling over multiple physical domains, and nonlinar behavior. Their analysis requires sophisticated numerical methods having the capability of integrating processes that occur in response to simultaneous independent driving forces. For example, coupling effects across the mechanical (applied pressure and tissue stress), thermal (elevated tissue temperature), and fluid flow (blood perfusion through the vasculature) domains present a highly nonlinear analysis challenge. We have developed generalized multiphysics modeling methods using finite elements adapted to tooth whitening with laser light technology [cite McGregor-Rego modeling paper]. In this paper we offer a brief presentation of the foundation for the governing physical model of the system and processes with adaptation to the morphology and constitutive properties of the composite tooth, followed by the solution of the model, presentation and discussion of the data, and recommendations for interpretation and application of the results.

Finite Element Model

The finite element method (FEM) of analysis has been used very widely as a tool to solve partial differential equation models in diverse fields including heat transfer, mass diffusion, fluid flow and solid mechanics, all of which apply to the current analysis of tooth whitening processes. A subject of interest is divided into numerous subcomponents called finite elements by constructing a mesh that represents the three-dimensional shape of the system. The mesh presents a finite number of intersection points for which the differential equations can be transformed into a large set of algebraic equations that can be solved numerically on a computer in conjunction with the appropriate boundary conditions for a problem. The FEM is a very powerful technology that has been applied to analyze and design huge numbers of challenging design and operational problems.

The FEM process model for tooth whitening is derived from our past work on analyzing the effect of coupled interactions between thermal, fluid flow, and mechanical loading on causing injury to soft tissues. Adaption to the laser-enhanced tooth whitening process requires information about processes and properties specific to tooth physiology and morphology and the components of treatment, as follows.

The model is based on governing equations that describe heat diffusion, mass diffusion, fluid flow (blood perfusion), and the kinetics of inflammatory-induced injury. Empirical data is required to define values for physical and physiological properties and kinetic constants. Much of this information can be obtained or extrapolated from existing literature as discussed in the Background section. This data was augmented with unpublished data provided by Proctor and Gamble as derived from internal studies.

We have previously developed the governing equations for the response to the loading of soft and hard tissue composites in the mechanical and thermal domains that interact with the perfusion of blood through the vasculature. Implementation for a description of the tooth whitening problem requires that a finite element mesh be set up to replicate tooth morphology and to embody relevant properties of the different tissue types that compose the tooth. To this end, we have taken a representative diagram of an incisor tooth and outlined the boundaries between the different tissue regions, as shown in Figure 3. Alternatively, a molar tooth geometry is also modeled. The geometry was assumed to be symmetric about the centerline as shown in Figure 4, with each region having unique physical properties and physiological behavior. The tooth drawing was digitized and manually traced with special software applied to create a defined boundary between the component tissues. The dimensions of the drawing outline were scaled or modified based on data from the dental anatomy literature. [Endodontics: Principles, Brokos et al ,Biuki et al, Martos et al 2 papers,]

The separate anatomical regions of the tooth and the corresponding finite element mesh for the molar and incisor teeth are shown in Figures 4 and 5. The mesh density is greatest at material interfaces and at the smallest radius of curvature where highest property gradients are anticipated to provide better resolution of the transport processes. The governing equations for the thermal, mechanical, and blood perfusion processes are solved on this grid using the COMSOL MultiPhysics commercial software package.

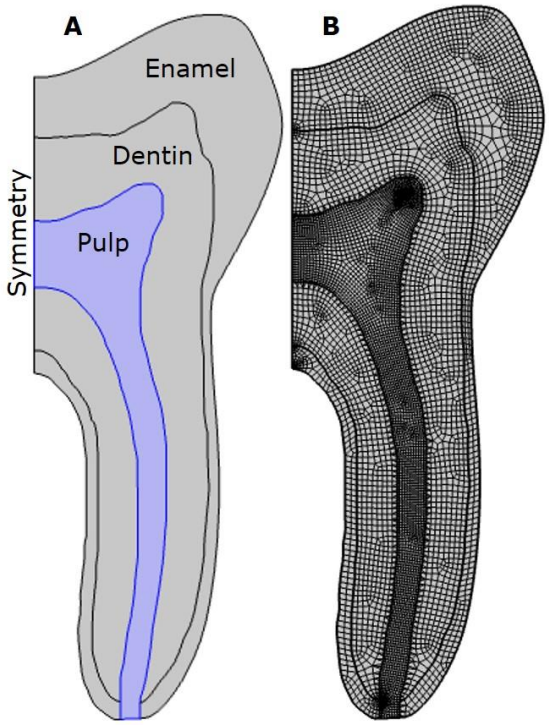

Figure 15 A shows the modeled molar domain with axis of symmetry. B is the a view of the mesh built and opttimized for running simulations

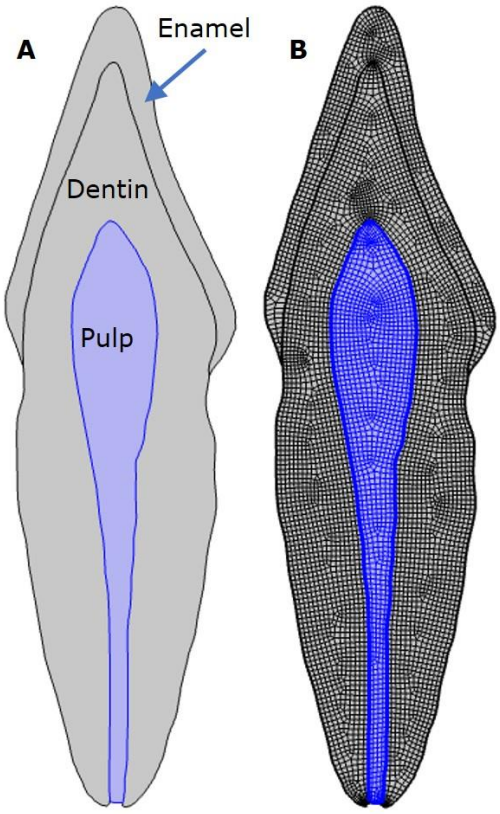

Figure 16 A shows the modeled incisor domain with axis of symmetry. B is the a view of the mesh built and opttimized for running simulations.

Physical Systems within FE Model

Fully Coupled Transient time-dependent problem

All physical subdomains of heat and mass diffusion, fluid flow, and mechanical stress defined in the model are fully coupled together through co-dependent variables, properties, and time. The model requires several physical domains to be solved to generate a solution. When integrating physical processes from traditionally independent functional domains, two primary approaches are used for obtaining a solution in Comsol. The first is called One-way coupling, which entails solving a solution in one physical domain and then passing that solution to the next domain solver for chaining the solutions together. One-way coupling is the most common and computationally efficient way for solving complex systems. However, a high level of dependency among the system variables across different domains can lead to solution errors, in which case several solver iterations are needed to generate a stable solution. An example of a one-way coupled problem is to first solve for heat transfer and temperature distribution within a material and then translate the temperature field data to a solid mechanics domain so thermal stresses can be calculated within the same material.

This approach works well for combined thermal and mechanical loading that is limited to processes involving only small deformations since the stress and strain from the solid mechanics analysis have little effect on the solution from the thermal model. A second method for analyzing combined thermaly, mechanical and fluid flow processes is fully coupled. In this case, most if not all of the system state variables must solved simultaneously. Downsides to this method are that it is often problematic to obtain convergence of the solution within the solver routine and long computer run times are required to obtain a solution. In some highly nonlinear problems, computer solution times are increased by order of magnitude above those required for one-way coupling methods.

The actualy physical system and processes embodied in laser mediated H_2O_2 diffusion to produce tooth whitening involve highly coupled interactions involving multiple domains of fields, forces and flows. Further, many constitutive material properties are cross domain dependent. Therefore, the time-dependent fully coupled model approach was selected for solution development. Fortunately, even though the system is nonlinear, its behavior is linear enough to not require sizeable computational time to obtain solutions. The incisor model had 5810 quadrahedral mesh elements with 89,568 degrees of freedom. The molar model had 6992 quadrahedral mesh elements with 146,232 degrees of freedom. A physical processing time of 12 hours was selected to simulate inflammatory injury mechanics to their completion. The average computer run time for a single tooth model was 1.5-20 min depending on boundary conditions on a machine using 8 Intel I9 tenth generation cores processors, 64 GB RAM Windows 10 pro multicore. Serial simulations

were conducted with incremental values of the governing physical parameters to identify the sensitivity of the outcome to specific physical properties and protocol design. The entire parameter sweep through all iterations required 2hrs 45 minutes of continuous computing.

The analysis principles are presented individually in the following sections of the paper for each of the individual process domains included in the model. The domains include: solid mechanics (stress / strain relationships); thermal effects (heat transfer and temperature driven injury processes); mass diffusion; development of inflammation; and cell injury and necrosis.

Solid Mechanics

Solid mechanics principles dictate the relationship between stress and strain within a tooth. Boundary conditions represent material constraints such as applying a physical load to the tooth, thermal expansion of the tooth resulting from heating procedures, swelling of pulp due to inflammatory response, and internal stresses generated from grinding operations from cavity removal. The material's mechanical properties are accounted for in the physical system to determine how the tooth will behave under changes to the environment.

Solid mechanics problems are solved by linear or nonlinear methods as a function of the extent of deformation that has occurred. Linear methods can be applied when deformations are small, which often is associated with very rigid materials. Nonlinear

methods are required when deformations are large as occurs in soft tissues of the heart and muscle, cushions and chairs, tires on a car. For the presented model, linear assumptions are applied due to the enamel's hardness. Large deformations result in fracture failure. Given that the pulp is encased in the rigid outer structures of the tooth, its deformations are also constrained to be small. The governing equations applied for the linear mechanical model used in this analysis are the following:

$$\nabla \cdot \sigma + \mathrm{F} = 0 \quad (1)$$

$$\varepsilon = \frac{1}{2}\left[(\nabla \mathbf{u})^{\mathrm{T}} + \nabla \mathbf{u}\right] \quad (2)$$

$$\sigma = \mathrm{C}\colon \varepsilon_{tot} \quad (3)$$

$$\mathrm{C} = C(E, \nu) \quad (4)$$

$$\varepsilon_{tot} = \varepsilon - \varepsilon_{inel} \quad (5)$$

$$\varepsilon_{inel} = \varepsilon_{th} + \varepsilon_{ifm} \quad (6)$$

$$\varepsilon_{th} = a(T)\left(T - T_{ref}\right) \quad (7)$$

σ is stress (N/m^2 or Pa)

F is boundary force (N)

ε is elastic strain

u is displacement (m)

C is second order tensor for storing material properties

E is Young's modulus

ν is Poisson's ratio

ε_{tot} is final or total strain

ε_{inel} is the inelastic strain

ε_{th} is strain from thermal expansion

ε_{ifm} is strain from inflammation

α is linear coefficient of thermal expansion ($1x10^{-6}$/°C)

Table 1 solid mechanics material properties used in the simulation for dental tissue.

Material	v	E [GPa]	α [$1x10^{-6}$/°C]
Enamel	0.33	84.1	17.0
Dentin	0.31	18.6	10.6
Pulp	0.45	0.002	180

Table 5 Mechanical properties of tooth materials, from Koycu et al

The single mechanical boundary condition applied is the constraint of no deflection on the root surface, as shown in Figure 6. The remainder of the tooth outside the axis of symmetry is free to move. With no external applied loading, the internal stresses and strains will result from thermal expansion due to temperature gradients and inflammatory swelling in soft tissue.

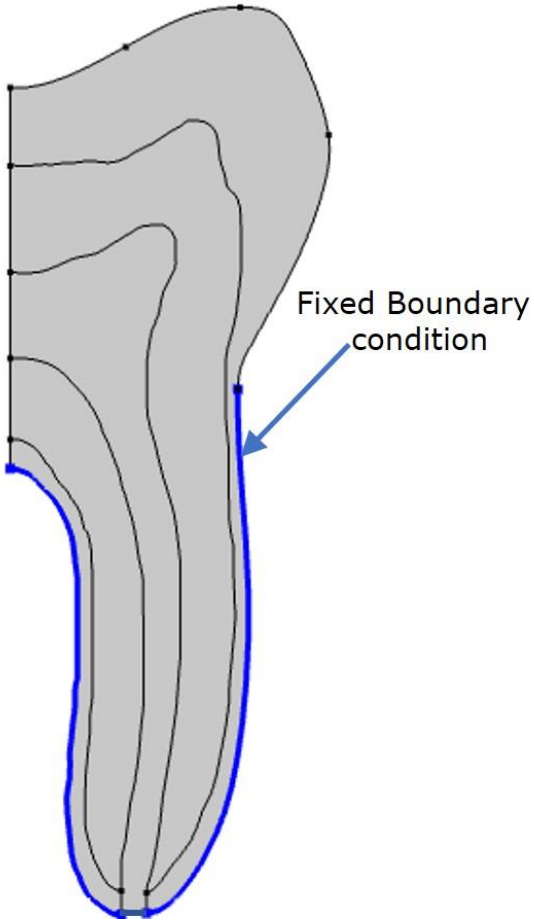

Figure 17 Mechanical boundary conditions for model. The blue line represents a fixed unmoveble boundary.

The solid mechanic governing equations are coupled to other physical systems through the dependency of material properties being dependent on non-mechanical properties such as temperature. Thus, temperature changes may result in a lower or higher yield strength and failure state.

Thermal Effects

Heat transfer processes play a vital role in the tissue response to laser irradiation. The system of interest is a tooth consisting of multiple composite materials, each having

unique properties and dimensions. Interactions with the environment include energy input via absorption of incident laser irradiation, convection with air in the mouth, conduction to adjacent tissues, and convection with blood perfused through the pulp. It is important to note that there is no single temperature associated with the tooth since thermal gradients will exist within the interior and is expected to change over time. Prediction of the spatial and temporal variations in temperature is a significant focus of the analysis presented in this paper.

Temperature modulates several potential injury processes. Most obviously a direct thermal injury occurs if a threshold temperature is reached. Temperature also influences the level of blood perfusion, the tissue mechanical properties, and sensitivity to pressure injuries. This coupling effect across multi-energy domains is complex and has been the subject of only limited prior systematic experimental and modeling studies. The current paper represents an initial foray into this arena.

The bioheat transfer system relates energy in the form of heat to the measurable property temperature. In standard heat transfer problems, conduction, convection, and radiation are solved to determine heat flow and temperature distribution in the material. In biological problems, modifications to the conduction equation are used to account for metabolic heat generation and internal convection within the tissue from blood flow. Temperature distribution within the model is important for biological processes and the material properties and temperature gradient within the enamel and dentin regions. Large temperature differences in the tooth can induce thermal stresses, leading to cracks within the enamel and dentin [Koycu,Iman]. Elevated temperatures in the soft tissue led to thermal

injuries. The current simulation only accounts for soft tissue damage. A temperature above 43 1/2 °C results in a burn given enough time [Henriques]. For every 1 °C above 44 results in an exponential time decrease when a burn forms based on the Arrhenius equation [Henriques].

In the model, the initial temperature of all materials is set to 37 °C. Thermal boundary conditions are defined in Figure 7. The governing equation for modeling tissue heat transfer is the Penne's equation (eq. (8)) which is a modification of the Fourier equation to account for internal convection with blood flow and cellular metabolism [Penne's cite]. The proposed version for the simulation add two special features to the Penne equation. The first is a spatially and temporally distributed heat generation term for laser irradiation. The second is a novel injury model that derives from the perfusion term as a function of internal stress to account for a reduction in blood flow due to increase internal stresses within the soft tissue domain. Since little is known about stress-related blood flow reduction within the dental pulp, an inverse linear relationship with diastolic blood pressure is a first approximation until future studies conducted.

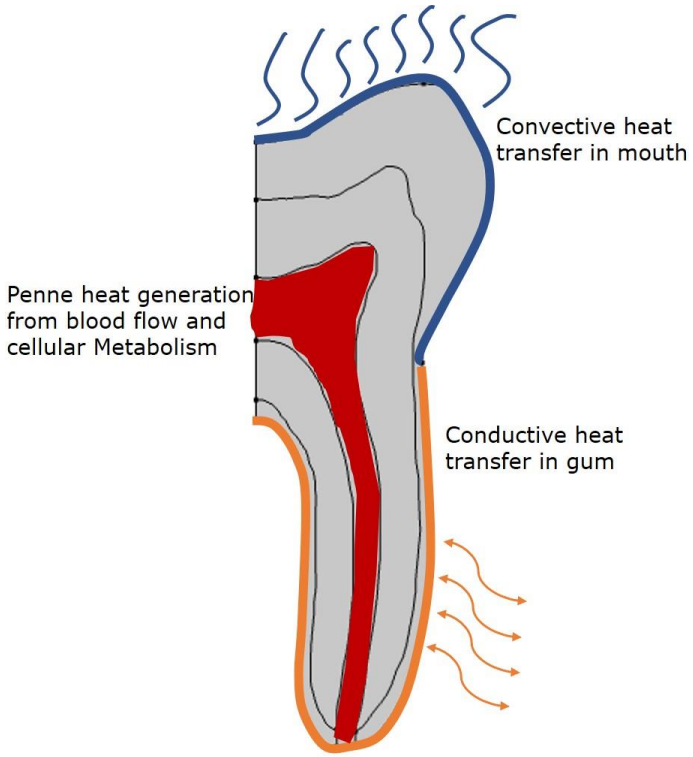

Figure 18 Thermal boundary conditions. Pulp shaded red acts as a heat generator. The blue boundary region of the tooth above the gum line and therefor has a convective boundary condition. The orange boundary condition is the region of the tooth below the gum line and is therefor a conductive boundary condition.

The orange region of Figure 7 is conduction within the root area is a constant boundary temperature of 37 °C. The exposed portion of the tooth in blue is given a constant convection coefficient of 15 W/m^2 with an air temperature of 37 °C. The boundary conditions are held constant from out the entire time domain of the simulation. The convection coefficient and air temperature are based on humans breathing out through their mouths. Alternatively, time-varying boundary conditions can be substituted to account for more realistic environmental conditions or different dental procedures and methods. One example would be removing the convective heat transfer coefficient and placing in

conductive heat transfer condition on the exposed portion of the tooth when anticipating a person closing their mouth over a particular period within the simulated time domain.

The equations used to model bioheat transfer are as follows:

$$\rho C \frac{\partial T}{\partial t} = \nabla \cdot (k \nabla T) + Q_{met} + \rho_b C_b \omega_f \omega_b (T_b - T) + Q_r \quad (8)$$

$$\omega_f = 1 - \frac{\sigma}{120 mmHg} \quad (9)$$

ρ is the density of tissue (kg/m^3)

C is the heat capacity at constant pressure in the tissue (J/(kg·K))

T is the absolute temperature of the tissue

k is the thermal conductivity (W/(m·K))

Q_{met} is the metabolic heat generation of the tissue (W/m^3)

ρ_b is the density of blood (kg/m^3)

C_b is the heat capacity at constant pressure in the blood (J/(kg·K))

ω_b is the blood profusion rate (1/s)

ω_f is the blood profusion fraction from internal stress rate (1/s)

T_b is the arterial blood temperature (K)

Q_r is the energy deposited by the radiative beam - light/laser source ((W/m^3))

For the purpose of this simulation the heat generation from cellular metabolism Q_{met} is set to a constant. It should be noted that this term can be substituted by alterative

functions that describe heat generation from cellular metabolism such as the Q_{10} model. The Q_{10} model regulates metabolic heat generation as a function of temperature.

Material	ρ [kg/m^3]	C [J/kg·K]	k [W/(m·K)]	ρ_b [kg/m^3]	C_b [J/kg·K]	ω_b [1/s]	T_{ref} [°K]	T_b [°K]	Q_{met} [W/m^3]	K [m^{-1}]
Enamel	2950[a]	750[a]	0.93[a]	-	-	-	310	310	-	120[d]
Dentin	2100[a]	1170[a]	0.63[a]	-	-	-	310	310	-	750[e]
Pulp	1000[b]	4200[b]	0.59[b]	1050[c]	3617[c]	0.0018[b]	310	310	1190[b]	10000[f]

Table 6 Thermal properties within the different tooth domains.
[a]Data adopted from literature [Lina et al]
[b]Data adopted from literature [Falahatka el, Kodonas et al, Meyer et al, Mathwes et al]
[c]Data adopted from literature [Hasgall et al]
[d]Data adopted from literature [Spitzer et al]
[e]Data adopted from literature [Jaap]
[f]Data adopted from literature [Kakino]

To account for the irradiance heat generation within the tooth from the dental laser or light, the Beer-Lambert Law is applied to the model. Figure 8 and Table 2 show the boundary conditions and material properties used for heat generation from a light source. The technique has been shown to be effective at producing temperature changes from light and laser sources [Zezell et al, Lin et al].

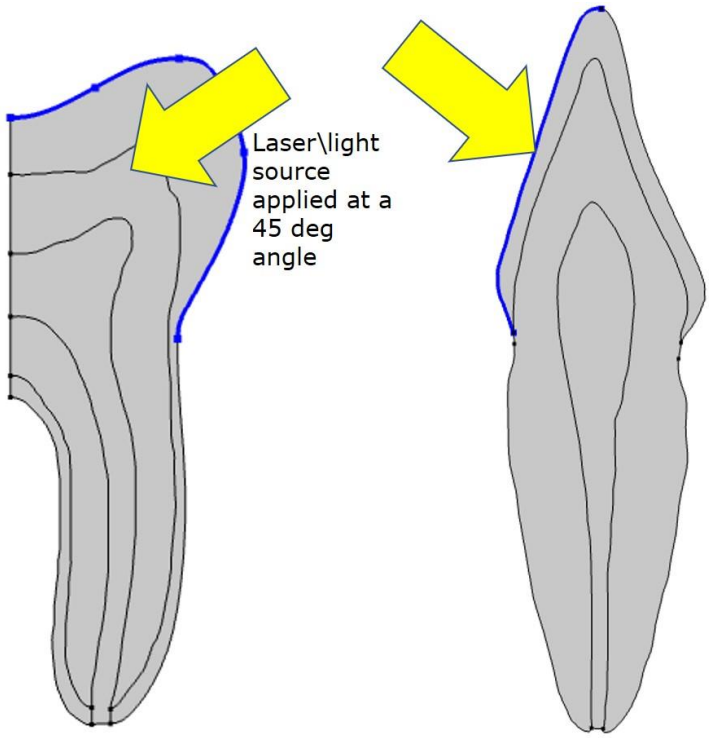

Figure 19 Light boundary conditions. The yellow arrow is the direction of the light source. The highlighted blue line is the applied surface the light source is in contact with.

$$\frac{\mathrm{e}}{\|\mathrm{e}\|} \cdot \nabla I = -\kappa I \tag{10}$$

$$Q_r = -\kappa I \tag{11}$$

I is the radiative intensity (W/m^2)

e is the orientation of the beam - light/laser source

κ is the absorption coefficient (m^{-1})

Q_r is the energy deposited by the radiative beam - light/laser source ((W/m^3))

The direction of the from figure 8 is at a 45° angle. Typically the absorption coefficient is a function of temperature, the wavelength of the laser/light source, and depth. The wavelength selected for the simulation is 450 nm and is held constant. The temperature changes are not large enough to alter an effective change in the absorption coefficient, and due to the opacity and thickness, the depth has little change. The absorption coefficient based on laser or light wavelength is documented in a number of studies, but a bulk value for pulp tissue is not [Spitzer and Ten Bosch 1975, Optical properties of dental hard tissues 2001 by Zijp Jacob Rudolf]. The existing studies that delve into the optical properties of pulp show the breakdown of absorption within the individual proteins and fluid within the tissue for the purpose of tissue health [Kakino et al, Takahiro et al]. Studying the anatomy, density, and blood profusion rate of the pulp, an assumption that the absorption coefficient value would fall somewhere between skin and blood.

[model development

Heat Transfer and Thermal Stress Analysis of a Mandibular Molar Tooth Restored by Different Indirect Restorations Using a Three-Dimensional Finite Element Method Koycu et al → key paper for mechanical and thermal model for parameters and theory

A review of heat transfer in human tooth—Experimental characterization and mathematical modeling *Lin* et al → key paper for HT theory in teeth and heat generation assumption

Heat Generation and Transfer on Biological Tissues Due to High-Intensity Laser Irradiation Zezell et al →

Stress behaviour across human tooth by temperature gradient resulting of laser irradiation Falahatkar et al → parameters and density of pulp helped the optical properties assumption]

[papers relation to pulp damage from temperature change

Heat Generation and Transfer on Biological Tissues Due to High-Intensity Laser Irradiation Zezell et al → reference the actual papers

Effects of blue-light irradiation during dental treatment Fumihiko Yoshino → reference the actual papers and has a table

Thermal risks from LED- and high-intensity QTH-curing units during polymerization of dental resins Serge Bouillaguet et al

Effect of simulated pulpal microcirculation on intrapulpal temperature changes following

application of heat on tooth surfaces Kodonas et al → also refences the paper for pulp profusion]

Mass transport of hydrogen peroxide (H_2O_2)

Tooth whiting is accomplished by apply a gel with a given concentration of Hydrogen peroxide H_2O_2 to the tooth over a given time period to allow the product to diffuse into the tooth. The diffused H_2O_2 into the tooth will react with the light source to enhance the whiting capabilities [Kwon]. The problem is when the H_2O_2 diffuses past the enamel and dentin into the soft tissue of the pulp. The H_2O_2 once in the pulp diffuses almost instantaneously and is toxic to the tissue creating inflammatory response [Vaz, Cohen, Colares]. Inflammation is a function of H_2O_2 located within the pulp tissue therefor creating a need to understand mass distribution of H_2O_2 within the tooth domain over a given time period and varying concentrations of peroxide in the gel. To model the mass transport behavior Fick's first and second law of diffusion was selected. The transient form of the equations relates to the concentration of a species diffusion through a material media. Equation 12-13 are the select form of Fick's laws to model mass transport. The use of Fick's laws for the transport of H_2O_2 within In Vitro studies of human teeth have been validate [Petersen].

$$\mathbf{J} = -D\nabla c \tag{12}$$

$$\frac{\partial c}{\partial t} + \nabla \cdot \mathbf{J} = R_a \tag{13}$$

$$R_a = -k \cdot c \tag{14}$$

$$D = D_o e^{\frac{E_a}{RT}} \tag{15}$$

$\mathbf{J}$ is mass flux diffusive flux vector (mol/(m^2·s))

D is the diffusion coefficient (cm^2/s)

D_o is the pre-exponential factor (cm^2/s)

c is the concentration of the species (mol/m^3)

k is the reaction rate constant (1/s)

R_a is a reaction rate expression for the species ($mol/(m^3 \cdot s)$)

R is ideal gas constant ($J/(mol \cdot K)$)

E_a is activation energy for diffusion (kJ/(mol))

T is temperature (K)

Assumptions:

There are some important assumptions being made.

First the material isotropic. Even though the material is anisotropic the isotropic assumption works due to slow diffusivity through the material as was shown through In Vitro studies [Peterson].

Second diffusion is function of temperature and not light source. In vitro studies indicate that light sources can increase the diffusion of H_2O_2 through both the enamel and dentin [Carman]. The studies did not isolate temperature from light activation so it is unknow what the exact effect light has on diffusion. The studies focus was on net effect and not derived material properties.

Third the concentration of H_2O_2 does not change over the application time. Concentration of H_2O_2 was shown in vitro to have small amount of change in the application gel over a period of 45 min period [Marson et al, Petersen]

Forth reaction consumption rate is homogenous. H_2O_2 reacts with the stains within the tooth to form an irreversible reaction [Petersen]. A constant reaction rate was shown to be an effective approximation for time dependent studies [Petersen]. This assumption can be altered in future models when H_2O_2 studies quantify the physical properties of reactions.

Fifth the activation energy for dentin was iteratively developed and a assigned pre-exponential factor is 2.5 times larger enamel. There is little in dental literature for derived material properties for enamel and dentin. According to studies dentin has 2.5 - 3 times the diffusivity as enamel at room temperature [Petersen,]. Since an activation energy and pre-exponential factor are unknow for dentin diffusion. Activation energy was developed using multiple studies and simulated iterations until a reliable value was found until a further research can provided the actual data [Petersen, P&G, Camps]. With the selected activation energy and setting equation 15 equal to room temperature then dentin will scale the pre-exponential to 2.5 times enamel at the same temperature.

The assumptions can be altered to fit alternative applications based on the modeling needs of the user

Boundary conditions for mass diffusion of hydrogen peroxide within a tooth can be seen in Figure 9. The purple top portion represents the application zone of H_2O_2 gel while the bottom portion in orange is a zero concentration boundary condition. The application zone is transient and is based on the procedures requirement for length of treatment. Once the end of the application time is reached the boundary condition returns to zero. For simplicity the change is almost instantons, but any number of time related function to reduce the concentration to zero can be used. The coefficients of the material properties are presented in Table 3. The application times for chosen for this study were 5, 10, 15, 30, 45, 60, 120 minutes with and without a light source.

The amount of H_2O_2 transporting into the pulp is needed to evaluate inflammatory response. Since this is a two dimensional problem standard methods for mass flow rate into the tissue can not be applied. According to Proctor & Gamble diffusion is assumed to be almost instantaneous so an artificially high diffusion coefficient was selectively chosen. Instead of having H_2O_2 react or absorb into the pulp tissue to account for the accumulated mass a zero concentration boundary condition is applied at the end of the root canal. A mass flux $\mu g/(s \cdot mm^2)$ can be averaged and using the diameter of the root canal approximately (0.3mm) [Buiki et al, Martos et al 2 papers, Torres-Ramos] area can be calculated and the mass flow rate can be estimated. Appling a time integral to the boundary total mass that entered the pulp cavity can be estimated.

A zero flux boundary condition was selected for the root section to make the model more in line in vitro studies conducted for H_2O_2 diffusion in the tooth for verification purposes.

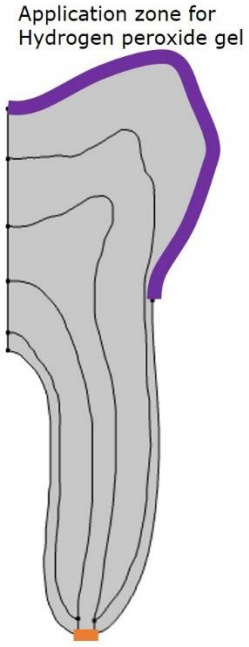

Figure 20 Mass Transport boundary condition. The purple highlighted section is the application zone of the hydrogen peroxide. The orange highlighted section is a zero concentration boundary condition.

Material	D_o [cm^2/s]	R [J/mol·K]	k [s^{-1}]	E_a [kJ/mol]
Enamel	17.55	8.314	1e-4	48.3
Dentin	44.25[a]	8.314	1e-4	40[a]
Pulp	9	-	-	-

Table 7 Mass transport properties within the different tooth domains.
[a]Data adopted from literature [Petersen] The Enamel is modified from the Petersen data to reflect changes in diffusion change with temperature based of publication. Pulp is artificially raise to give a near instantaneous diffusion within the pulp based on its reaction with tissue. [information supplied by P&G]

[papers for light supporting diffusion of h2O2]

"Penetration of 38% Hydrogen Peroxide into the Pulp Chamber in Bovine and Human Teeth Submitted to Office Bleach Technique" Carmen

[papers for H2O2 mass transfer to be used in this paper]

"Quantitative analysis of the diffusion of hydrogen peroxid through teeth" Petersen

"In vitro determination and quantification of 30% hydrogen peroxide penetration through dentin and cementum during bleaching" Rotstein, Ilan

"Penetration of hydrogen peroxide and degradation rate of different bleaching products" Marson

"Time-Course Diffusion of Hydrogen Peroxide Through Human Dentin: Clinical Significance for Young Tooth Internal Bleaching" Camps

"Penetration of 38% Hydrogen Peroxide into the Pulp Chamber in Bovine and Human Teeth Submitted to Office Bleach Technique" Camargo

"Hydrogen peroxide penetration into the pulp chamber and dental permeability after bleaching" Berger

[inflammation]

"Inflammatory response of human dental pulp to at-home and in-office tooth bleaching" VAZ

"Human pulpal response to bleaching procedures on vital teeth" Cohen

"Hydrogen peroxide-based products alter inflammatory and tissue damage-related proteins in the gingival crevicular fluid of healthy volunteers: a randomized trial" Colares

Inflammation Strain Model in Pulp

The inflammatory model is inspired by strain ε_{th} from thermal expansion and hydroscopic swelling. It was important to find a relationship between the concentration or mass of hydrogen peroxide within the tissue and the swelling which would occur as it diffused through the dental pulp. The strain from the inflammation could be factored into the total overall inelastic strain. In a rigid system such as dental pulp being cased within the dental enamel of the tooth which would form a rigid body not allowing tissue expansion therefore creating higher internal stress and increasing the potential to damage cells as seen in Figure 10. The Equation 16 was developed by the author as a development start to relate local inflammation in terms of strain based off a local variable. Equation 16 relates local mass diffusion of H_2O_2 to internal tissue strain.

$$\varepsilon_{ifm} = \frac{K}{\left(1 + e^{\left(-a(mass-\beta)\right)}\right)} \quad (16)$$

ε_{ifm} is strain from inflammation

$mass$ is total accumulated mass of H_2O_2 in the pulp chamber (μg)

a is the sensitivity of the tissue to H_2O_2, effects the how quickly the strain will reach the max threshold as mass accumulates in the pulp (1/ μg)

β is the lower threshold coefficient for when H2O2 starts to cause injury in the issue (μg)

K is the theoretical peak strain from inflammation

Material	K	α	β
Pulp	0.3	0.03324	183.9

Table 8 Inflammatory Model coefficient

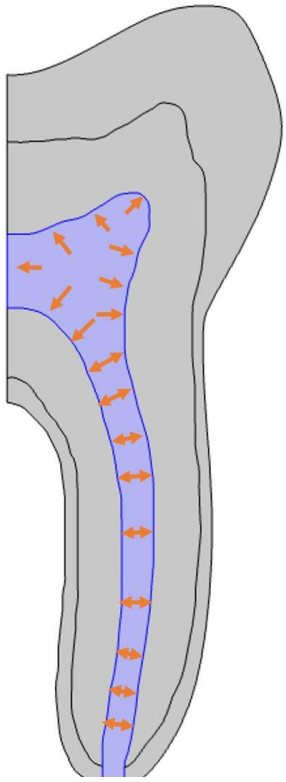

Figure 21 Representation of how the inflammatory model works. As the total mass of hydrogen peroxide increases the pulp will swell pushing on the ridged cavity

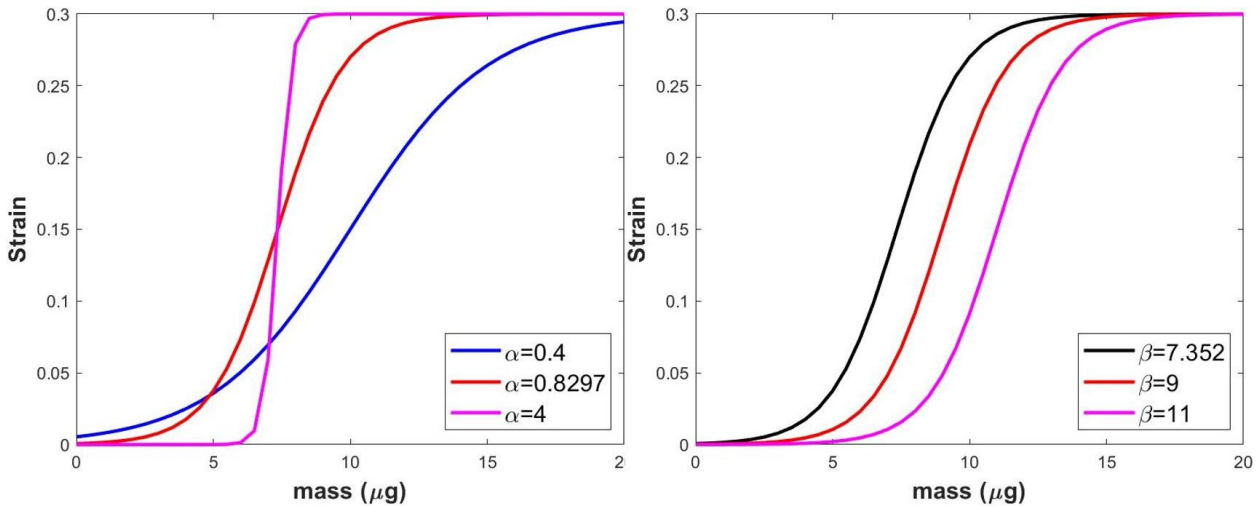

Figure 22 Example of the inflammatory model shape and behavior using different values for the coefficients. α effects the how quickly the strain will reach the max threshold as mass accumulates in the pulp. β effects the point were mass accumulation starts to have an affect on strain inflammation.

There currently are no research studies relating inflammatory stress and strain in pulp tissue to total amount of mass of hydrogen peroxide diffused. To develop an inflammatory model literature was objectively quantified to find a relationship to pulp damage and mass transfer of H_2O_2. It is well documented that the 15% concentration gels caused little irritation and 38% was around the max threshold used in practice with application times of 45 – 60 min [Kwon, Vaz, Cohen, Colares]. It is assumed a 50% concentration gel applied to a incisor over an hour period would certainly be toxic to the pulp tissue and produce irreversible damage leading to a higher measurable internal stress and strain. By using the simulated H_2O_2 mass diffused in the pulp chamber and potential injury thresholds collected from studies a strain relationship could be sujectivly derived.

Since no data exists on inflammatory mechanical responses to the mass of hydrogen peroxide, the coefficients used in the model act as competent placeholder until more experimental data is obtained to verify the relationship between the kinetics of peak strain between peroxide diffusion within dental pulp. All the coefficients presented in the inflammatory model are approximation and not derived from a specific experiment. Each part was iterated on until it fit a logical result in reversable and irreversible cell damage from inflammation. The presented coefficients will show as mass concentration increases in the pulp chamber swelling will occur. It will not be accurate to the specifics amounts of peroxide and exact internal strain.

Cell Damage Model in Pulp

The injury model was developed by McGregor et al to describe cell death for both thermal and thermally modified pressure injury. Pure thermal injury is considered burns, and is the denaturing of protein due to elevated temperature [Moritz]. A pressure injury is a combination of several factors such as direct deformation of the cell, ischemia, and inflammatory response [Geffen 2018]. These factors are further altered by temperature and time, dictating the severity and onset of the injury. The mathematical fundamentals of the model are explained in detail [journal name] and are outside of the scope of this paper. The model predicts cell death in the tissue domain from pressure, temperature, and time. The

tissue injury coefficients are optimized from three studies, Iaizzo et al, Moritz & Henrique, and Rylander.

$$\Omega(t,T,\omega) = e^{-\int_0^t \left[\left(e^{\lambda^*}\right)^k k \cdot e^{\beta_T \cdot T(\tau)+\beta_\omega \cdot \omega(\tau)} \cdot \tau^{k-1}\right] d\tau} \quad (17)$$

λ^* is scale term, simplified, overall impact physiological variables have on injury term

k is shape term, simplified, once injury occurs how suddenly will cell viability change

β_T weighs the effect temperature has on injury development outside of homeostasis

β_ω weighs the effect blood profusion has on injury development outside of homeostasis

ω is the blood profusion in the tissue

τ & t is time (s)

Material	λ	k	B_T	B_ω
Pulp pressure injury	-6.8595	1.8554	0.2573	-0.0105
Pulp pure thermal injury	-12.6210	2.9298	0.8880	0

Table 9 Coefficients for the injury model. Coefficients are developed from the Ioizzo studies [McGregor et al].

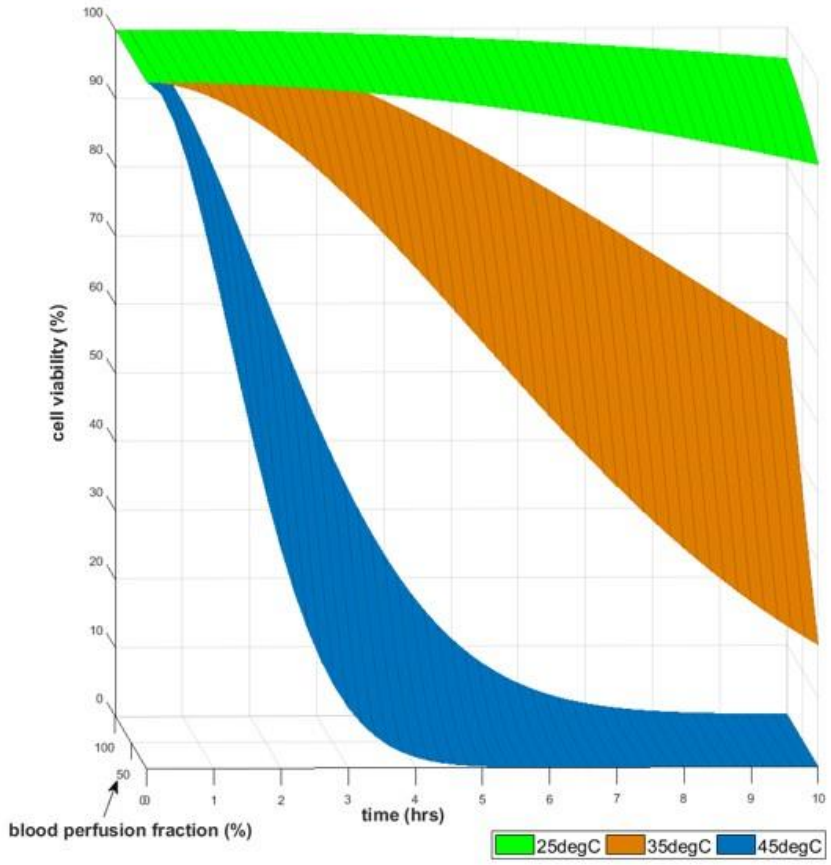

Figure 23 Behavior of the injury model in 3D under isothermal conditions steady state conditions. Each isothermal represents the cell viability if the dental pulp is held at a constant temperature and a fraction of original blood flow over time. The simulation algorithm self corrects for blood flow above 91% not allowing a pressure injury to accrue.

The perfusion term ω is assumed to be a linear relationship between local stress in the tissue and the potential diastolic blood pressure (120mmHg) produced by the heart. The simplified assumption is made for the purpose of creating a damage model with ischemia as a driving factor for injury. The linear relationship is a first approximation, which can be replaced by a more complex relationship based on theoretical or clinical data. Last this term is not limited to ischemic damage and can be built around several cell damaging factors such as rupturing or large sheer deformation. The linear assumption is oversimplification of the blood flow to tissue but serves as good starting point to understand impact stress has on creating damage potential.

The injury model combined with the inflammation model lumps all the damage factors together. It does not in its present state differentiate between damage to the cells from stress or direct damage from the H_2O_2 reactions. It is assumed that once H_2O_2 inters the pulp chamber reaction that occur result in an inflammatory response which will drive the rate of injury in the soft tissue with temperature and time.

There exist no data on pulp damage and direct inflammation driven stresses in the tissue. To serve as a place holder for the damage model properties, dermis the highly perfused portion of the skin was select. This dermis is sensitive to tissue loading,

temperature and time [Iaizzo]. This should serve as a competent first approximation until actual pulp data can be obtained.

The equation, when implemented in the FEA model uses and conditional algorithm to determine version of the equation is applied. If the temperature is above 44°C the pure thermal injury is given priority. When the temperature is below the burn set point, the pressure injury becomes the dominant the model. There are safe conditions built in to hold off on injury. Stress below 10mmHg will not trigger the injury model. This prevents the simulation from overshooting cell death predictions. The injury model produces a value between one and zero. One represents 100% cell viability as zero indicates 0%. Anything below 50% would be an indicator of fully irreversible cellular necrosis.

Boundary values and application time.

Light intensity and H_2O_2 concentration are varied on the molar and incisor to simulate which combination could be harmful. Table 6 list the different application scenarios to be simulated. A total of 93 simulations was carried out. H_2O_2 concentration of 15% and 30% are inline with home and office products [Colares]. The 50% concentration was selected to represent an expected toxic threshold. Light Intensity was selected based on initial test requirements from Proctor & Gamble. Scenarios without light or H_2O_2 concentration are used to isolate tissue damage from either case. The combination of both is for analyzing synergistic relationship increasing temperature domain within the tooth and its affects on peroxide diffusion with overall tissue damage.

Parameter sweep of H_2O_2 concentration with light source Intensity							
H_2O_2 Concentration & Light Intensity	Application time in minutes						
15%, 30% ,50% H_2O_2 -- no light	5	10	15	30	45	60	120
0% H_2O_2 -- 100 mW/cm^2	5	10	15	30	45	60	-
0% H_2O_2 -- 200 mW/cm^2	5	10	15	30	45	60	-
0% H_2O_2 -- 300 mW/cm^2	5	10	15	30	45	60	-
15%, 30% ,50% H_2O_2 -- 100 mW/cm^2	5	10	15	30	45	60	-
15%, 30% ,50% H_2O_2 -- 200 mW/cm^2	5	10	15	30	45	60	-
15%, 30% ,50% H_2O_2 -- 300 mW/cm^2	5	10	15	30	45	60	-

Table 10 shows the list of all different scenarios simulated. Left side of the list the applied H_2O_2 concentration and ligh intensity of the light source. The right side list how long H_2O_2 and light are applied to the tooth.

Results

Thermal responses within the tooth domain

Figure 12 and 16 shows temperature distributions within the tooth domain all three light intensities from an initial temperature of 37 °C. Peak temperature for the molar as see in Figure 15 is reached within the first three minutes of application regardless of light intensity. Figure 19 shows peak temperature in the incisor occurs around 12 minutes for the three light sources. Figures 13 and 14 shows a line slice through the molar with the temperature at each point along the axis. Figure 14 regardless light application time 5 or 60 minutes the temperature distribution is relatively stable. Figures 17 and 18, incisor temperature distribution for 5 and 60 minutes. The incisor takes longer for the temperature to stabilize. This is most likely due to geometrical differences with each tooth domain. The enamel has the lowest amount of light absorption and is the thickest in the molar. The

incisor has a greater amount of surface area and thinner enamel allowing more light penetration to the dentin and pulp regions within the tooth.

[**get Dr. Diller's help on what else to say here**]

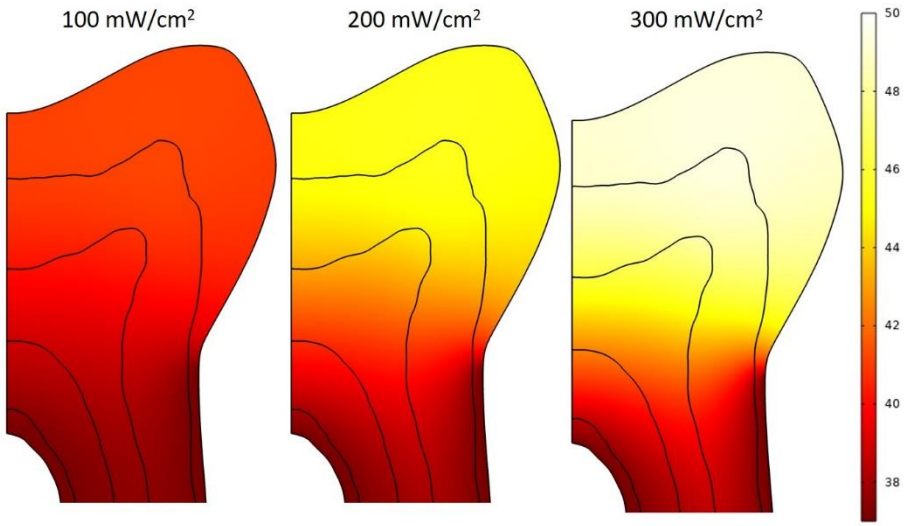

Figure 24 Molar Temperature distribution under different light intensities. Left 100 mW/cm^2. Center 200 mW/cm^2. Right 300 mW/cm^2

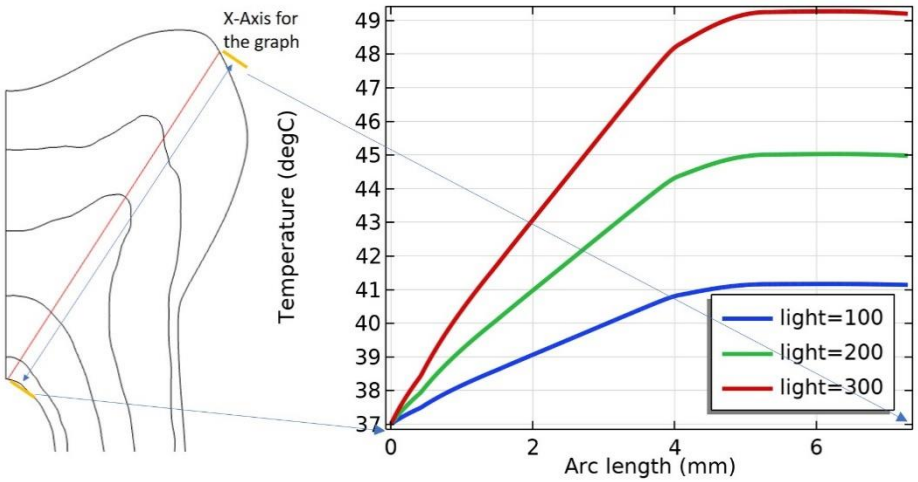

Figure 25 Temperature distribution on a cross-section axis. The closer to the light source the higher the temperature.

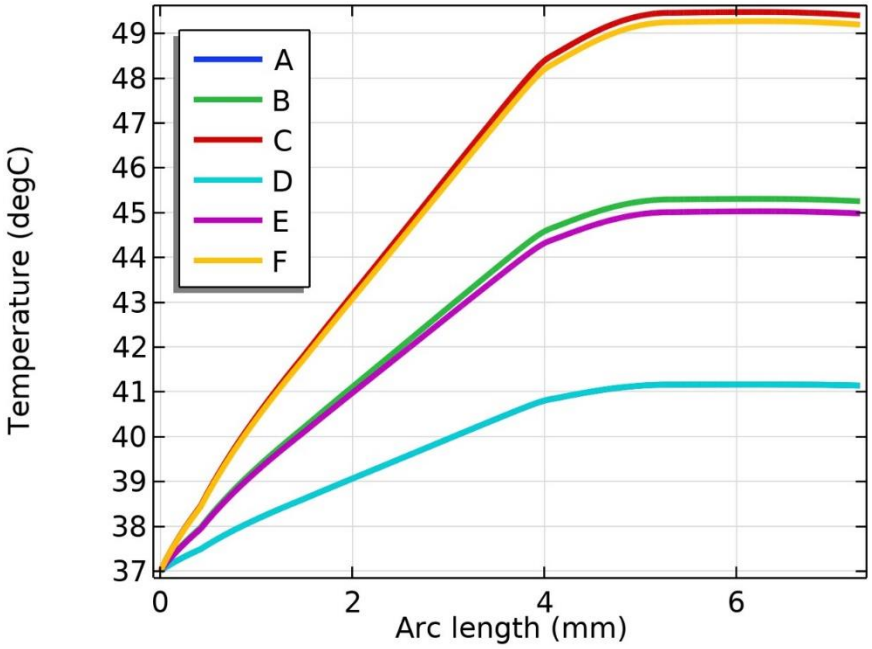

Figure 26 Plot of the temperature distribution using the same axis from figure 13 for different light intensities and at 5 and 60 minutes. A is 100 mW/cm^2 for 60 min. B is 200 mW/cm^2 for 60 min. C is 300 mW/cm^2 for 60 min. D is 100 mW/cm^2 for 5 min. E 100 mW/cm^2 for 5 min. F is 100 mW/cm^2 for 5 min. In the pair of A&D, B&E, C&F little difference in the temperature distribution between 5 and 60 minutes. The major of the temperature change happens within the first 5 minutes.

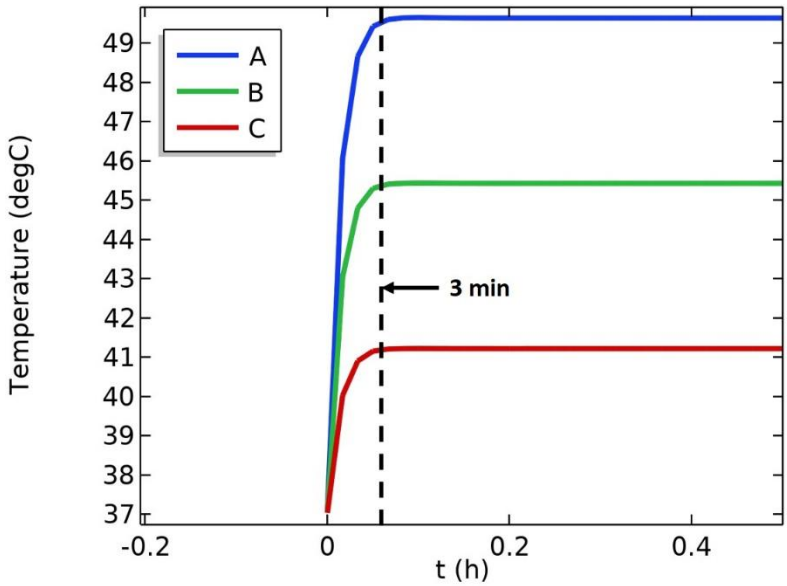

Figure 27Molar max temperature within the tooth over time. The peak temperature is achieve around 3 minutes regardless of light intensity. A is 300 mW/cm^2, B is 200 mW/cm^2, C is 100 mW/cm^2

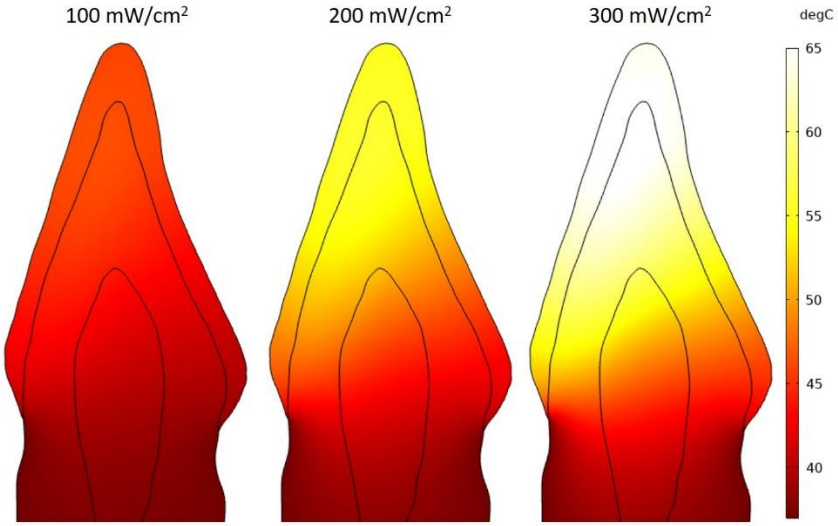

Figure 28 Incisor Temperature distribution under different light intensities. Left 100 mW/cm^2. Center 200 mW/cm^2. Right 300 mW/cm^2

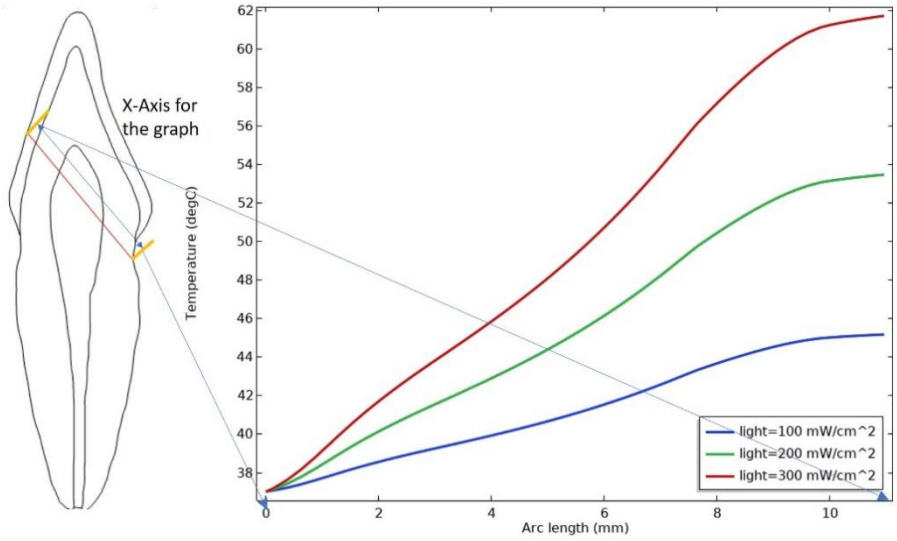

Figure 29 Temperature distribution on a cross-section axis. The closer to the light source the higher the temperature.

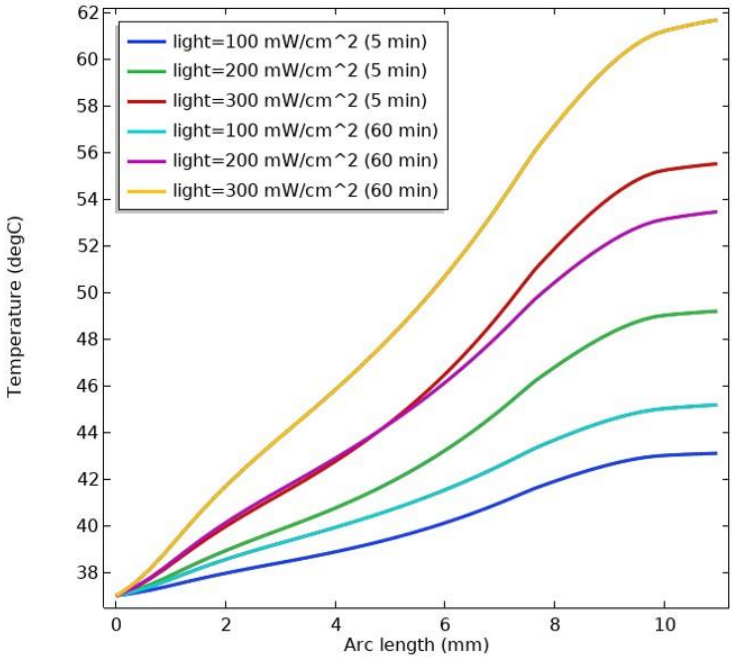

Figure 30 Plot of the temperature distribution using the same axis from figure 13 for different light intensities and at 5 and 60 minutes. Unlike the molar the incisor take longer to hit steady-state temperature

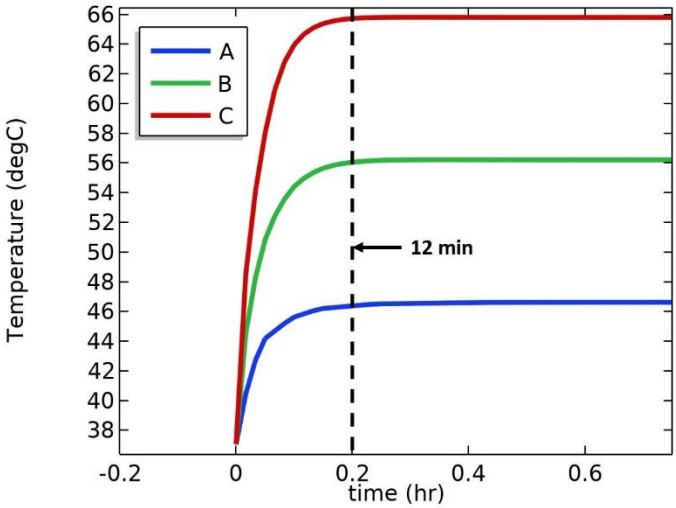

Figure 31 Incisor max temperature within the tooth over time. The peak temperature is achieve around 12 minutes regardless of light intensity. A is 300 mW/cm^2, B is 200 mW/cm^2, C is 100 mW/cm^2

Mass diffusion of H_2O_2 within the pulp tissue

Figures 20 and 22 present a visual color map of peroxide concentration and vector line of mass flow. The images where taken from a 200 mW/cm^2 light intensity 30% H_2O_2 concentration with an application time of 1 hour at the 1 hour time interval. So the question is how much does concentration, application time, and light intensity affect mass diffusion of peroxide into the tooth pulp? Dental literature measurement time scale for peroxide diffusion into the pulp chamber is generally at the end of application time period. Due to the porosity and absorption within the tooth it can take up to several hours for diffusion is complete [dentin diffusion paper, Petersen]. Figures 21 and 23 show the peroxide mass in the pulp chamber over time under different application times and concentrations with no

light source maintaining a tooth temperature of 37 °C. At the end of each application time peroxide is allowed to flow back out of the application surface or into the pulp chamber. For 15% H_2O_2 concentration applied for 30min and then removed could take hours for the mass of peroxide to finish diffusing into the pulp chamber. Table 10 and 14 shows peroxide within the pulp chamber at different application times and the finial 12 hour time period. This shows with a 60 minute application time how much mass is in the pulp chamber under different concentrations. The values from Table 10 and 14 match experimental results conducted internally by P&G. Although there are several papers on H_2O_2 diffusion in the tooth they focus on a sample of the of the over all geometry.

A summery of the total peroxide mass diffused in pulp tissue is presented in Tables 7, 8, 9 for the molar and Tables 11, 12, 13 for the incisor at 12 hours. Increasing the concentration and light intensity allows for larger accumulation of peroxide in the pulp chamber. Regardless of concentration for short application times of effect of light on diffusion is low. As application times for light increase the stronger the effect on total accumulated peroxide in the pulp.

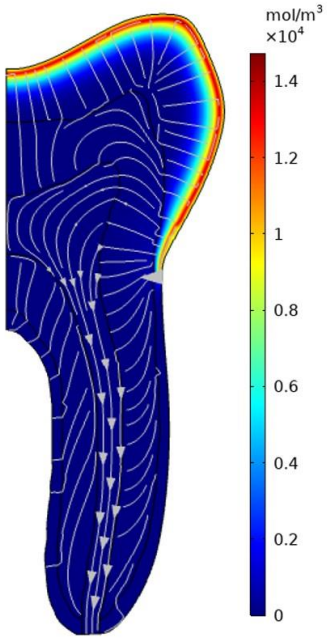

Figure 32 Molar H_2O_2 spatial concentration and mass diffusion pathways through the tooth. Lines show the exit of peroxide out of the root. This how the mass of peroxide is totaled for the 2D model and added to the accumulation term of the inflammatory model.

15% H_2O_2 (µg) total diffusion pulp chamber (after 12hr)				
Application Time (min)	0 (mW/cm²)	100 (mW/cm²)	200 (mW/cm²)	300 (mW/cm²)
5	1.86	2.07	2.33	2.63
10	3.70	4.21	4.80	5.50
15	5.57	6.38	7.29	8.40
30	11.15	12.88	14.89	17.19
45	16.75	19.44	22.68	26.66
60	22.28	25.86	30.58	36.09
120	44.70	-	-	-

Table 11 Molar total mass H_2O_2 diffused into the dental pulp after 12 hours using a 15% concentration.

30% H_2O_2 (µg) total diffusion pulp chamber (after 12hr)				
Application Time (min)	0 (mW/cm²)	100 (mW/cm²)	200 (mW/cm²)	300 (mW/cm²)
5	3.69	4.16	4.64	5.24
10	7.41	8.41	9.60	10.95
15	11.15	12.72	14.61	16.80
30	22.30	25.75	29.83	34.82
45	33.49	38.76	45.37	53.32
60	44.55	52.06	61.10	72.23
120	89.35	-	-	-

Table 12 Molar total mass H_2O_2 diffused into the dental pulp after 12 hours using a 30% concentration.

50% H_2O_2 (µg) total diffusion pulp chamber (after 12hr)				
Application Time (min)	0 (mW/cm²)	100 (mW/cm²)	200 (mW/cm²)	300 (mW/cm²)
5	6.18	6.92	7.76	8.79
10	12.35	13.96	15.99	18.27
15	18.59	21.27	24.36	27.27
30	37.18	42.91	49.68	57.67
45	55.67	64.77	75.66	88.82
60	73.71	86.81	101.68	120.49
120	148.93	-	-	-

Table 13 Molar total mass H_2O_2 diffused into the dental pulp after 12 hours using a 50% concentration.

H_2O_2 (µg) total diffusion pulp chamber Zero Light application time 60 (min)			
H_2O_2 Concentration	Mass H_2O_2 30 min	Mass H_2O_2 60 min	Mass H_2O_2 12 hrs
15% H_2O_2	2.07	9.18	22.28
30% H_2O_2	4.14	18.36	44.54
50% H_2O_2	6.91	30.58	73.71

Table 14 Molar total mass H_2O_2 diffusion in dental pulp with an application time of 60 minutes using no light at different time intervals. Mass continues to rise well after application time ends due to the concentration of H_2O_2 remaining in the enamel and dentin.

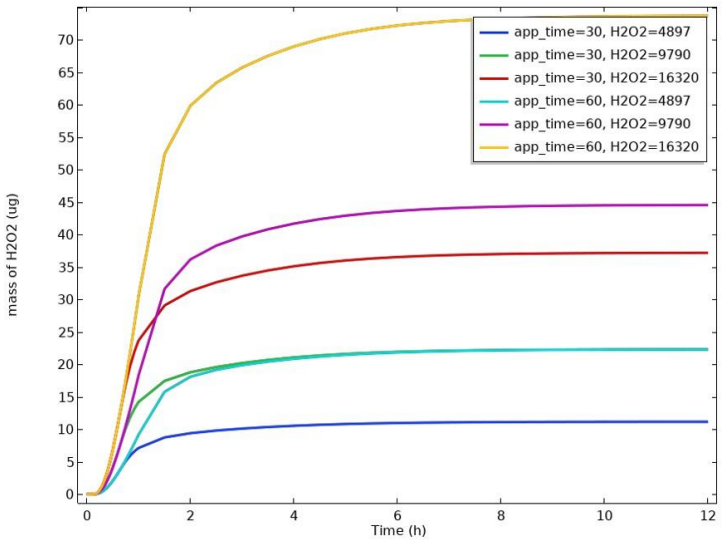

Figure 33Molar total mass in the pulp tissue over time for 15%, 30%, 50% concentrations applied for 30 & 60 mins no light. Note there more H_2O_2 in the pulp for 30% applied to the tooth for 60 mins, than 50% concentration applied for 30 mins.

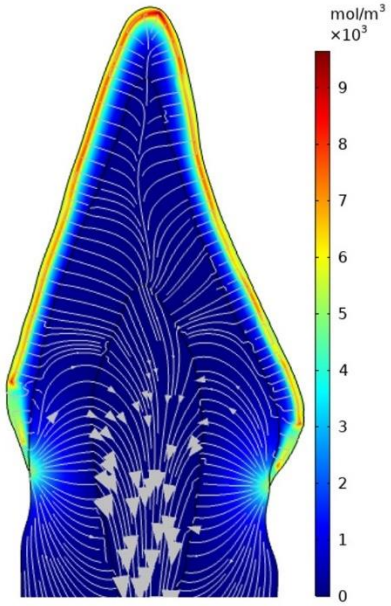

Figure 34 Incisor H_2O_2 spatial concentration and mass diffusion pathways through the tooth

15% H_2O_2 (µg) total diffusion pulp chamber (after 12hr)				
Application Time (min)	0 (mW/cm²)	100 (mW/cm²)	200 (mW/cm²)	300 (mW/cm²)
5	5.87	6.23	6.58	7.13
10	11.73	12.61	13.69	15.14
15	17.69	19.16	20.97	23.56
30	35.44	38.95	43.61	50.21
45	53.15	58.91	66.79	78.28
60	70.87	79.03	90.50	107.32
120	141.76	-	-	-

Table 16 Incisor total mass H_2O_2 diffused into the dental pulp after 12 hours using a 15% concentration.

30% H_2O_2 (µg) total diffusion pulp chamber (after 12hr)				
Application Time (min)	0 (mW/cm²)	100 (mW/cm²)	200 (mW/cm²)	300 (mW/cm²)
5	11.71	12.41	13.24	14.27
10	23.57	25.33	27.45	30.38
15	35.21	38.20	42.12	47.22
30	70.82	77.69	87.11	100.38
45	106.20	117.72	133.23	156.39
60	141.49	157.97	180.72	214.83
120	283.39	-	-	-

Table 15 Incisor total mass H_2O_2 diffused into the dental pulp after 12 hours using a 30% concentration.

50% H_2O_2 (µg) total diffusion pulp chamber (after 12hr)				
Application Time (min)	0 (mW/cm²)	100 (mW/cm²)	200 (mW/cm²)	300 (mW/cm²)
5	19.65	20.75	21.94	23.74
10	39.32	42.20	45.96	50.65
15	58.82	63.87	70.27	78.44
30	118.01	129.56	144.86	167.17
45	177.04	196.40	144.86	260.31
60	235.35	263.25	301.33	357.96
120	472.23	-	-	-

Table 17 Incisor total mass H_2O_2 diffused into the dental pulp after 12 hours using a 50% concentration.

H_2O_2 (µg) total diffusion pulp chamber Zero Light application time 60 (min)			
H_2O_2 Concentration	Mass H_2O_2 30 min	Mass H_2O_2 60 min	Mass H_2O_2 12 hrs
15% H_2O_2	7.54	29.00	70.87
30% H_2O_2	15.09	59.98	141.49
50% H_2O_2	25.13	99.99	235.35

Table 18 Incisor total mass H_2O_2 diffusion in dental pulp with an application time of 60 minutes using no light at different time intervals. Mass continues to rise well after application time ends due to the concentration of H_2O_2 remaining in the enamel and dentin.

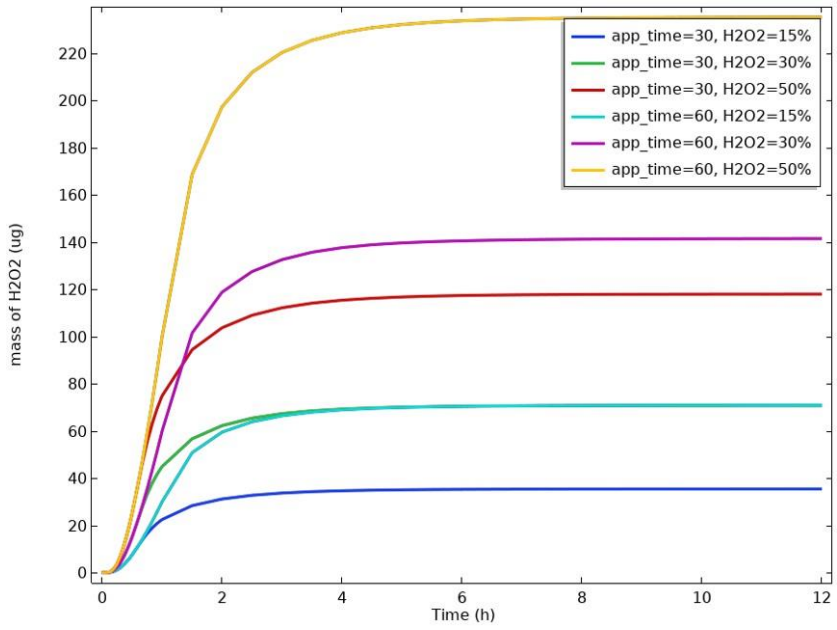

Figure 35 Incisor total mass in the pulp tissue over time for 15%, 30%, 50% concentrations applied for 30 & 60 mins no light. Note there more H_2O_2 in the pulp for 30% applied to the tooth for 60 mins, than 50% concentration applied for 30 mins.

Solid Mechanics

Stress and strain in the tooth for this particular simulation is caused thermal expansion and a inflammation with no other outside or internal effects. Figure 25 and 27 show peak stress for the molar and incisor which coincides with the peak temperature. For the molar and incisor the peak times are 3 mins and 12 mins. The stress in the enamel and dentin regions are important if reached a critical point could cause cracking [Oskui]. Thermal stress can and does affect the pulp region [Oskui]. Drawing from knowledge of pressure ulcers/injury cellular damage can happen as low a 1.3 kPa if given enough time [McGregor et al, Iazzio et al]. Stress in the pulp region see Figures 26 and 28 is caused by combination of thermal and inflammatory strain. Figures 26 and 28 a, b, c are the stress maps from at peak temperature from the three different light sources. Parts d, e, f are stress maps from inflammation after 12 hours from peroxide infiltration. Last Figures 29 and 30 show in red any stress value above 1.3 kPa during peak thermal temperature. From these figures is becomes obvious that temperature alone can cause sensitivity or pain. This could be further complicated if any sharp or irregular geometry within pulp. Thermal expansion or contraction could give another explanation why teeth can be thermally sensitive. Imperfection, spurs, cracks, and sharp transition will be make the issue worse. It is highly unlikely that large long term damage would occur in the pulp due to the thermal stress. As will discussed in the next section there would more likely be thermal damage. Damage

from internal stress will most likely come from inflammatory response due to its long-term presence. However, further investigation would be require.

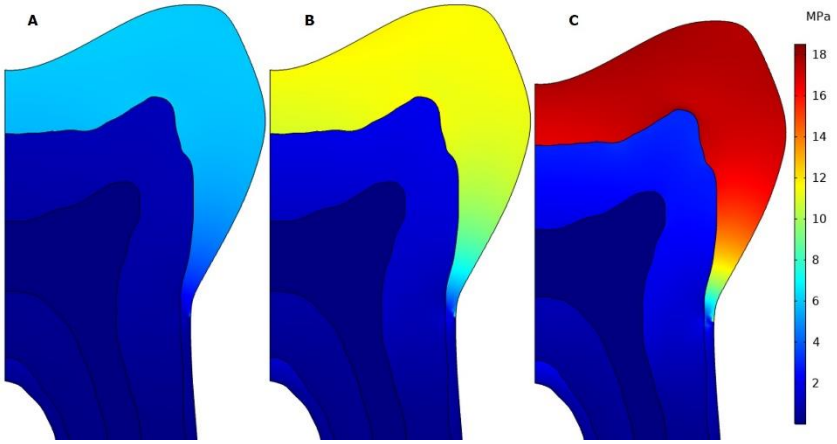

Figure 36 Molar stress distribution due to thermal expansion from heating. A is 100 mW/cm^2, B is 200 mW/cm^2, C is 300 mW/cm^2

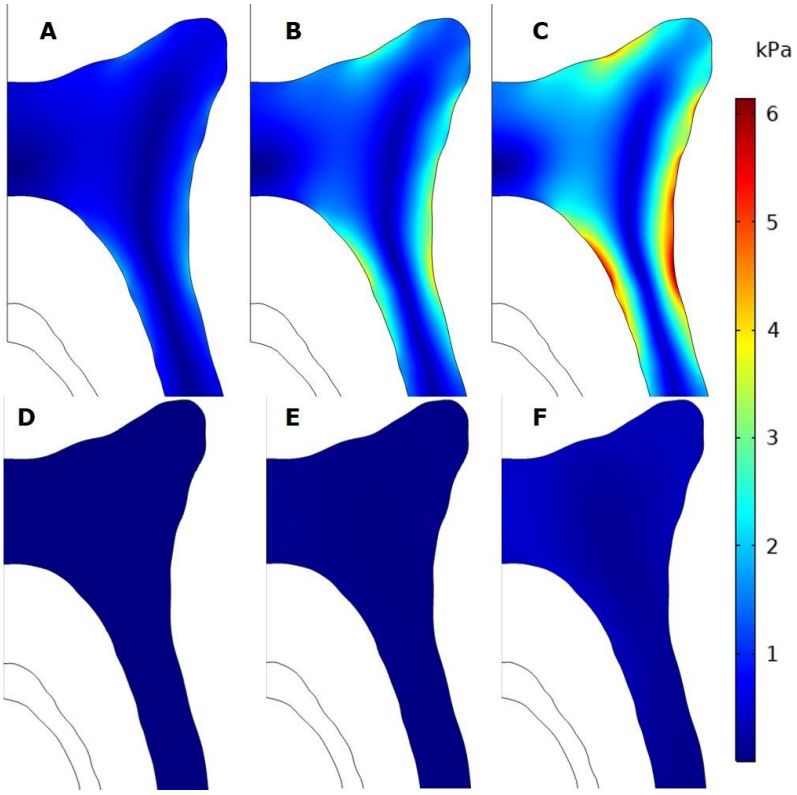

Figure 37 Molar peak stress distribution due to the thermal expansion from heat and H_2O_2 diffusion into the pulp. A is 100 mW/cm^2 at 3 min, B is 200 mW/cm^2 at 3 min, C is 300 mW/cm^2 at 3 min, D is 300 mW/cm^2 15% concentration at 12 hrs, E is 300 mW/cm^2 30% concentration at 12 hrs, D is 300 mW/cm^2 50% concentration at 12 hrs. The thermal stress are greater than the inflammatory stress. After the heat is removed the thermal stresses dissipate with only the inflammatory persisting.

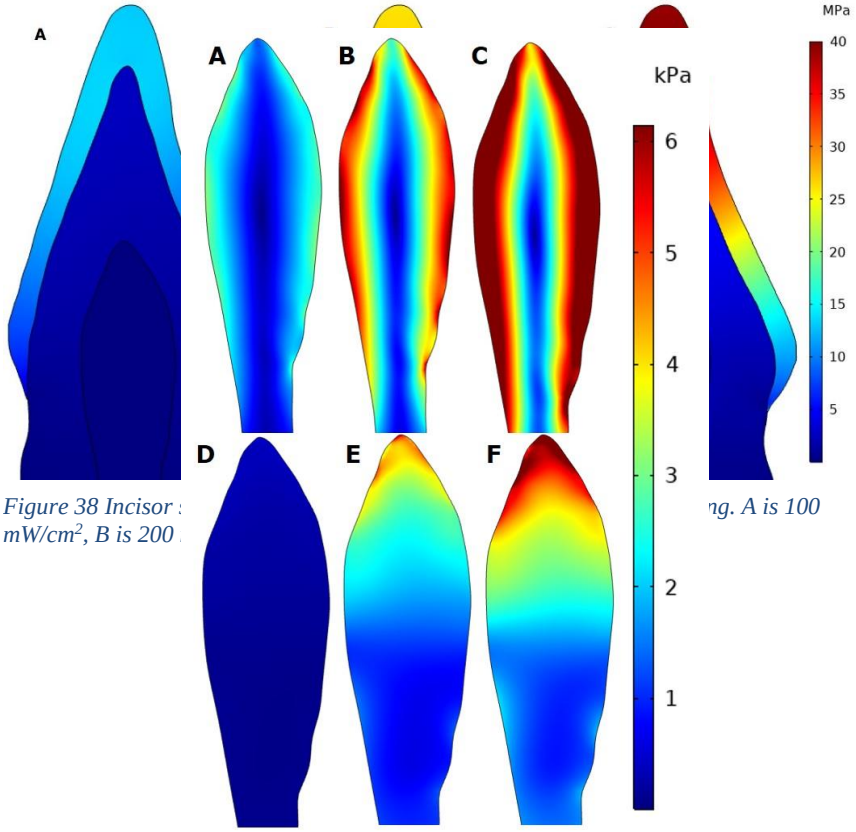

Figure 38 Incisor s *ng. A is 100 mW/cm^2, B is 200*

Figure 39 Incisor peak stress distribution due to the thermal expansion from heat and H_2O_2 diffusion into the pulp. A is 100 mW/cm^2 at 3 min, B is 200 mW/cm^2 at 3 min, C is 300 mW/cm^2 at 3 min, D is 300 mW/cm^2 15% concentration at 12 hrs, E is 300 mW/cm^2 30% concentration at 12 hrs, D is 300 mW/cm^2 50% concentration at 12 hrs. The thermal stress are greater than the inflammatory stress. After the heat is removed the thermal stresses dissipate with only the inflammatory persisting.

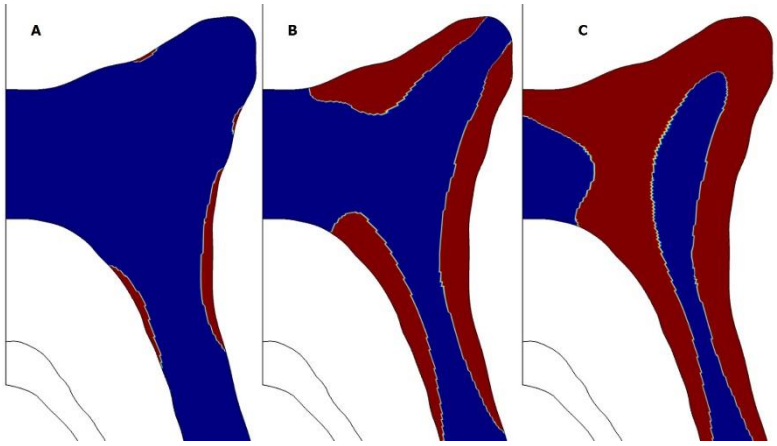

Figure 40 Molar peak stress above 10 mmHg is shaded in red. Areas where stress is above 10 mmHg of stress will have an impact on injury formation if held at an elevated temperature for a specific amount of time. It is expected that a subject would have a noticeable feel to the change in internal pressure. A is 100 mW/cm^2, B is 200 mW/cm^2, C is 300 mW/cm^2

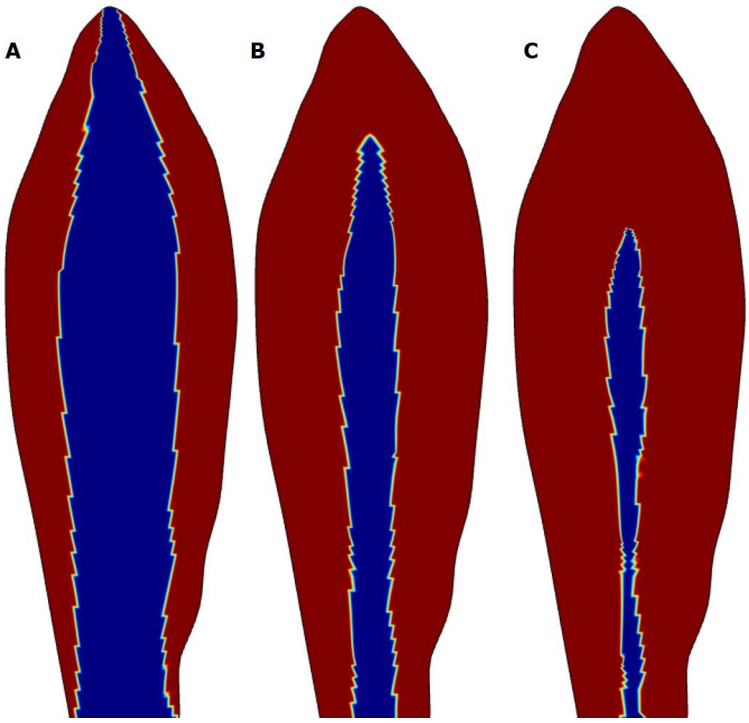

Figure 41 Incisor peak stress above 10 mmHg is shaded in red. Areas where stress is above 10 mmHg of stress will have an impact on injury formation if held at an elevated temperature for a specific amount of time. It is expected that a subject would have a noticeable feel to the change in internal pressure. A is 100 mW/cm^2, B is 200 mW/cm^2, C is 300 mW/cm^2

Injury in the pulp tissue

Pure thermal injury

Pure thermal damage. For the pure thermal damage H_2O_2 concentration is set to zero and only light intensity and application time is considered. The molar with a 100

mW/cm^2 light source regardless of application time did not create any visible injury. Figures 31 and 32 present special damage throughout the pulp under different constraints. Figure 31 a, b the molar pulp takes little to no damage with c showing sign of what would amount to is micro-blisters and reversable damage. The remaining d, e, f all showing irreversible burn damage at the top right of the pulp and some reversible damage around the parameter from thermal stress. Figure 32 only section A does not contain irreversible damage. This indicates that the heat produced by the 300 mW/cm^2 create a sensitive environment in the tissue for cell damage. Table 16 is a summary of the results from all the constraints. The percentage is obtained through integrating damage temporally and spatially. The values are rounded to the nearest whole number. The second number is the minimum recorded value for damage temporally and spatially from one to zero. One equals 100% cell viability with 50% or below irreversible damage. Looking at the 100 mW/cm^2 column although the total volume damage is 100% intact the minimum value for the 60 minute is 0.94. Due to rounding this means a small percentage of the tissue experienced some damage.

Table 15 The 200 mW/cm^2 light will thermally destroy tissue if left on for a long time period. The 300 mW/cm^2 even after 5 minutes will experience some micro damage. The results are inline with Zach and Cohen work which is a widely cited paper in pulp thermal injury journal publications [Zach and Cohen]. Their experiment results showed a 4 degree increase in pulp tissue for 20-35 seconds could produce a small amount of micro blisters that were fully reversible and were indistinguishable from the control after 7 days.

They labeled 10 °C the critical temperature for exposure time period. Fifteen percent of the teeth heated to 10 °C degrees failed to recover quoting that they were smaller of the samples. The remaining 85% fully recovers minus some histologic stigmata. Almost everything above 20 °C invariably destroyed the pulp [Zach and Cohen]. The peak temperature in the pulp at 5 minutes using the 300 mW/cm^2 light was slightly above 48 °C for a small fraction of the tissue. This would lead to a small amount of reversible pulp cell damaged. In Henriques and Moritz pivotal papers thermal injury severity is a function of temperature and time [Henriques and Moritz]. The longer the tissue is exposed to thermal stimulus the greater the potential injury. For 300 mW/cm^2 scenarios only the 5 minute application time does not respond in irreversible damage.

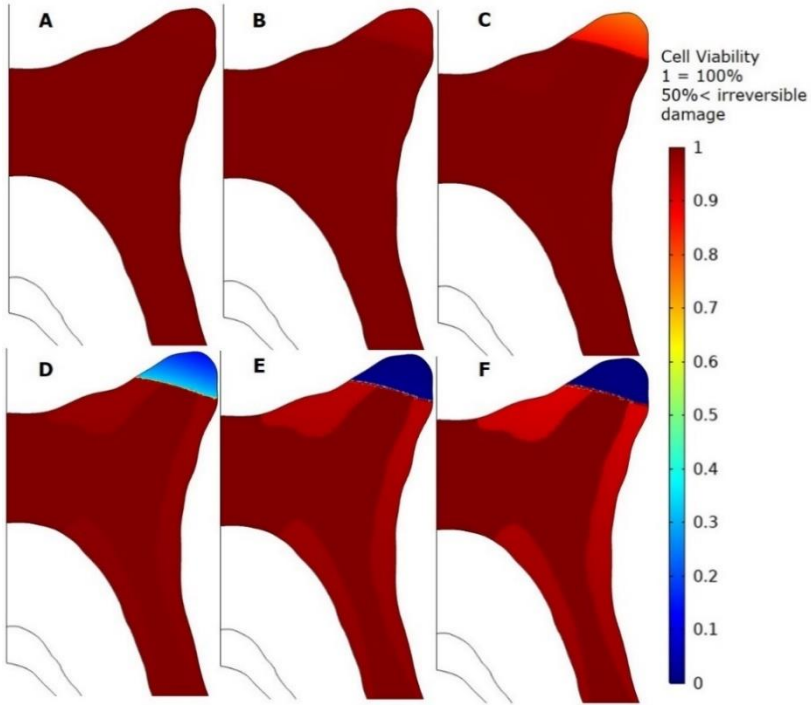

Figure 42 Molar cell viability with light intensity of 200 mW/cm^2 no H_2O_2 applied, results are pure thermal injury. A is 5 min application time, B is 10 min application time, C is 15 min application time, D is 30 min application time, E is 45 min application time, F is 60 min application time. Below 50% is irreversible damage.

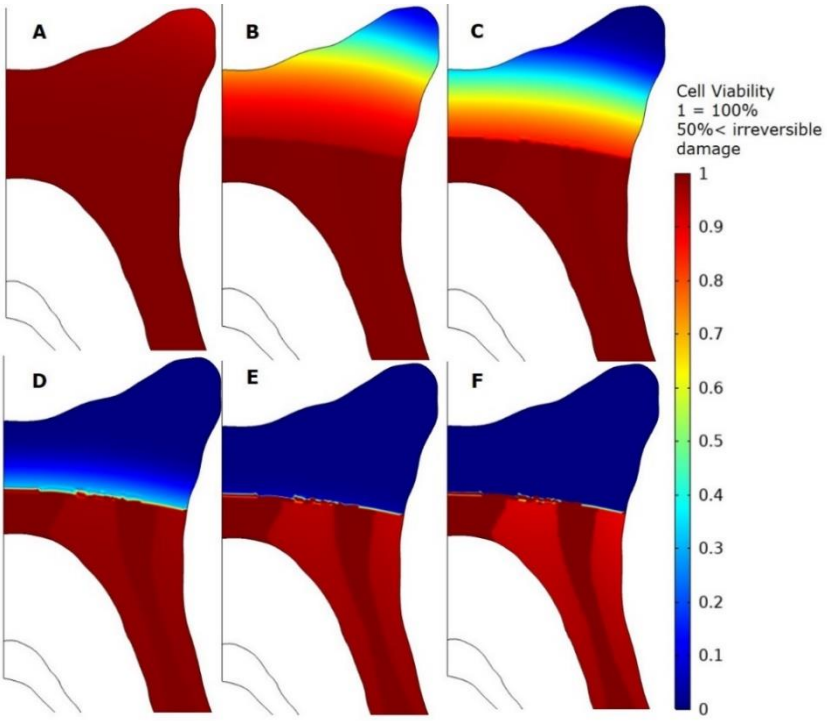

Figure 43 Molar cell viability with light intensity of 300 mW/cm^2 no H_2O_2 applied, results are pure thermal injury. A is 5 min application time, B is 10 min application time, C is 15 min application time, D is 30 min application time, E is 45 min application time, F is 60 min application time. Below 50% is irreversible damage.

% Total pulp tissue viability Pure thermal damage by volume & (minimum cell viability) No H_2O_2 Application			
Application Time (min)	100 (mW/cm^2)	200 (mW/cm^2)	300 (mW/cm^2)
5	100 (1)	100 (0.99)	100 (93)
10	100 (1)	100 (0.96)	91 (0.08)
15	100 (0.99)	99 (0.76)	82 (0)
30	100 (0.98)	97 (0.1)	70 (0)
45	100 (0.98)	96 (0)	67 (0)
60	100 (0.94)	96 (0)	67 (0)

Table 19 Molar pure thermal injury summary chart. Summation of the pulp volume viability and the minimum cell viability located within the tissue domain.

Figures 33-35 display the spatial damage for the incisor pulp and Table 16 list the total percent damage injury and minimum viable cell. The incisor shows a greater degree damageability do due to it's higher peak temperatures. Viewing Figure 33 and Table 16 the 100 mW/cm^2 can result in irreversible damage unlike the molar. Figure 33 C the top portion shows some discoloration. The peak temperature is 44 °C. According to Table 16 although this is reversible but it getting close to adding permanent long term damage. The only safe application time for the 200 mW/cm^2 light is 5 minutes. There is no safe application time for the 300 mW/cm^2 light source within the presented scenarios. The incisor is thinner and has a large effected parameter allow more of the light to penetrate into the dentin and pulp.

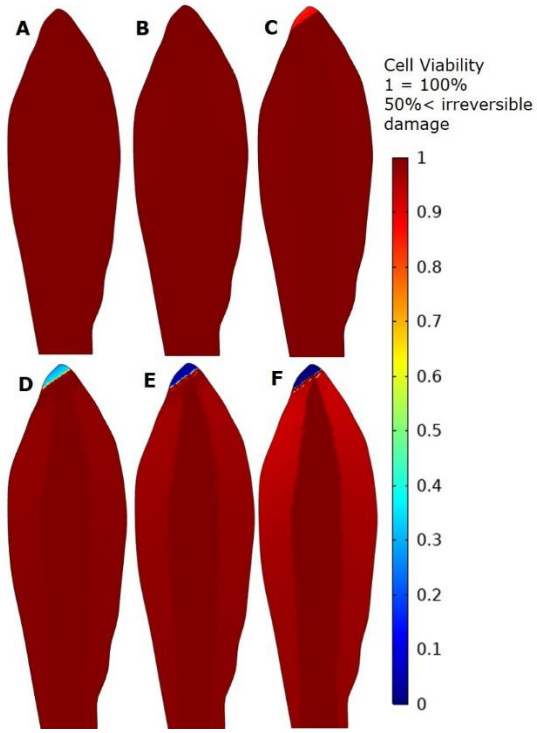

Figure 44 Incisor cell viability with light intensity of 100 mW/cm^2 no H_2O_2 applied, results are pure thermal injury. A is 5 min application time, B is 10 min application time, C is 15 min application time, D is 30 min application time, E is 45 min application time, F is 60 min application time. Below 50% is irreversible damage.

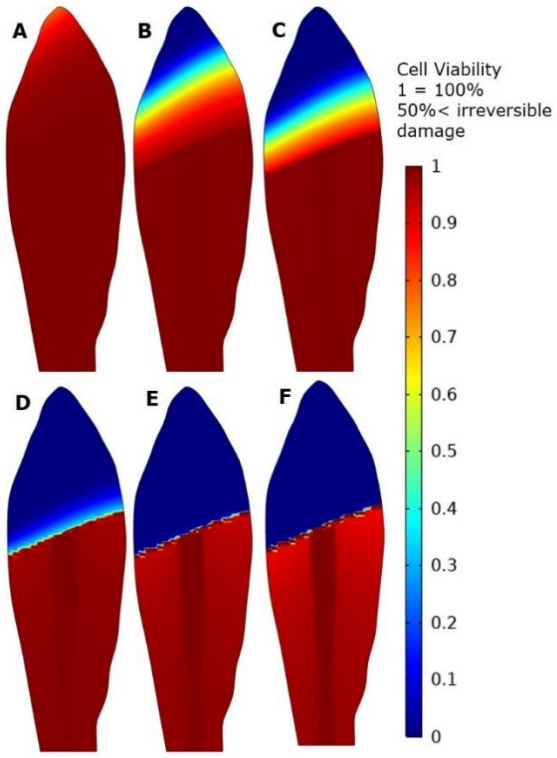

Figure 45 Incisor cell viability with light intensity of 200 mW/cm^2 no H_2O_2 applied, results are pure thermal injury. A is 5 min application time, B is 10 min application time, C is 15 min application time, D is 30 min application time, E is 45 min application time, F is 60 min application time. Below 50% is irreversible damage.

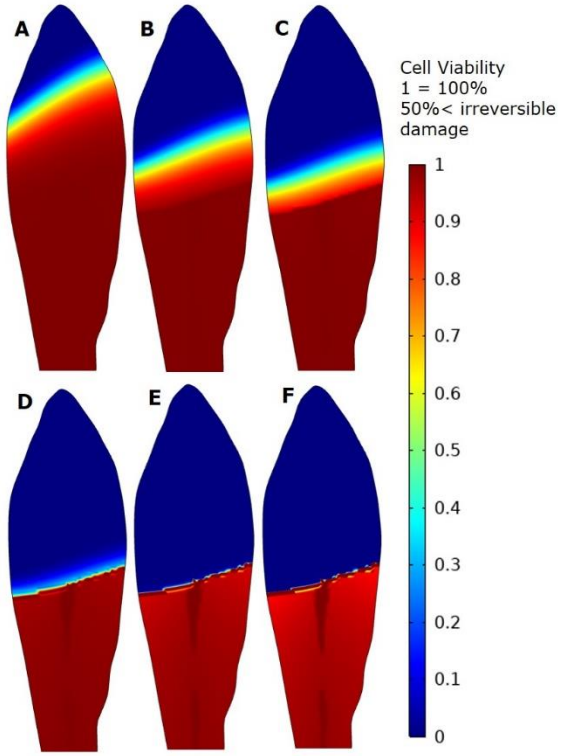

Figure 46 Incisor cell viability with light intensity of 300 mW/cm^2 no H_2O_2 applied, results are pure thermal injury. A is 5 min application time, B is 10 min application time, C is 15 min application time, D is 30 min application time, E is 45 min application time, F is 60 min application time. Below 50% is irreversible damage.

% Total pulp tissue viability Pure thermal damage by volume & (minimum cell viability) No H_2O_2 Application			
Application Time (min)	100 (mW/cm^2)	200 (mW/cm^2)	300 (mW/cm^2)
5	100 (99)	99 (0.76)	87 (0)
10	100 (96)	90 (0)	74 (0)
15	99 (0.74)	83 (0)	68 (0)
30	99 (0.12)	75 (0)	62 (0)
45	99 (0.01)	74 (0)	61 (0)
60	98 (0)	73 (0)	60 (0)

Table 20 Incisor pure thermal injury summary chart. Summation of the pulp volume viability and the minimum cell viability located within the tissue domain.

Pure inflammatory injury

For pure inflammatory damage scenarios various concentration of hydrogen peroxide gel are applied to the tooth with on light. The entire system maintains an average 37 ℃ temperature. Since no damage can come from the light, mass diffusion of peroxide into the pulp chamber is the only mechanism driving damage. As peroxide accumulates into the pulp chamber the internal stress will increase. For the current select inflammatory parameters there is no damage accrued in the pulp chamber for the molar see Figure 36 and Table 17. The predictive capability of the model in it's current form lacks the necessary experimental data or refinement to detect any injury.

Figure 37 and Table 18 pertains to the peroxide damage to the pulp in the incisor. From clinical knowledge percentages of H_2O_2 concentration of up to 37% or below are safe given the appropriate application time [cohen and chase, Colares]. Reviewing Table 18 15% H_2O_2 for up to 2 hour treat showed no damage. This result agrees with the findings according to literature [Colares et al, Vaz et al]. For concentration of 30% H_2O_2 or below are safe until 1 hour mark which the start of cell damage. In Vaz et al and Cohen et al study the clinical times applied where 30-45 minutes. All finding suggest this to safe threshold with some minor morphological changes to the cell structures. Past 1 hour cell vitality rapidly devolves. For 50% H_2O_2 the toxicity of application time 30 minutes. To the authors knowledge there is no know in vitro studies for this concentration to compare to due to its potential toxicity level to surrounding tissue. This does reinforce that increasing peroxide

concentration will lower the safe application time with no light activation. Figure 37 shows the results after 12 hour of a 2 hour application time with the three different concentrations. The rapid acceleration of damage can be explained in Figure 38. The constants α and β dictate the starting point for stain inflammation and how quickly it accelerates up to a theoretical maximum. The choices selected meet the base requirements for the model to fit clinical application.

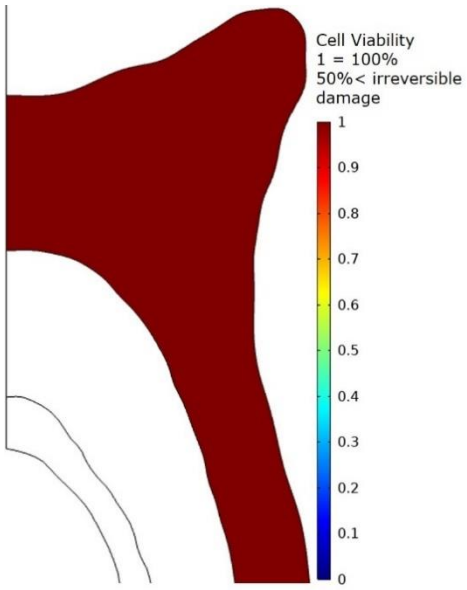

Figure 47 Molar pulp cell viability with no light. Regardless of the concentrations and application time no tissue damage was perceived.

% Total pulp tissue viability Pure H_2O_2 damage (after 12hr) by volume & (minimum cell viability) No light source			
Application Time (min)	15% H_2O_2	30% H_2O_2	50% H_2O_2
5	100 (1)	100 (1)	100 (1)
10	100 (1)	100 (1)	100 (1)
15	100 (1)	100 (1)	100 (1)
30	100 (1)	100 (1)	100 (1)
45	100 (1)	100 (1)	100 (1)
60	100 (1)	100 (1)	100 (1)
120	100 (1)	100 (1)	100 (1)

Table 21 Molar pure inflammatory injury summary chart. Summation of the pulp volume viability and the minimum cell viability located within the tissue domain.

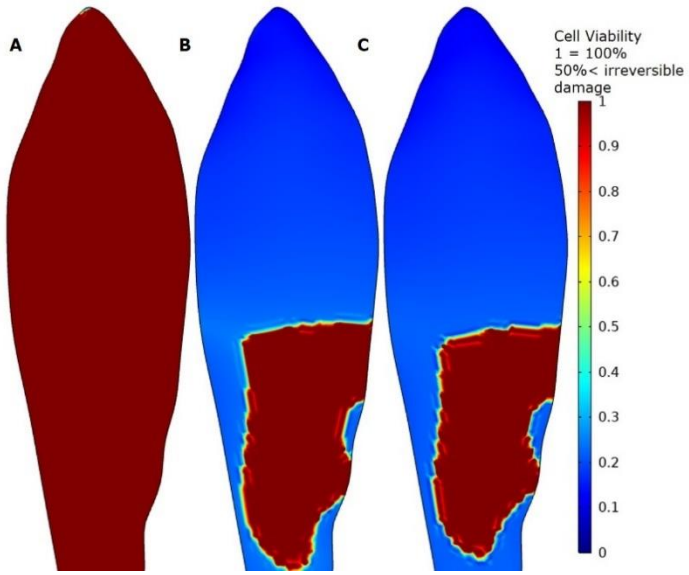

Figure 48 Incisor pulp cell viability with no light. A is 15% concentration 120 min application time, A is 30% concentration 120 min application time, A is 50% concentration 120 min application time.

% Total pulp tissue viability Pure H_2O_2 damage (after 12hr) by volume & (minimum cell viability) No light source			
Application Time (min)	15% H_2O_2	30% H_2O_2	50% H_2O_2
5	100 (1)	100 (1)	100 (1)
10	100 (1)	100 (1)	100 (1)
15	100 (1)	100 (1)	100 (1)
30	100 (1)	100 (1)	100 (1)
45	100 (1)	100 (1)	87 (0.15)
60	100 (1)	100 (0.13)	50 (0.08)
120	100 (0.13)	38 (0.06)	35 (0.04)

Table 22 Incisor pure inflammatory injury summary chart. Summation of the pulp volume viability and the minimum cell viability located within the tissue domain.

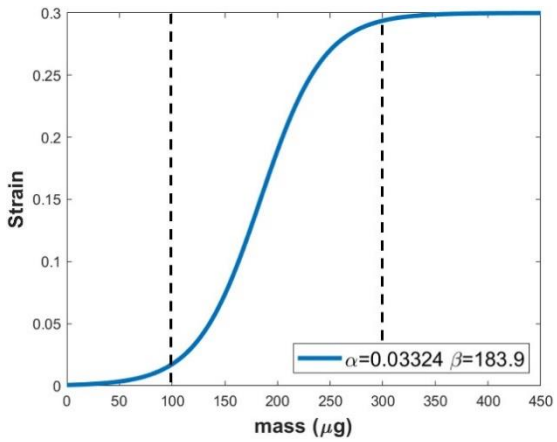

Figure 49Inflammatory model relationship of strain to total mass of H_2O_2.

Combined damage molar and incisor

Image description

Cover table results

Complications with combined damage

Combination of Pressure and Thermal Injury

Mass diffusion of peroxide is increase to the with increasing the temperature of the tooth material. As temperature increases the greater the amount of hydrogen peroxide infiltrates the pulp chamber. However the changes in the mass transfer is relative low to application time versus temperature change. Higher temperatures are more likely to create a thermal injury than to increase the increase the peroxide to a toxic level. Figure 39 and Tables 19-21 show the combined damage results for the molar. Since the pure peroxide had notedly little effect on the molar the damage results look like the burn damage.

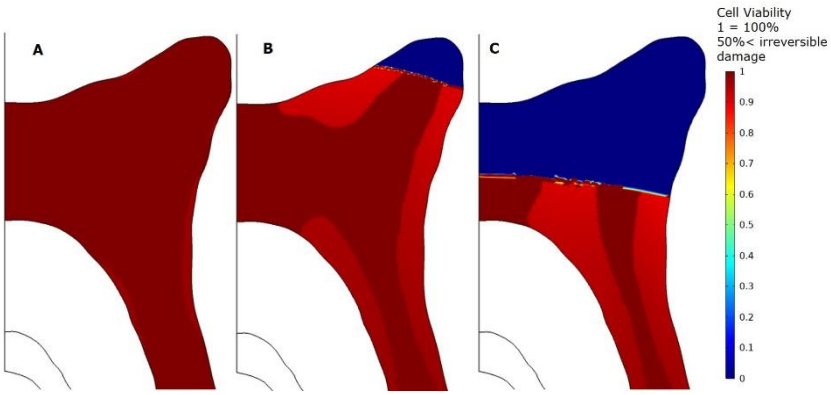

Figure 50 Molar cell viability with both light and H_2O_2. A is 100 mW/cm^2, B is 200 mW/cm^2, B is 300 mW/cm^2, ***need the peroxide concentration***

% Total pulp tissue viability combination of thermal & H_2O_2 Application damage (after 12hr) by volume & (minimum cell viability) 100 mW/cm^2			
Application Time (min)	15% H_2O_2	30% H_2O_2	50% H_2O_2
5	100 (1.00)	100 (1.00)	100 (1.00)
10	100 (1.00)	100 (1.00)	100 (1.00)
15	100 (0.99)	100 (0.99)	100 (0.99)
30	100 (0.98)	100 (0.98)	100 (0.98)
45	100 (0.96)	100 (0.96)	100 (0.96)
60	100 (0.93)	100 (0.93)	100 (0.93)

Table 23 Molar combine thermal and inflammatory injury summary chart for 100 mW/cm^2. Summation of the pulp volume viability and the minimum cell viability located within the tissue domain.

% Total pulp tissue viability combination of thermal & H_2O_2 Application damage (after 12hr) by volume & (minimum cell vibility) 200 mW/cm^2			
Application Time (min)	15% H_2O_2	30% H_2O_2	50% H_2O_2
5	100 (0.99)	100 (0.99)	100 (0.99)
10	100 (0.92)	100 (0.92)	100 (0.92)
15	99 (0.75)	99 (0.75)	99 (0.75)
30	97 (0.10)	97 (0.10)	97 (0.10)
45	96 (0.00)	96 (0.00)	96 (0.00)
60	96 (0.00)	96 (0.00)	95 (0.00)

Table 24 Molar combine thermal and inflammatory injury summary chart for 200 mW/cm^2. Summation of the pulp volume viability and the minimum cell viability located within the tissue domain.

% Total pulp tissue viability combination of thermal & H_2O_2 Application damage (after 12hr) by volume & (minimum cell viability) 300 mW/cm^2			
Application Time (min)	15% H_2O_2	30% H_2O_2	50% H_2O_2
5	99 (0.76)	99 (0.76)	99 (0.76)
10	92 (0.1)	92 (0.1)	92 (0.1)
15	83 (0)	83 (0)	83 (0)
30	70 (0)	70 (0)	70 (0)
45	67 (0)	67 (0)	61 (0)
60	67 (0)	67 (0)	47 (0)

Table 25 Molar combine thermal and inflammatory injury summary chart for 300 mW/cm^2. Summation of the pulp volume viability and the minimum cell viability located within the tissue domain.

A greater amount of peroxide does penetrate into the incisor but it also has an increased max temperature. There is a greater amount of total damage combining both peroxide and light see Figure 40 and Tables 22-24. The overall extent of the total damage is increase, but even 1% of cell death should be avoided. Figure 41 is a comparison of total percentage over time for high concentrations of H2O2 and application time with no light to a high concentration with 100 mW/cm^2. [what else to say here]

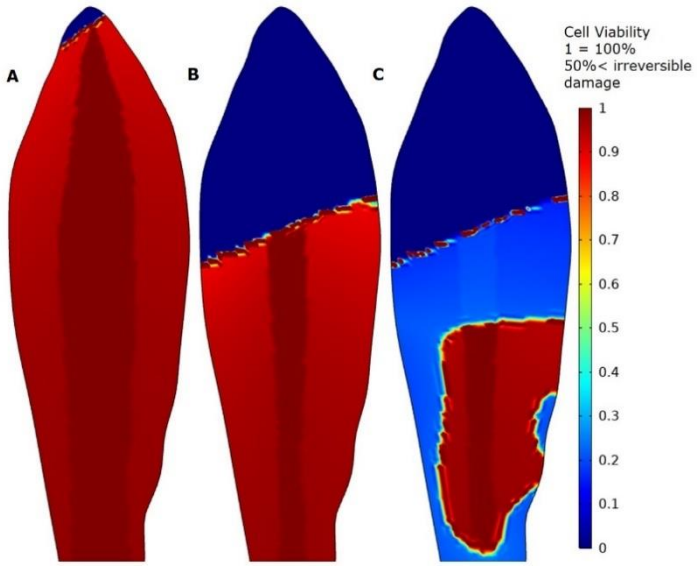

Figure 51 Incisor cell viability with both light and H_2O_2. A is 100 mW/cm^2, B is 200 mW/cm^2, B is 300 mW/cm^2, ***need the peroxide concentration***

% Total pulp tissue viability combination of thermal & H_2O_2 Application damage (after 12hr) by volume & (minimum cell vibility) 100 mW/cm^2			
Application Time (min)	15% H_2O_2	30% H_2O_2	50% H_2O_2
5	100 (1)	100 (1)	100 (1)
10	100 (0.96)	100 (0.96)	100 (0.96)
15	100 (0.83)	100 (0.83)	100 (0.83)
30	97 (0.18)	97 (0.16)	97 (0.15)
45	96 (0)	96 (0)	96 (0)
60	95 (0)	96 (0)	65 (0)

Table 26 Incisor combine thermal and inflammatory injury summary chart for 100 mW/cm^2. Summation of the pulp volume viability and the minimum cell viability located within the tissue domain.

% Total pulp tissue viability combination of thermal & H_2O_2 Application damage (after 12hr) by volume & (minimum cell viability) 200 mW/cm²			
Application Time (min)	15% H_2O_2	30% H_2O_2	50% H_2O_2
5	98 (0.41)	98 (0.41)	98 (0.41)
10	89 (0)	89 (0)	89 (0)
15	83 (0)	83 (0)	83 (0)
30	75 (0)	75 (0)	75 (0)
45	74 (0)	74 (0)	50 (0)
60	73 (0)	73 (0)	32 (0)

Table 27 Incisor combine thermal and inflammatory injury summary chart for 200 mW/cm^2. Summation of the pulp volume viability and the minimum cell viability located within the tissue domain.

% Total pulp tissue viability combination of thermal & H_2O_2 Application damage (after 12hr) by volume & (minimum cell viability) 300 mW/cm²			
Application Time (min)	15% H_2O_2	30% H_2O_2	50% H_2O_2
5	86 (0)	86 (0)	86 (0)
10	74 (0)	73 (0)	73 (0)
15	68 (0)	68 (0)	68 (0)
30	62 (0)	62 (0)	62 (0)
45	61 (0)	61 (0)	47 (0)
60	60 (0)	47 (0)	28 (0)

Table 28 Incisor combine thermal and inflammatory injury summary chart for 300 mW/cm^2. Summation of the pulp volume viability and the minimum cell viability located within the tissue domain.

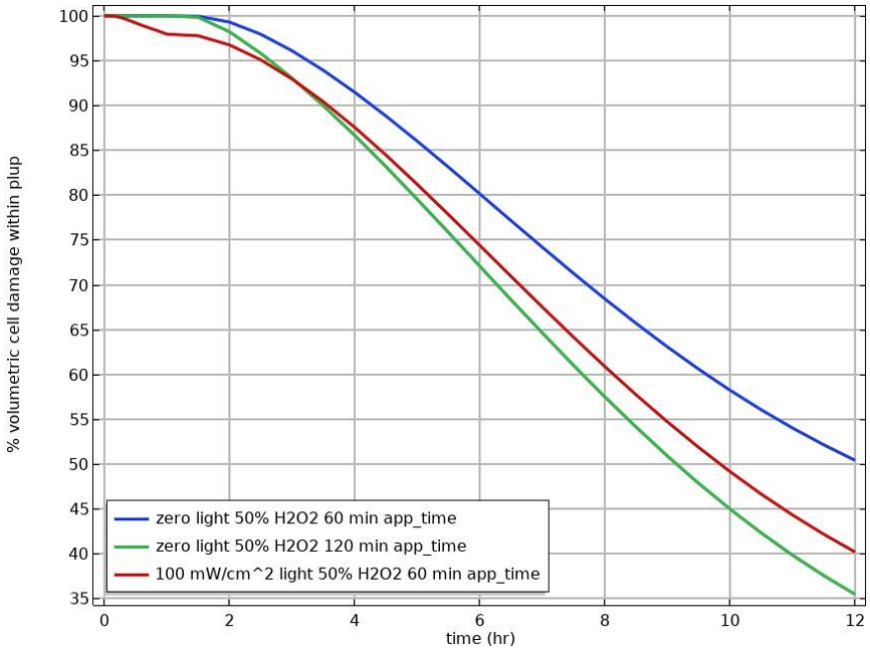

Figure 52 Incisor graph comparing volumetric cell viability with %50 concentration of H_2O_2 over time. The blue and green lines represent zero light with peroxide application time of 60 & 120 minutes. The red lines is %50 H_2O_2 & 100 mW/cm^2 applied for 60 minutes. For the red the initial dip is viability is from the thermal injury from the light. Once the light is turned off the remainder of the damage is from the leaching of peroxide into the pulp cavity. The red graph line ends with 10% more damage than the blue nonlight. This due to the increase in diffusion created by the light source allowing more hydrogen peroxide into the pulp.

Discussion

The need to start out with 2D model is useful for building the structure of a complex model with multiple domains. The reduction in computation time is crucial for building a simulation with many parts and parameter checks. The iterations involve for building such a simulation can be immense. Starting off with basic shapes or 2D construction served to reduce computational times. Due to the tooths irregular geometry certain approximations where needed in the case estimating fluxes for mass. Moving from cross-sections to different cross-sections of the same tooth could lead to different results. Nonetheless 2D can give important insights into the physiological mechanisms while building the system equations to be applied to a 3D geometry.

Temperature in this particular experiment increases with the use of a light source applied to the one side of the tooth at a 45 degree angle. Light intensity is evenly distributed based on the parameter of the applied surface based on the light power. This is an approximation since light sources follow a distribution based on center point and distance from said point similar to a flash light. This makes the model conservative on temperature increases but still practical enough to gain physiological insight sight while developing the simulation technique. Light power increases high multiplicative effect. As light intensity increases temperature increases in the tooth significantly. This in turn creates a temporary increase in internal stresses in the tooth pulp while increasing the diffusivity of hydrogen peroxide within the enamel and dentin. Most importantly it increases the chance to thermally damage the tooth.

The two damage mechanisms are included within the model thermal and inflammatory. The McGregor-Rego Model is used to account for the overall accumulated damage [McGregor et al]. The model is broken down into piecewise steps to applied to the simulated domain. Depending on the physical parameters such and temperature or pressure the model is activated or deactivated while damage is accrued over the physical domain. The simulation shows that thermal injuries happen very quickly relative to inflammation. Depending on the light intensity this can happen in 5 minutes or less. The inflammation model developed by McGregor for the purpose of this paper is driven by peroxide mass accumulated in the pulp. Since the mass of peroxide diffusion through the porous media of the tooth is relatively slow it can take up to 12 hours to see the full extent of damage create. Although temperature does increase diffusion in the current state of the model it has small effect relative to increasing application time. More experiments on material properties of dentin and enamel will be needed to be definitive on the gap between increase in mass flow based on increasing application time or temperature. The current hypothesis is although light increases diffusion the largest driver is H_2O_2 concentration application time. This means outside of using the most effective light for whiting the tooth increasing intensity will more likely cause thermal injury than an inflammatory pressure injury within the range of tested parameters.

The inflammatory model increases local strain within tissue based on the peroxide absorbed. Temperature increases will cause increase strain from thermal expansion. Since the dentin and enamel are stiff materials there is little in terms of pliability for the pulp to

expand thus increasing internal stress. Based on pressure injury portion of the McGregor-Rego model stress increase from temperature change could be damaging over prolonged times which could partially explain why temperature changes in the tooth can be painful. However, the time periods are not long enough to cause large amounts permeant damage. This is due to the longer time periods needed to form a pressure related injury based on current experimental data on skin, fat, and muscle. This means the majority of the pressure injury model will be driven by the inflammatory model. The application time and concentration of hydrogen peroxide have the strongest drivers for mass diffusion into the pulp. With the current material properties this can take several hours after the application ended to completely absorb into the pulp. The full extent of inflammation will not be seen till 2-12 hours depending on the tooth geometry, concentration, and application time. The strain caused by the inflammatory model was but together anecdotally from a string of paper and observations. Actual, experimental data is needed to increase modeling accuracy. Clinically the model matches inflammatory stain to expected damage. Using at home product of 15% H_2O_2 concentration for up to 2 hours is safe with some potential for full reversable damage. A at office product of 30% H_2O_2 concentration can be applied safely up to 1 hour. The simulation predicts that a 2 hour of application would result in full irreversible damage. The actual extent of damage is uncertain due to a lack of physical data. Currently the inflammatory model ramps up quickly once a threshold of peroxide is obtained see Figure 38. A concentration of 50% H_2O_2 which is not clinically practical due to the irritation it would cause to the surrounding tissue was selected based on it's

usefulness in future in vitro experiments. Based on simulation results, an application of 30 minutes using no light before peroxide levels in the pulp chamber will reach a toxic level.

Using both light and H_2O_2 over long periods will engage both the thermal injury and pressure injury portion of the McGregor-Rego model. Increasing the application time of both for the incisor and molar will result in burn injury before inflammation. The damage model in only being applied to the pulp so any cracks or failures in the enamel and dentin due to the temperature change are not accounted for at the present moment.

Useful paper [Kwon et al]

Conclusion and Recommendations

For the first time a working 2D multi-domain model for pulp damage has been demonstrated. The model showed the relationship of application time of H_2O_2 concentration and light have on the different physical domains and effects they have on pulp damage. A multipurpose damage and inflammation strain model was introduced for the first time in a tooth simulation. The McGregor-Rego damage model accounts for both thermal injury and pressure injury using a computational piecewise method. The inflammation model increases internal strain based on the absorbed mass of peroxide in the pulp.

Damage to the pulp using both light and peroxide for long periods of time will likely result in thermal injury before pressure injury would occur. Long application times

of peroxide have a greatest effect for developing a pressure injury. Pressure injuries take a longer time to form verses a burn. Temperature change can create stress in the dental pulp that could potentially cause noticeable pain.

The simulation can serve as a plate form to not just tooth whiting.

There are several areas to move forward from a simulation and experimental front. Converting a 3D CT scan of serval adult human tooth to use for modeling. This will account for the complex surfaces, internal geometries, and complex reactions different directions due to its morphology. Variations within humans and age groups can accounted. Compare none standard tooth geometries in terms of defects, alterations, and disease. There already exist good example of CT conversion of 3D models [Buti et al].

Several of the material parameters are missing or need further investigation. There needs to be a replication of Petersen's study for both human enamel and dentin mass diffusion properties. Although Petersen's study covered enamel it was conducted on bovine which according to Camargo et al have a large enough difference to matter [Camargo et al]. Thermally and optically further investigation into optical properties with not only the same but different light waves and the heat generated using the Beer-Lambert Law. A development of look up table be beneficial several areas of dentistry applications. Another component to consider is it has been shown that obtaining the optical properties for teeth

can be affect by how the surface was prepared using different dental restorative materials [Elgendy et al].

No data exist in regrades to a stress strain relationship for inflammation within the tooth pulp. Experiments need to be carried out to not verify the model but to define the coefficients for the strain behavior to peroxide. This opens up several areas of investigation into not just inflammatory strain but also thermal strain within the tooth pulp.

The damage model is using tissue data from skin. Experiments are needed to see how the pulp tissue receives damage over time from a variety of factors. These will help determine thermal injury from pressure injury. The pressure injury and inflammatory model lump any direct damage received to the tissue from hydrogen peroxide together which should help in translating experimental data for the model. The terms in the damage model can be altered to suit future adaptions model as our understanding grows. Some of these relationships that are directly involved in damage to the cell such as sheer stress, strain energy, ischaemia, inflammation factors, and more.

The present simulation can assist in the development and planning of experiments. The simulation can be setup to replicate in vitro experiments and help determine time scale, measurement accuracy, and experimental conditions to test. A replication of the experiment can be virtually produced to see if there is anything that requirements or any unforeseeable

circumstances which need to be addressed. The model while applied to the experiments may garner insight as to why a specific outcome is happen.

The boundary condition can be improved on the better simulate both in vitro and in vivo environments. The concentration currently held constant which is okay for in vitro studies but according to Proctor & Gamble quickly diminishes with in vivo. A dilution rate can be assigned to simulate this effect. The light is held at a constant intensity across the surface of the application zone. A statical distribution or equation can be add with a focal point for the center to represent light pattern behavior. The thermal boundary condition is held at a constant convection and gel is treated as thin none interacting layer. The boundary conditions in the model can vary over time to simulate both conduction and convection as a person opens and closes their mouth. The gel can be assigned a thickness and thermal properties to understand its significance in heat transfer.

There are also future additions that can be developed to increase the simulation potential benefit to dental product development and fundamental research. The particular focus of this study was on damage to the pulp while undergoing a tooth whiting procedure. The model can be adapted support a myriad of other applications. Some the applications include. The whiting of teeth and the effects of different treatment conditions. Pain potential to a patient due to thermal response from different types of dental procedures. Laser and mechanical cavity removal. Dental implants effect on surrounding tissue during

and after procedure. Include enamel and dentin into the damage model. The listed possible simulation applications are to just to name a few.

The groundwork for providing a mutli-domain has been shown. Important insights can be gleaned from understand how these systems interact with each other. The hope is to provide a useful tool and stepping stone for future development and understanding of dental procedures and support research endeavors.

Bibliography

[1] 2015, “The Agency for Healthcare Research and Quality’s (AHRQ)” [Online]. Available: https://www.ahrq.gov/topics/pressure-ulcers.html. [Accessed: 02-Apr-2020].
[2] 2017, “Centers for Disease Control and Prevention, National Center for Injury Prevention and Control. Web-Based Injury Statistics Query and Reporting System (WISQARS)” [Online]. Available: www.cdc.gov/injury/wisqars. [Accessed: 02-Apr-2020].
[3] NPUAP, 2016, “NPUAP Pressure Injury Stages,” NPUAP 2016 Staging Consens. Conf., pp. 1–2.
[4] Amit Gefen, 2018, “The Future of Pressure Ulcer Prevention Is Here: Detecting and Targeting Inflammation Early,” EWMA J., 19(2), pp. 7–13.
[5] Coleman, S., Nixon, J., Keen, J., Wilson, L., Mcginnis, E., Dealey, C., Stubbs, N., Farrin, A., Dowding, D., Schols, J. M. G. A., Cuddigan, J., Berlowitz, D., Jude, E., Vowden, P., Schoonhoven, L., Bader, D. L., Gefen, A., Oomens, C. W. J., and Nelson, E. A., 2014, “A New Pressure Ulcer Conceptual Framework,” J. Adv. Nurs., 70(10), pp. 2222–2234.
[6] Moritz, a. R., and Henriques, F. C., 1947, “STUDIES OF THERMAL INJURY II. The Relative Importance of Time and Surface Temperature in the Causation of Cutaneous Burns.,” Am J Pathol, 23, pp. 695–720.
[7] Moritz, A. R., 1947, “STUDIES OF THERMAL INJURY III. The Pathology and Pathogenesis of Cutaneous Burns An Experimental Study,” Am. J. Pathol., 13(6), pp. 915–941.
[8] Iaizzo, P. A., Kveen, G. L., Kokate, J. Y., Leland, K. J., Hansen, G. L., and Sparrow, 1995, “Prevention of Pressure Ulcers by Focal Cooling: Histological Assessment in a Porcine Model.,” Wounds A Compend. Clin. Res. Pract., 7(5), pp. 161–169.
[9] Kokate, J. Y., Leland, K. J., Sparrow, E. M., and Iaizzo, P. A., 1997, “Critical Thresholds for Pressure Ulcer Formation in a Porcine Model,” Wounds, 9(4), pp. 111–121.
[10] Hansen, G. L., Sparrow, E. M., Kokate, J. Y., Leland, K. J., and Iaizzo, P. A., 1997, “Wound Status Evaluation Using Color Image Processing,” IEEE Trans. Med. Imaging, 16(1), pp. 78–86.
[11] Kokate, J. Y., Leland, K. J., Held, a M., Hansen, G. L., Kveen, G. L., Johnson, B. a, Wilke, M. S., Sparrow, E. M., and Iaizzo, P. a, 1995, “Temperature-Modulated Pressure Ulcers: A Porcine Model.,” Arch. Phys. Med. Rehabil., 76(7), pp. 666–673.
[12] Zeevi, T., Levy, A., Brauner, N., and Gefen, A., 2018, “Effects of Ambient Conditions on the Risk of Pressure Injuries in Bedridden Patients—Multi-Physics Modelling of Microclimate,” Int. Wound J., 15(3), pp. 402–416.
[13] Schwartz, D., Magen, Y. K., Levy, A., and Gefen, A., 2018, “Effects of Humidity on Skin Friction against Medical Textiles as Related to Prevention of Pressure Injuries,” Int. Wound J., 15(6), pp. 866–874.

[14] Kottner, J., Black, J., Call, E., Gefen, A., and Santamaria, N., 2018, "Microclimate: A Critical Review in the Context of Pressure Ulcer Prevention," Clin. Biomech., 59(September), pp. 62–70.
[15] European Pressure Ulcer Advisory Panel, National Pressure Injury Advisory Panel, and Pan Pacific Pressure Injury Alliance, 2019, Prevention and Treatment of Pressure Ulcers/Injuries: Clinical Practice Guideline, The International Guideline.
[16] Gefen, A., Alves, P., Ciprandi, G., Coyer, F., Milne, C. T., Ousey, K., Ohura, N., Waters, N., and Worsley, P., 2020, "Device-Related Pressure Ulcers: SECURE Prevention," J. Wound Care, 29(Sup2b), pp. S1–S52.
[17] Pearce, J. A., 2013, "Comparative Analysis of Mathematical Models of Cell Death and Thermal Damage Processes," Int. J. Hyperth., 29(4), pp. 262–280.
[18] Pearce, J. A., 2015, "Improving Accuracy in Arrhenius Models of Cell Death: Adding a Temperature-Dependent Time Delay," J. Biomech. Eng., 137(12), pp. 1–7.
[19] Pearce, J. A., 2009, "Relationship between Arrhenius Models of Thermal Damage and the CEM 43 Thermal Dose," Energy-based Treat. Tissue Assess. V, 7181(February 2009), p. 718104.
[20] He, X., and Bischof, J. C., 2003, "Quantification of Temperature and Injury Response in Thermal Therapy and Cryosurgery," Crit. Rev. Biomed. Eng., 31(5–6), pp. 355–422.
[21] STOLL, A. M., and GREENE, L. C., 1959, "Relationship between Pain and Tissue Damage Due to Thermal Radiation," J. Appl. Physiol., 14(3), pp. 373–382.
[22] Henriques, F. C., 1947, "STUDIES OF THERMAL INJURY V. The Predictability and the Signinficance of Thermally Induced Rate Processes Leading to Irreverible Epidermal Injury," 43(5), pp. 489–502.
[23] Moritz, A. R., Henriques, F. C., Durtra, F. R., and Weisiger, J. R., 1947, "STUDIES OF THERMAL INJURY IV. An Exploration of the Casualty-Producing Attributes of Conflagrations; Local and Systemic Effects of General Cutaneous Exposure to Excessive Circumambient (Air) and Circumradiant Heat of Varying Duration and Intensity," Arch. Pathol., 43(5), pp. 466–488.
[24] Henriques, F. C., and Moritz, A. R., 1947, "STUDIES OF THERMAL INJURY I. The Conduction of Heat to and through Skin and the Temperatures Attained Therein. A Theoretical and an Experimental Investigation.," Am. J. Pathol., 23(4), pp. 530–549.
[25] O'Neill, D. P., Peng, T., Stiegler, P., Mayrhauser, U., Koestenbauer, S., Tscheliessnigg, K., and Payne, S. J., 2011, "A Three-State Mathematical Model of Hyperthermic Cell Death," Ann. Biomed. Eng., 39(1), pp. 570–579.
[26] Feng, Y., Oden, J. T., and Rylander, M. N., 2008, "A Two-State Cell Damage Model under Hyperthermic Conditions: Theory and in Vitro Experiments," J. Biomech. Eng., 130(4), pp. 1–10.
[27] Xue, C., Friedman, A., and Sen, C. K., 2009, "A Mathematical Model of Ischemic Cutaneous Wounds," Proc. Natl. Acad. Sci. U. S. A., 106(39), pp. 16782–16787.
[28] Linder-Ganz, E., and Gefen, A., 2009, "Stress Analyses Coupled with Damage Laws to Determine Biomechanical Risk Factors for Deep Tissue Injury during Sitting," J. Biomech. Eng., 131(1), pp. 1–13.

[29] Friedman, R., Shabshin, N., Payan, Y., and Gefen, A., 2019, “Heel Ulcers: Investigating Injurious Tissue Load Thresholds in Humans, Based on a Patient-Specific Computational Heel Model,” Innovations and Emerging Technologies in Wound Care, pp. 123–139.
[30] Cox, D. R., 1972, “Regression Models and Life-Tables Authors (s): D . R . Cox Source : Journal of the Royal Statistical Society . Series B (Methodological), Vol . 34 , No . 2 Published by : Wiley for the Royal Statistical Society Stable URL : Http://Www.Jstor.Org/Stable,” J. R. Stat. Soc., 34(2), pp. 187–220.
[31] Rylander, M. N., Feng, Y., Zimmermann, K., and Diller, K. R., 2010, “Measurement and Mathematical Modeling of Thermally Induced Injury and Heat Shock Protein Expression Kinetics in Normal and Cancerous Prostate Cells,” Int. J. Hyperth., 26(8), pp. 748–764.
[32] Rylander, M. N., Diller, K. R., Wang, S., and Aggarwal, S. J., 2005, “Correlation of HSP70 Expression and Cell Viability Following Thermal Stimulation of Bovine Aortic Endothelial Cells,” J. Biomech. Eng., 127(5), pp. 751–757.
[33] Wang, S., Xie, W., Rylander, M. N., Tucker, P., Aggarwal, S. J., and Diller, K. R., 2008, “HSP70 Kinetics Study by Continuous Observation of HSP–GFP Fusion Protein Expression on a Perfusion Heating Stage,” Biotechnol. Bioeng., 99(1), pp. 146–154.
[34] Schwartz, D., and Gefen, A., 2020, “An Integrated Experimental-Computational Study of the Microclimate under Dressings Applied to Intact Weight-Bearing Skin,” Int. Wound J., (December 2019), pp. 1–16.
[35] Linder-Ganz, E., and Gefen, A., 2004, “Mechanical Compression-Induced Pressure Sores in Rat Hindlimb: Muscle Stiffness, Histology, and Computational Models,” J. Appl. Physiol., 96(6), pp. 2034–2049.
[36] Loerakker, S., Manders, E., Strijkers, G. J., Nicolay, K., Baaijens, F. P. T., Bader, D. L., and Oomens, C. W. J., 2011, “The Effects of Deformation, Ischemia, and Reperfusion on the Development of Muscle Damage during Prolonged Loading,” J. Appl. Physiol., 111(4), pp. 1168–1177.
[37] SAE, 2015, "Recommendation for Acceptable Operating Parameters of Heated Automobile Seats in Order to Mitigate Occupant Injury, J3047-2015-10-21."
[38] Stoll, A. M., 1960, "A Computer Solution for Determination of Thermal Tissue Damage Integrals from Experimental Data," IRE Transactions on Medical Electronics, ME-7(4), pp. 355-358.
[39] Stoll, A. M., 1967, "Heat Transfer in Bioethcnology," Advances in Heat Transfer, 4, pp. 65-141.
[40] Bull, J. P., and Lawrence, J. C., 1979, "Thermal Conditions to Produce Skin Burns," Fire and Materials, 3(2), pp. 100-105.
[41] Lawrence, J. C., and Bull, J. P., 1976, "Thermal Conditions Which Cause Skin Burns," J. Inst. Mech. Eng. Engineering in Medicine, 5(1), pp. 61-63.
[42] Log, T., 2017, "Modeling Skin Injury from Hot Spills on Clothing," Int J Environ Res Public Health, 14(11).
[43] Stoll, A. M., and Chianta, M. A., 1968, "Burn Production and Prevention in Convective and Radiant Heat Transfer," Aerospace Medicine, 39, pp. 1097-1100.

[44] Stoll, A. M., and Chianta, M. A., 1969, "Method and Rating System for Evaluation of Thermal Protection," Aerospace Medicine, 40(11), pp. 1232-1237.
[45] Stoll, A. M., Chianta, M. A., and Munroe, L. R., 1964, "Contact Flame Studies," JOURNAL OF HEAT TRANSFER-TRANSACTIONS OF THE ASME, 86(3), pp. 449-456.
[46] Chato, J. C., and Subramanian, B., 1998, "Safe Touch Temperatures for Hot Plates," Journal of Biomechanical Engineering, 120(6), pp. 727-736.
[47] Stoll, A. M., Chianta, M. A., and Piergallini, J. R., 1979, "Thermal Conduction Effects in Human Skin," Aviation space Environmental Medicine, 50(8), pp. 778-787.
[48] Diller, K. R., 1985, "Analysis of Skin Burns," Heat Transfer in Medicine and Biology: Analysis and Applications, A. Shitzer, and R. C. Eberhart, eds., Plenum Publishing Co., New York, pp. 85-134.
[49] Diller, K. R., 1991, "Analysis of Burns Caused by Long-Term Exposure to a Heating Pad," Journal of Burn Care & Rehabilitation, 12, pp. 214-217.
[50] Diller, K. R., 1998, "Modeling Thermal skin Burns on a Personal Computer," Journal of Burn Care and Rehabilitation(19).
[51] Buettner, K., 1952, "Effects of Extreme Heat and Cold on Human Skin. III. Numberical Analysis and Pilot Experiments on Penetrating Flash Radiation Effects," Journal of Applied Physiology, 5(5), pp. 207-220.
[52] Abraham, J. P., Plourde, B. D., Vallez, L. J., Nelson-Cheeseman, B. B., Stark, J. R., Sparrow, E. M., and Gorman, J. M., 2018, "Skin Burns," Theory and Applications of Heat Transfer in Humans, D. Shrivastava, ed., John Wiley & Sons, New York, pp. 723-739.
[53] Orgill, D. P., Porter, S. A., and Taylor, H. O., 2005, "Heat injury to cells in perfused systems," Ann N Y Acad Sci, 1066, pp. 106-118.
[54] Southwood, W. F. W., 1955, "The Thickness of the Skin," Plastic and Reconstructive Surgery, 15, pp. 423-429.
[55] Leider, M., and Buncke, C. M., 1954, "Physical Dimensions of the Skin," AMA Archives of Dermatology and Syphilology, 69, pp. 563-569.
[56] de Rigal, J., Excoffier, C., Querleux, B., Faivre, B., Agache, P., and Leveque, J.-L., 1989, "Asssessment of Aging of the Human Skin by In Vivo Ultrasonic Imaging," Journal of Investigative Dermatology, 93, pp. 621-625.
[57] Whitton, J. R., and Everall, J. D., 1973, "The Thickness of the Epidermis," British Journal of Dermatology, 89, pp. 467-476.
[58] Abraham, J. P., Plourde, B. D., Vallez, L. J., and Nelson-Cheeseman, B. B., 2016, "Correcting a prevalent misunderstanding of burns," Burns, 42(4), pp. 715-716.
[59] Diller, K. R., 2011, "Car Seat Heaters As a Potential Burn Hazard: a Clarification," J Burn Care Res, 32(2), pp. e33-34; author reply e35-36.
[60] Maguiña, P., Palmieri, T. L., and Greenhalgh, D. G., 2003, "Car Seat Heaters: A Potential Hazard for Burns," Journal of Burn Care & Rehabilitation, 24(5), pp. 315-316.
[61] Benjamin, C., Gittler, M., and Lee, R., 2011, "Burn from car seat heater in a man with paraplegia: case report," J Spinal Cord Medicine, 34(3), pp. 332-334.
[62] Demir, E., O'Dey, D. M., Fuchs, P. C., Block, F., and Pallua, N., 2006, "[Heated car seats--a potential burn risk for paraplegics]," Nervenarzt, 77(2), pp. 201-203.

[63] Sever, C., Kulahci, Y., Uygur, F., and Oksuz, S., 2010, "An Unusual Burn Caused by Heated Car Seat," Eplasty, 10(e28), pp. 231-232.
[64] Ketterer, A. R., and Hogrefe, C. P., 2019, "Gluteal Burns from a Car Seat Heater in a Neurologically Intact Patient: A Case Report," J Emerg Med, 56(6), pp. e107-e109.
[65] Yon, J. R., Fredericks, C., Mentzer, C., Kubasiak, J. C., and Poulakidas, S., 2021, "The end of the assembly line: Shifting patterns of automotive burns," Burns, 47(3), pp. 728-732.
[66] Bouten, C. V., Oomens, C. W., Baaijens, F. P., and Bader, D. L., 2003, "The etiology of pressure ulcers: skin deep or muscle bound?," Archives of Physical Medicine and Rehabilitation, 84(4), pp. 616-619.
[67] Gefen, A., 2008, "How Much Time Does it Take to Get a Pressure Ulcer? Integrated Evidence from Human, Animal, and In Vitro Studies," Ostomy Wound Management, 54(10), pp. 26-35.
[68] Gefen, A., 2019, "Prevention and Treatment of Pressure Ulcers/Injuries: Clinical Practice Guideline."
[69] Oomens, C. W., Bader, D. L., Loerakker, S., and Baaijens, F., 2015, "Pressure induced deep tissue injury explained," Annals of Biomedical Engineering, 43(2), pp. 297-305.
[70] Council, N. P. I. A., 2012, Pressure Ulcers: Prevalence, Incidence and Implcations for the Future.
[71] Gefen, A., 2019, "How medical engineering has changed our understanding of chronic wounds and future prospects," Med Eng Phys, 72, pp. 13-18.
[72] Gefen, A., Beienza, D., Edsberg, L., Milton, W., Murphy, C., Oomens, C. W. J., Perry, L., and Sari, Y., 2019, The Etiology of Pressure Injuries, Prevention and Treatment of Pressure Ulcers/Injuries: Clinical Practice Guideline. 3rd Ed., European Pressure Ulcer Advisory Panel (EPUAP), National Pressure Injury Advisory Panel (NPIAP), and Pan Pacific Pressure Injury Alliance (PPPIA).
[73] Zhang, J. D., Mak, A. F. T., and Huang, L. D., 1997, "A Large Deformation Biomechanical Model for Pressure Ulcers," Journal of Biomechanical Engineering, 99(4), pp. 406-408.
[74] Agam, L., and Gefen, A., 2007, "Pressure Ulcers and Deep Tissue Injury: a Bioengineering Perspective," Journal of Wound Care, 16(8), pp. 336-342.
[75] Linder-Ganz, E., Shabshin, N., Itzchak, Y., Yizhar, Z., Siev-Ner, I., and Gefen, A., 2008, "Strains and stresses in sub-dermal tissues of the buttocks are greater in paraplegics than in healthy during sitting," J Biomech, 41(3), pp. 567-580.
[76] Linder-Ganz, E., Yarnitzky, G., Yizhar, Z., Siev-Ner, I., and Gefen, A., 2009, "Real-time finite element monitoring of sub-dermal tissue stresses in individuals with spinal cord injury: toward prevention of pressure ulcers," Ann Biomed Eng, 37(2), pp. 387-400.
[77] Brienza, D., Vallely, J., Karg, P., Akins, J., and Gefen, A., 2018, "An MRI investigation of the effects of user anatomy and wheelchair cushion type on tissue deformation," J Tissue Viability, 27(1), pp. 42-53.
[78] Sae-Sia, W., Wipke-Tevis, D. D., and Williams, D. A., 2005, "Elevated sacral skin temperature (T(s)): a risk factor for pressure ulcer development in hospitalized neurologically impaired Thai patients," Appl Nurs Res, 18(1), pp. 29-35.

[79] McGregor, G., and Diller, K. R., 2021, "Modeling and Simulation of Coupled Pressure and Thermal Injury," Journal of Heat Transfer, in review.
[80] "COMSOL Multiphysics," COMSOL, Inc, Burlington, MA 01803.
[81] "Sim4Life," ZMT Aurich MedTech AG, Zurich, Switzerland.
[82] Espino, D. M., Shepherd, D. E., and Hukins, D. W., 2013, "Development of a transient large strain contact method for biological heart valve simulations," Comput Methods Biomech Biomed Engin, 16(4), pp. 413-424.
[83] Levy, A., Kopplin, K., and Gefen, A., 2014, "An air-cell-based cushion for pressure ulcer protection remarkably reduces tissue stresses in the seated buttocks with respect to foams: finite element studies," J Tissue Viability, 23(1), pp. 13-23.
[84] Roselli, R. J., and Diller, K. R., 2011, Biotransport: Principles and Applications, Springer, New York.
[85] Pennes, H. H., 1948, "Analysis of Tissue and Arterial Blood Temperatures in the Resting Human Forearm," Journal of Applied Physiology, 1(2), pp. 93-122.
[86] Fanger, P. O., 1970, "Conditions for Thermal Comfort. Introduction of a General Comfort Equation," Physiological and Behavioral Temperature Regulation, J. D. Hardy, A. P. Gagge, and J. A. J. Stolwijk, eds., Charles C Thomas, Springfield, pp. 152-176.
[87] Olney, C. M., Simone, A., Hanowski, K., Rector, T. S., Goldish, G. D., Hansen, A. H., and Ferguson, J. E., 2018, "Microclimate evaluation of strap-based wheelchair seating systems for persons with spinal cord injury: A pilot study," J Tissue Viability, 27(3), pp. 181-187.
[88] Swaine, J. M., Moe, A., Breidahl, W., Bader, D. L., Oomens, C. W. J., Lester, L., O'Loughlin, E., Santamaria, N., and Stacey, M. C., 2018, "Adaptation of a MR imaging protocol into a real-time clinical biometric ultrasound protocol for persons with spinal cord injury at risk for deep tissue injury: A reliability study," J Tissue Viability, 27(1), pp. 32-41.
[89] Lustig, M., Levy, A., Kopplin, K., Ovadia-Blechman, Z., and Gefen, A., 2018, "Beware of the toilet: The risk for a deep tissue injury during toilet sitting," J Tissue Viability, 27(1), pp. 23-31.
[90] Gefen, A., 2007, "The Biomechanics of Sitting-Acquired Pressure Ulcers in Patients with Spinal Cord Injury or Lesions," International Wound Journal, 4(3), pp. 222-231.
[91] Linder-Ganz, E., Scheinowitz, M., Yizhar, Z., Margulles, S. S., and Gefen, A., 2005, "Frequency and Extent of Spontaneous Motion to Relief Tissue Loads in Normal Individuals Seated in a Wheelchair," 2005 Summer Bioengineering Conference, ASME, Vail, CO.
[92] Yang, Y. S., Chang, G. L., Hsu, M. J., and Chang, J. J., 2009, "Remote monitoring of sitting behaviors for community-dwelling manual wheelchair users with spinal cord injury," Spinal Cord, 47(1), pp. 67-71.
[93] Kwon, S. R., and Wertz, P. W., 2015, “Review of the Mechanism of Tooth Whitening,” J. Esthet. Restor. Dent., **27**(5), pp. 240–257.
[94] Rodrigues, F. T., Serro, A. P., Polido, M., Ramalho, A., and Figueiredo-Pina, C. G., 2017, “Effect of Bleaching Teeth with Hydrogen Peroxide on the Morphology, Hydrophilicity, and Mechanical and Tribological Properties of the Enamel,” Wear, **374**–**375**, pp. 21–28.

[95] Goldberg, M., Grootveld, M., and Lynch, E., 2010, “Undesirable and Adverse Effects of Tooth-Whitening Products: A Review,” Clin. Oral Investig., **14**(1), pp. 1–10.
[96] Silva-Costa RSG, Ribeiro AEL, Assunção IV, Araújo Júnior RF, Araújo AA, Guerra GCB, B. B., 2018, “In-Office Tooth Bleaching with 38 % Hydrogen Peroxide Promotes Moderate / Severe Pulp Inflammation FGF-2 and Osteocalcin in Rats Abstract,” J. Appl. Oral Sci., **26**(1), pp. 1–9.
[97] Colares, V. L. P., Lima, S. N. L., Sousa, N. C. F., Araújo, M. C., Pereira, D. M. S., Mendes, S. J. F., Teixeira, S. A., Monteiro, C. de A., Bandeca, M. C., Siqueira, W. L., Moffa, E. B., Muscará, M. N., and Fernandes, E. S., 2019, “Hydrogen Peroxide-Based Products Alter Inflammatory and Tissue Damage-Related Proteins in the Gingival Crevicular Fluid of Healthy Volunteers: A Randomized Trial,” Sci. Rep., **9**(1), pp. 1–11.
[98] Cohen, S. C., and Chase, C., 1979, “Human Pulpal Response to Bleaching Procedures on Vital Teeth,” J. Endod., **5**(5), pp. 134–138.
[99] Kim, S., 1985, “Microcirculation of the Dental Pulp in Health and Disease,” J. Endod., **11**(11).
[100] Kim, S., 1990, “Neurovascular Interactions in the Dental Pulp in Health and Inflammation,” J. Endod., **16**(2).
[101] Fekrazad, R., Alimazandarani, S., Kalhori, K. A. M., Assadian, H., and Mirmohammadi, S. M., 2017, “Comparison of Laser and Power Bleaching Techniques in Tooth Color Change,” J. Clin. Exp. Dent., **9**(4), pp. e511–e515.
[102] Henriques, F. C., 1947, “STUDIES OF THERMAL INJURY V. The Predictability and the Signinficance of Thermally Induced Rate Processes Leading to Irreverible Epidermal Injury,” **43**(5), pp. 489–502.
[103] Petersen, B. K., 2012, “Quantitative Analysis of the Diffusion of Hydrogen Peroxide through Teeth,” UCLA.
[104] Spitzer, D., and Ten Bosch, J. J., 1975, “The Absorption and Scattering of Light in Bovine and Human Dental Enamel,” Calcif. Tissue Res., **17**(2), pp. 129–137.
[105] Turrioni, A. P. S., De Oliveira, C. F., Basso, F. G., Moriyama, L. T., Kurachi, C., Hebling, J., Bagnato, V. S., and De Souza Costa, C. A., 2012, “Correlation between Light Transmission and Permeability of Human Dentin,” Lasers Med. Sci., **27**(1), pp. 191–196.
[106] Elgendy, H., Maia, R. R., Skiff, F., Denehy, G., and Qian, F., 2019, “Comparison of Light Propagation in Dental Tissues and Nano-Filled Resin-Based Composite,” Clin. Oral Investig., **23**(1), pp. 423–433.
[107] Zach, L., and Cohen, G., 1965, “Pulp Response to Externally Applied Heat,” Oral Surgery, Oral Med. Oral Pathol., **19**(4), pp. 515–530.
[108] Bouillaguet, S., Caillot, G., Forchelet, J., Cattani-Lorente, M., Wataha, J. C., and Krejci, I., 2005, “Thermal Risks from LED- and High-Intensity QTH-Curing Units during Polymerization of Dental Resins,” J. Biomed. Mater. Res. - Part B Appl. Biomater., **72**(2), pp. 260–267.
[109] Sulieman, M., Addy, M., and Rees, J. S., 2005, “Surface and Intra-Pulpal Temperature Rises during Tooth Bleaching: An in Vitro Study,” Br. Dent. J., **199**(1), pp. 37–40.

[20] Zezell, D. M., Ana, P. A., Pereira, T. M., Correa, P. R., and Velloso, W., 2011, "Heat Generation and Transfer on Biological Tissues Due to High-Intensity Laser Irradiation," *Developments in Heat Transfer*, BoD–Books on Demand, pp. 227–246.
[21] Kramer, I. R. H., 1960, "The Vascular Architecture of the Human Dental Pulp," Arch. Oral Biol., **2**(3).
[22] Van Hassel, H. J., 1971, "Physiology of the Human Dental Pulp," Oral Surgery, Oral Med. Oral Pathol., **32**(1), pp. 126–134.
[23] Matthews, B., and Andrew, D., 1995, "Microvascular Architecture and Exchange in Teeth," Microcirculation, **2**(4).
[24] Bragin, D. E., Statom, G. L., Yonas, H., Dai, X., and Nemoto, E. M., 2014, "Critical Cerebral Perfusion Pressure at High Intracranial Pressure Measured by Induced Cerebrovascular and Intracranial Pressure Reactivity," Crit. Care Med., **42**(12), pp. 2582–2590.
[25] Dick, S. K., Chistyakova, G. G., Terekh, A. S., Smirnov, A. V., Salimi Zadeh, M. M., and Barun, V. V., 2014, " Characterization of Blood Flow Rate in Dental Pulp by Speckle Patterns of Backscattered Light from an in Vivo Tooth ," J. Biomed. Opt., **19**(10), p. 106012.
[26] Meyer, M. W., 1993, "Pulpal Blood Flow: Use of Radio-labelled Microsoheres," Int. Endod. J., **26**(1).
[28] Vaz, M. M., Lopes, L. G., Cardoso, P. C., de Souza, J. B., Batista, A. C., Costa, N. L., Torres, É. M., and Estrela, C., 2016, "Inflammatory Response of Human Dental Pulp to At-Home and in-Office Tooth Bleaching," J. Appl. Oral Sci., **24**(5), pp. 509–517.